Trinity College Dublin
Coláiste na Tríonóide, Baile Átha Cliath
The University of Dublin

Elucidating the therapeutic potential of Q8 in Glioblastoma Multiforme

Masters by Research Thesis

March 2024

Submitted to Trinity College Dublin in fulfilment

of the thesis requirements for masters:

Sean Lonergan

18328834

Supervisor: Dr Melissa Conroy

Neuroscience

Department of Physiology

School of Medicine

Trinity College Dublin

Declaration of Integrity

I declare that this thesis has not been submitted as an exercise for a degree at this or any other university and it is entirely my own work.

I agree to deposit this thesis in the University's open access institutional repository or allow the Library to do so on my behalf, subject to Irish Copyright Legislation and Trinity College Library conditions of use and acknowledgement.

I consent to the examiner retaining a copy of the thesis beyond the examining period, should they so wish (EU GDPR May 2018).

Name: Sean Lonergan

Signature: 

Date: 28/03/2024

Table of Contents

List of Tables and Figures

Abstract

Glioblastoma multiforme (GBM) is the most common and aggressive form of brain cancer in humans. Despite advancements in treatment and care, patient outcomes and survival rates are abysmal, with a five-year survival rate of 6.8%. In addition, treatment resistance and tumour recurrence are major contributing factors to GBM severity. Novel therapeutic strategies are urgently needed to combat these issues. Anti-angiogenic drugs reduce the formation of blood vessels by tumours which in turn cuts off blood and nutrient flow and can limit growth and invasion. 1,4-dihydroxy quininib, (Q8), is a novel anti-angiogenic molecule with proven efficacy in other hard-to-treat cancers and here we will test its utility in GBM. Natural killer (NK) cells are a highly specialised innate immune cell that target cancer cells and exhibit a potent anti-tumour response. Here, we showed the ability of Q8 to decrease GBM cell viability in the U251 GBM cell line model at doses above 10μM. In addition, Q8 displayed potent immunostimulatory activity, most notably in the promotion of IL-2 secretion. Finally, we demonstrated Q8's ability to enhance expression of activating NK receptor ligands MICA/B and B7-H6 on U251 and T98G GBM cells, eluding to its potential use in combination with NK cell-based therapies. Interestingly, Q8-treated GBM cell supernatants also enhanced activating NK receptor Nkp46 and activation marker CD69 on NK cell therapy KHYG-1 cells, indicating an immunostimulatory effect on NK cell function and is in line with the drug's induction of IL-2 in GBM cells. In contrast, Q8 increased inhibitory NK receptor ligand HLA-E on GBM cell lines and therefore it's cumulative effects on NK cell responses requires further investigation. Overall, our *in vitro* data suggests that Q8 elicits both direct and indirect anti-cancer effects in GBM and should be considered for further interrogation in *ex vivo* and *in vivo* models.

Acknowledgements

I would like to thank my supervisor Dr. Melissa Conroy for her patience and unwavering support throughout the year. Her guidance, motivation, and encouragement during this research allowed me to complete this work to the highest degree, and this continued counselling is a testament to the success of this research. I am truly grateful for the time and wisdom she gave which have no doubt helped me to grow as a scientist and as an academic.

Thank you to the Department of Physiology for allowing me to conduct my research and granting me access to their resources, without which this research would not be possible. A special thanks to Marianna Mekhaeil for familiarising me with, and integrating me into, the department, and for helping with planning some of the experiments I undertook. Also, to Caroline Marion for her expertise and advice in cancer cell culture. Many thanks to those in the Department of Physiology and the Department of Anatomy who gave advise and feedback on presentation talks, experimental design, and thesis presentation. I would also like to acknowledge Eimear Mylod who's previous research on the NK ligand receptor profile in the T98G cell line is utilised here and built upon in subsequent experiments.

Finally, to my mother Emer, my father Gerard, and my sister Sarah. Their constant love and support during the year cannot be understated. At times when I wanted to give up, they were always there with the right thing to say. No challenge or set-back could not be overcome with their support behind me, and that has meant the world.

Abbreviations

(d)H_2O	(Distilled) water
(d)PBS	(Dulbecco's) phosphate buffered saline
ADAM	A disintegrin and metalloproteinase
APC	Antigen-presenting cell
ATP	Adenosine triphosphate
BBB	Blood-brain-barrier
BSA	Bovine serum albumin
CAR	Chimeric antigen receptor
CO_2	Carbon dioxide
CRC	Colorectal cancer
CRT	Chemoradiotherapy
CysLt(R)	Cysteinyl leukotriene (receptor)
DMEM	Dulbecco's Modified Eagle Medium
DMSO	Dimethyl sulfoxide
DNA	Deoxyribonucleic acid
ECM	Extracellular matrix
ELISA	enzyme linked immunosorbent assay
EMMPRIN	Extracellular matrix metalloproteinase inducers
FACS	Fluorescence-activated cell sorting
FAK	Focal adhesion kinase
FBS	Foetal bovine serum
FDA	Food and Drug Administration
FGF	Fibroblast growth factor
FOLFOX	Folinic acid, fluorouracil and oxaliplatin
GBM	Glioblastoma multiforme
GI	Gastrointestinal
H_2O_2	Hydrogen peroxide
H_2SO_4	Sulfuric acid
HIF1α	Hypoxia inducible factor-1 alpha
IDH	Isocitrate dehydrogenase
IFN-γ	Interferon gamma

IL	Interleukin
ILC	Innate lymphoid cell
KIR	Killer immunoglobulin-like receptor
LILR	Leukocyte immunoglobulin-like receptor
MGMT	O-6-methylguanine methyltransferase
MHC	Major histocompatibility complex
MMP	Matrix metalloproteinase
MTT	3-(4,5-dimethylthiazol-2-yl)-2,5-diphenyltetrazolium bromide
NK	Natural killer
NKG2D	Natural killer group 2 member D
Nrf2	Nuclear factor erythroid 2-related factor 2
OPD	o-phenylenediamine dihydrochloride
P1GF	Placental growth factor
PDGF	Platelet-derived growth factor
PGE2	Prostaglandin E2
Q8	1,4-dihydroxy quininib
RNA	Ribonucleic acid
SEM	standard error of the mean
SFM	Serum free medium
TCA	Tricarboxylic acid cycle
TGF-α	Transforming growth factor
TIE	TEK tyrosine kinase
TKI	Tyrosine Kinase Inhibitor
TMZ	Temozolomide
TNF-α	Tumour necrosis factor-α
UM	Uveal melanoma
VCAM	Vascular cell adhesion molecule
VEGF	Vascular endothelial growth factor
WHO	World Health Organisation

1. Introduction

1.1 Glioblastoma multiforme (GBM)

1.1.1 GBM is a hard-to-treat malignancy

Glioblastoma multiforme (GBM) is the most common and aggressive form of brain cancer in humans. GBM is commonly diagnosed late into tumour development, Grade III or IV in accordance with the 2021 WHO cancer classification system (Sejda et al., 2022). Late diagnosis is attributed to the subtlety of its symptoms including headache, nausea, drowsiness, and weakness, followed by more sinister seizures, unilateral weakness, memory loss, speech impediment and visual deficiency (Penn Medicine, 2023). Current treatments including surgical resection and chemoradiotherapy (CRT) are effective in slowing cancer growth and reducing symptomology, however GBM remains incurable with a survival rate of ~14.6 months post diagnosis (Wirsching, Galanis & Weller, 2016). The annual incidence of GBM is between 0.59-5 people per 100000, with a 17% survival rate two years post diagnosis, plummeting to 6.8% after 5 years (Glioblastoma Research Organization, 2022), and even then approximately 90% of GBM patients will relapse within two years of their initial diagnosis (Visser et al., 2015). Radiation therapy in combination with TMZ provides the best clinical results in newly diagnosed GBM patients (Dhermain, 2014).

The exact cause of GBM has not been fully elucidated. The only known common risk factor is exposure to high dose ionizing radiation which may cause DNA mutation of glial cells, while more recent studies have posited that spontaneous mutations of genetic material in astrocytes may also lead to dysregulation of regular cell growth and function resulting in more spontaneous instances of GBM (Hanif et al., 2017). Furthermore, the clinical course of GBM is dependent on where the tumour arises in the brain and its physiological capabilities to metabolise, grow, and invade surrounding tissue. This means there is no typical presentation of GBM, and no two patients are ever the same, adding to the complexity of this disease.

GBM tumours can be characterised both phenotypically, including cellular morphology, growth patterns, and their rate of mitosis, and genotypically often based on the status of isocitrate dehydrogenase 1 (IDH1) in accordance with 2021 WHO guidelines i.e., either IDH-wildtype, IDH-mutant, or IDH-unspecified (Sejda et al., 2022). IDH1 is a gene that encodes the functional enzyme isocitrate dehydrogenase-1 which catalyses the oxidative decarboxylation of isocitrate to α-ketoglutarate, a crucial reaction in the TCA

cycle in glucose metabolism (Dimitrov et al., 2015). IDH1 mutations are linked to better clinical outcomes, doubling survival time to ~30 months (Molenaar et al., 2014). The exact reason for this is unclear, however evidence suggests that the point mutation causes a structural change at the protein active site, in turn reducing its efficacy in the TCA cycle and negatively impacting glucose metabolism. This decreased metabolic function would therefore make IDH-mutant GBM tumours less aggressive, improving patient prognosis (Bascur et al., 2018). Other mutations affecting cell receptor expression cause dysfunction in key cell signalling pathways, with the most pertinent mutations being those encoding proteins involved in extrinsic and intrinsic apoptotic pathways which converge in a caspase cascade resulting in cell shrinkage, DNA fragmentation and eventual cell death (Krakstad & Chekenya, 2010). Interventional strategies aim to target such mechanisms in an attempt to rescue cellular function and induce programmed cell death.

1.1.2 Chemoradiotherapy resistance in GBM

The first line chemotherapeutic agent for GBM, Temozolomide (Figure 1), is a lipophilic prodrug capable of crossing the BBB with anti-cancer activity. High dose TMZ elicits extensive tumouricidal potential, however toxic side effects, including hepatoxicity, acute cardiomyopathy and pneumonia, do not allow such doses to be used clinically (Kumari et al., 2017). TMZ increases patient survival from 12 to 14.4 months post-diagnosis (Filippi-Chiela et al., 2013).

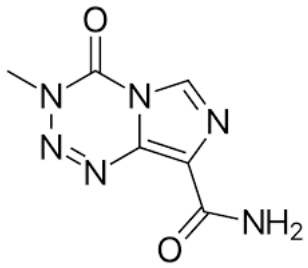

Figure 1: The chemical structure of temozolomide. TMZ is an imidazotetrazine lipophilic prodrug used as a standard treatment for Glioblastoma multiforme.

Despite the clinical success of chemoradiotherapy short-term in GBM patients, approximately 50% of TMZ treated patients do not respond to drug treatment due to intrinsic or acquired resistance (Lee, 2016). Comparable results are seen when recurrent GBM cases are rechallenged with TMZ, alluding to retained resistance to the drug. A possible mechanism of such resistance is via O-6-methylguanine methyltransferase (MGMT), a DNA repair enzyme, which has the ability to reverse methylation damage by alkylating agents such as TMZ (Tomar et al., 2021). Studies have shown that decreased expression of MGMT correlates with prolonged survival in GBM patients, while an increase in MGMT expression infers resistance to TMZ. Hence, MGMT has been established as a marker of intrinsic resistance to TMZ. Ongoing research and clinical trials are elucidating the possible benefits of MGMT inhibition in resensitising GBM tumours to radiation therapy. Such inhibitors include lomustine which has undergone phase 3 clinical trials (Herrlinger et al., 2019) and lomeguatrib which has proven radiosensitising capabilities *in vitro* (Kirstein et al., 2021). Furthermore, there is evidence to suggest that extracellular matrix metalloproteinase inducers (EMMPRINs) such as CD147 may also incur TMZ resistance by inhibiting nuclear factor erythroid 2-related factor 2 (Nrf2) degradation by increased Akt activation, thus promoting tumour growth and resistance to oxidants via an increase in Nrf2-mediated antioxidant gene expression (Bu et al., 2021; Ma, 2013).

Further to drug resistance GBM displays mechanisms of radioresistance, with a host of factors implicated including the tumour microenvironment, hypoxia, metabolic changes, heterogeneity, cell cycle and DNA damage, and microRNAs (Ali et al., 2020). The full picture remains unclear but there is evidence to support an underlying pathomechanism which enables GBM cells to resist the exogenous radiation damage. For this, a host of radiosensitising drugs have been considered such as ascorbate and motexafin gadolinium, however none have demonstrated significant improvements to patient outcomes as of yet (Ali et al. 2020). Overall, it is clear that new and improved therapeutic options are urgently warranted to improve survival rate for GBM patients.

1.1.3 Immune evasion, invasion, and angiogenesis – hallmarks of cancer and key events in GBM progression

GBM tumours are extremely aggressive in terms of growth and spread and are also rather brilliant when it comes to evading the host immune system, enabling such a rapid and destructive pathophysiology. The hallmarks of cancer as originally described by

Hanahan and Weinberg (2000) outline six biological capabilities acquired and deployed during the development and progression of human tumours. The original six include resisting cell death, sustaining proliferative signalling, evading growth suppressors, activating invasion and metastasis, replicative immortality, and inducing angiogenesis. The concept further evolved to include two more acquired capabilities including deregulated metabolism and immune system evasion, as well as two enabling characteristics encompassing genomic instability and tumour-promoting inflammation (Hanahan & Weinberg, 2011). Most recently, four new hallmarks and enabling characteristics have been posited by original author Douglas Hanahan (2022) including phenotypic plasticity, non-mutational epigenetic reprogramming, polymorphic microbiomes, and senescent cells. These hallmarks serve as the foundation of interventional research for cancer, with the focus of this research being the induction of angiogenesis and how targeting this mechanism may prevent tumour growth. Moreover, many of these hallmarks have been observed as contributory factors to GBM growth and survival and their compound activities are what establish the harsh GBM tumour microenvironment (Hanahan & Monje, 2023).

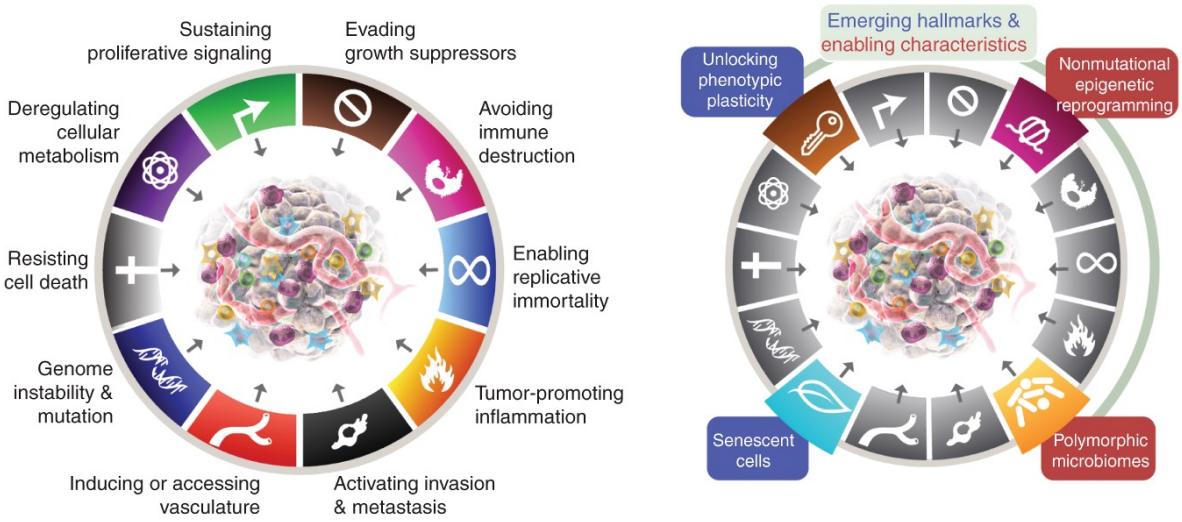

Figure 2: The hallmarks of cancer (Hanahan, 2022). This illustration depicts the original (left) and emerging (right) hallmarks of cancer, first outlined by Hanahan and Weinberg in their 2000 Cell publication. These hallmarks encapsulate the key characteristics shared across cancer species that allow tumourigenesis, growth, metastasis, and evasion to occur. They have also served as crucial targets for drug intervention strategies either singularly or in multi-model options. Although the list has grown and will continue to grow, they provide key insights into the development of cancer, and offer researchers a multitude of targets to intercept and treat.

Tumour promoting inflammation and evading growth suppressors: The GBM microenvironment is characteristically hypoxic, necrotic, and functionally immunosuppressive. There is a marked increase in the production of cytokines and chemokines including IL-1β, IL-6, IL-8, IL-10, prostaglandin E2 (PGE2), transforming growth factor (TGF-β), and basic fibroblast growth factor (bFGF) that dampen the anti-tumour response by blocking T-cell activation, inhibiting IL-2 production, and limiting NK cell activity (Chen et al., 2020). In particular, IL-10 enhances growth and inhibits the production of immune signalling markers such as interferon gamma (IFN-γ) and tumour necrosis factor-α (TNF-α) (Razavi et al., 2016). As is the case in many cancers, the T cell response becomes exhausted over time and their anti-tumour immune response diminishes (Z. Zhang et al., 2020). Continuous stimulation of T cells results in senescence, indicated by the presence of CD57, a surface cell marker. CD57 positive cells can secrete cytokines but do not proliferate. In addition, these resident cells have been shown to downregulate co-stimulatory molecules such as CD27, contributing further to immune dysfunction (Pearson et al., 2020). Furthermore, increased expression of immune checkpoint molecules such as PD-1, LAG-3, TIGIT, and CTLA-4 suppress T-cell function by competitively binding to activation sites, thus reducing the anti-cancer response (Sivori et al., 2019). It has also been shown that increased frequencies of T regulatory lymphocytes (Tregs) in GBM patients suppress antigen-presenting cell (APC) function via increased IL-10, granzyme and perforin secretion, transendocytosis of CD80 and CD86, and trogocytosis of major histocompatibility complexes (MHC), contributing to the aforementioned T-cell senescence (Humphries et al., 2010; Kondělková et al., 2010).

Activating invasion and metastasis: Having successfully evaded the local immune barrage, GBM then employs highly aggressive, coordinated invasion strategies to spread into the surrounding brain parenchyma. Tumour cell adherence is modulated primarily by integrins and/or cadherins (Demuth & Berens, 2004). Integrins allow tumour cells to modify attachment behaviour by recruiting signal proteins for processes such as phosphorylation and dephosphorylation via focal adhesion kinase (FAK), allowing for changes in adherence and motility of cancer cells (Wolfenson et al., 2013). Furthermore, matrix metalloproteinases (MMPs), ADAMS and cathepsins expressed by GBM cells enables migration by degrading and remodelling the extracellular matrix (ECM) through which the cells are passing (Vollmann-Zwerenz et al., 2020). As these cells migrate, they attract surrounding cells including microglia, astrocytes and endothelial cells which secrete proteases to further enhance their movement. Recent evidence points to the existence of

tumour microtubes, which allow precise communication between migrating tumour cells and neighbouring recruits (Osswald et al., 2015). In addition, *in vitro* analysis of CD147/EMMPRIN expression in GBM cells revealed an increased stimulation, and subsequent activation, of the production of pro-MMP-2 which may facilitate invasion *in vivo* (Sameshima et al., 2000). Further attention will be given in coming sections to the role of angiogenesis in GBM progression and survival.

Inducing angiogenesis: Angiogenesis is the formation of new blood vessels. Tumours require a source of nutrients and oxygen in order to maintain cellular function and a way of eliminating metabolic waste and carbon dioxide (Lugano et al., 2019). Several factors have been identified as key to the formation of tumour neovasculature including vascular endothelial growth factor (VEGF), platelet-derived growth factor (PDGF), TGF-β, bFGF, and angiopoietins. There are three key mechanisms employed by tumours to facilitate the formation of blood vessels, outlined in Figure 3: VEGF-dependant angiogenesis occurs due to increased expression of VEGF in response to the secretion of hypoxia inducible factor-1 alpha (HIF1α). Normally, HIF1α is secreted during times of hypoxia signalling a need for increased oxygen and blood flow to that area, for example during ischemic stroke. However, in solid malignancies such as GBM, this factor is increased as a result of the tumours own hypoxic core, upregulating VEGF expression and hence the stimulation of vascularisation from the surrounding endothelium (Park & Lee, 2022).

VEGF-independent angiogenesis posits that as a result of the hypoxic tumour microenvironment there is an increase in other angiogenic factors such as angiopoietin 1 & 2, calpain-2, MMPs, etc., which aim to remodel and stabilise tumour vascularity, and support its plasticity for further growth and migration (Crivellato, 2011). The TIE-2/angiopoietin pathway is an important cell signalling pathway in regular neurological function and is heavily implicated in abnormal angiogenesis in GBM. GBM is characterised by the overexpression of angiopoietin-1, angiopoietin-2, and TIE-2, and studies have reported that radiation therapy may promote angiogenesis via this pathway in the face of decreased VEGF-signalling which may contribute to GBM recurrence (Deshors et al., 2019). Furthermore, angiopoietin expression is linked to poorer overall survival in patients, justifying the use of therapeutics that target this pathway as an interventional strategy.

Finally, there is evidence to suggest that glioma stem cells within the tumour core are capable of differentiating into endothelial and pericyte precursors which in turn would lead to the formation of de novo blood vessels (Cheng et al., 2013).

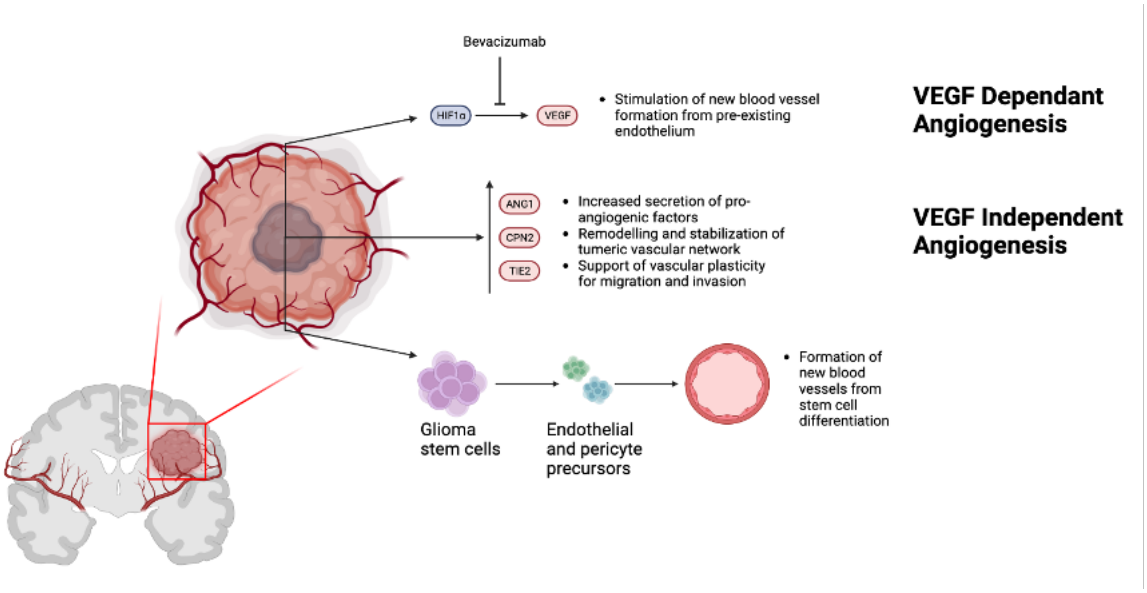

Figure 3: The proposed mechanisms of angiogenesis employed by GBM. This figure illustrates three potential mechanisms identified through which GBM angiogenesis occurs. VEGF-dependant angiogenesis relies on the stimulation of blood vessel formation as a result of VEGF secretion. VEGF is stimulated in turn by HIF1α whose expression is upregulated due to the hypoxic core of the tumour itself. VEGF-independent angiogenesis is facilitated through the production of pro-angiogenic factors which promote remodelling and stabilisation of new and existing vasculature. The third is a novel mechanism proposing glioma stem cells differentiate into vascular precursors and form blood vessels *de novo*.

VEGF is the most prominent angiogenic factor in GBM development, with overexpression correlating with poorer prognosis in patients (Shibuya, 2011). Current anti-angiogenic treatments target this VEGF-dependent pathway, with bevacizumab (Avastin) being the lead compound in GBM since gaining FDA approval in 2004 for use in GBM treatment. Avastin is also approved for, and is successful in, the treatment of colorectal cancer, ovarian cancer, and cervical cancer (Garcia et al., 2020). In GBM, Avastin is effective in slowing tumour growth by inhibiting VEGF-A activity but unfortunately does not affect the overall survival of GBM patients (Diaz et al., 2017). Furthermore, bevacizumab was found to be ineffective against recurrent GBM (Friedman et al., 2009). Combinatorial approaches with other anti-angiogenics might elicit more efficacy for these drugs in GBM.

1.2 Anti-angiogenic compounds under clinical and pre-clinical investigation

The exact mechanism through which anti-angiogenics limit cancer growth is still under investigation. Initially, and rather intuitively, it was thought that these agents prevented new vessel formation as well as pruning existing tumour vessels leading to substrate deprivation and shrinking. However more recent theories claim that these agents work to normalise the highly abnormal GBM vascular network, which would improve tumour perfusion, aid the delivery of cytotoxic therapies, and enhance their efficacy (J. Park et al., 2016). Therapeutic intervention of angiogenesis is an ever growing field of clinical research, and a review by A. B. Zhang et al. (2023) outlines some of the more recent anti-angiogenics that have entered trial phases, which are summarised below.

1.2.1 Anti-VEGF Inhibitors

Afibercept is a human recombinant fusion protein that binds VEGF-A, VEGF-B, and placental growth factor (P1GF) meaning it should show increased efficacy due to its multi-faceted antagonism, however phase II clinical trials found no significant improvements in patient survival. Ramucirumab is a human monoclonal antibody and antagonist that has a high affinity for the extracellular domain of VEGF receptor 2. It received FDA approval in 2014 for single-agent use in gastric cancer following prior standard chemotherapy and showed improved progression-free and overall survival in recurrent glioblastoma patients during phase II clinical trials. Dovitinib is another dual action inhibitor to both VEGFR and bFGF, however it has failed to show any meaningful alterations as a single agent or in combination with other anti-angiogenic treatments

(namely bevacizumab) on progression-free survival in patients with recurring GBM during a phase II clinical trial.

1.2.2 Small Molecular Tyrosine Kinase Inhibitors (TKIs)

Small Molecular Tyrosine Kinase Inhibitors (TKIs) act by reversible, competitive inhibition of adenosine triphosphate (ATP) binding domains of VEGFRs. Sunitinib is a multi-target anti-angiogenic that blocks downstream transduction, stunting angiogenesis, and tumour growth. Phase II studies have shown no significant effect on progression-free survival in recurrent GBM. Sorafenib targets VEGF, PDGFR, and the RAS/RAF/MEK pathways and was found to reduce angiogenesis in orthotopic GBM models. Following this, it was included as a combination phase II trial with bevacizumab and although this pairing showed no improvement to patient outcomes, it warranted consideration of dual anti-angiogenic therapy with multiple simultaneous targets.

Based on the studies described in the above sections, there is clear evidence pre-clinically that shows that targeting angiogenesis in GBM is a worthwhile endeavour, however it has yet to translate in improved patient outcomes long-term. A novel approach should be taken that steps away from VEGF pathway intervention and towards other, equally pertinent, angiogenic factors.

1.2.3 The anti-cancer capabilities of 1,4-dihydroxy quininib (Q8): a novel anti-angiogenic with potential utility in GBM

1,4-dihydroxy quininib (Q8) is a small anti-angiogenic compound and is an antagonist of cysteinyl leukotriene receptors 1 & 2 (CysLtR1 & CysLtR2, respectively). Q8 is a structural analogue of its parent CysLtR antagonist quininib (2-[(E)-2-(Quinolin-2-yl) vinyl] phenol). During development, Q8 exhibited a more potent anti-angiogenic effect in a zebrafish intersegmental vessel assay and was hence chosen as a lead compound for future studies. Q8 works via a VEGF-independent mechanism of action, modulating the production and expression of angiogenic and inflammatory mediators (Butler et al., 2019). Importantly, such mediators have been shown to facilitate GBM progression and indicate that Q8 might have utility beyond gastrointestinal (GI) cancers thus providing rationale for its selection as the investigational product for this study.

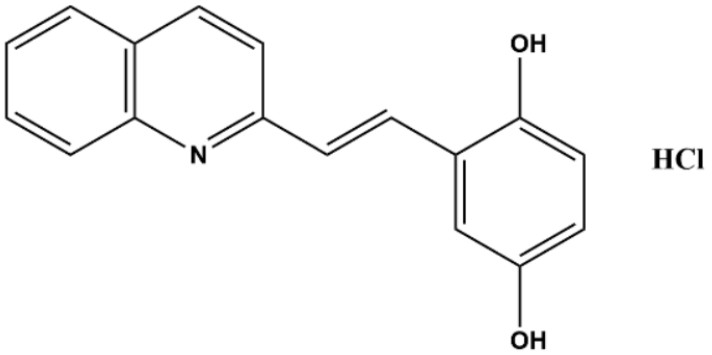

Figure 4: The chemical structure of 1,4-dihydroxy quininib (Q8). Q8 is a small anti-angiogenic molecule and an antagonist of cysteinyl leukotriene receptors 1 & 2.

CysLtR1 is a G-coupled receptor that is activated by ligand binding, those being cysteinyl leukotriene C4, D4, and E4. Increased CysLtR1 expression has been observed in other cancer types including transitional cell carcinoma of the bladder, prostate cancer, and CRC. Its expression is limited in the brain parenchyma, however it is highly localised in areas that experience trauma and in tumours. When bound, CysLtR1 activates a series of signalling pathways, outlined in Figure 5, that are implicated in cell survival and proliferation, multidrug resistance, and angiogenesis (Burke et al., 2016). This was confirmed by studying the effects of other CysLtR1 antagonists like Montelukast and Zafirlukast which were found to inhibit cell growth and induce cell cycle arrest and death in the A172 and U-87 GBM cell lines (Tsai et al., 2021). Q8 appears to be unique in its mechanism of action in that it modulates pro-angiogenic and inflammatory mediator expression, while other CysLtR1 antagonists induce cellular apoptosis pathways or inhibit cell proliferation.

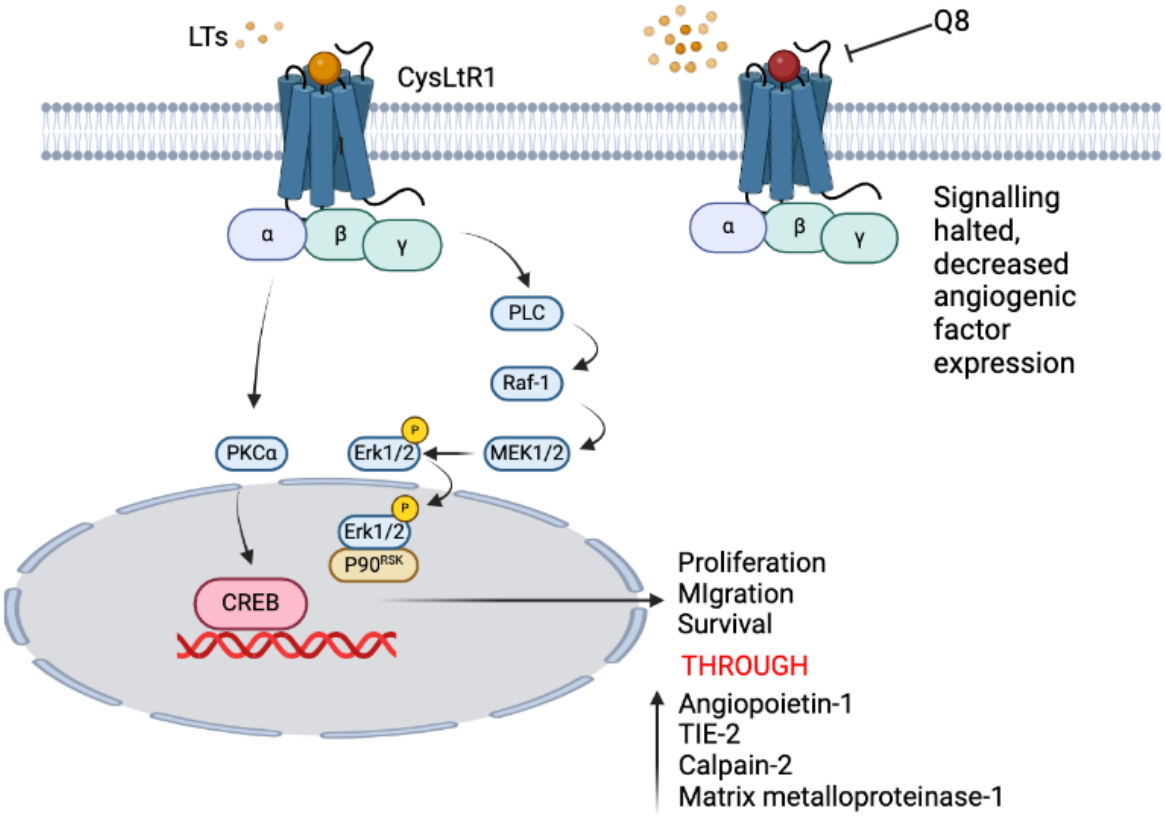

Figure 5: CysLtR1 binding results in activation of the Ras/Raf/MEK/Erk pathway which increases angiogenic factor secretion, and enables proliferation, migration, and survival. Upon stimulation, conformation changes of the receptor subunits result in activation of phospholipase C (PLC), Raf-1, and mitogen-activated protein kinase (MEK1/2). Activation of this pathway causes translocation of phosphorylated extracellular signal-regulated kinase (p-Erk1/2) from the cell cytosol to the nucleus where it interacts with $p90^{RSK}$, a regulatory effector protein involved in cell growth, proliferation, and survival via downstream signalling cascades including the Tie-2/angiopoietin signalling pathway. This function is also achieved by the activation of protein kinase Cα (PKCα) which induces upregulation of the cAMP response element-binding protein (CREB) transcription factor, an important pathway for cancer survival and malignant cell transformation (Steven & Seliger, 2016). Q8 is an antagonist of this receptor, therefore it blocks leukotriene ligand binding and hinders the associated signalling cascades. Generated using BioRender.com.

CysLtR tumour expression is correlated to poorer patient outcomes in breast cancer and colorectal cancer (CRC) cohorts due to its ability to up-regulate proliferative and survival pathways *in vitro* (Burke et al., 2016). Q8 dramatically reduced secretion of TIE-2, vascular cell adhesion molecule 1 (VCAM-1), and calpain-2 expression and displayed similar efficacy in human CRC explants and tumour xenografts (Butler et al., 2019). Calpain-2 is known to influence GBM cell migration and invasion and is also a downstream target of the TIE-2/angiopoietin pathway. It is significantly increased in GBM tissue and is implicated in TMZ resistance. Calpain-2 shRNA knockdown experiments have shown significant decreases in GBM migration as well as sensitisation of GBM cells to TMZ treatment (Stillger et al., 2023). Reduction in these key angiogenic factors showed Q8 was a high affinity antagonist to CysLtR1 in CRC and had a direct effect on the TIE-2/angiopoietin signalling pathway. Furthermore, when tested in combination with bevacizumab, and in combination with the chemotherapy folinic acid, fluorouracil and oxaliplatin (FOLFOX), Q8 reduced TIE-2 expression and significantly increased the expression of dendritic cell maturation markers, positing Q8 as a potentially efficacious combination therapeutic (Kennedy et al., 2020). In addition, Q8 exhibited secretome modulatory effects both *in vitro* and *in vivo* in uveal melanoma (UM). Significant alterations to the secretion of IL-13, IL-2, and TNF-α showed the drug's ability to significantly reduce angiogenic factors associated with CysLtR1 activation and poorer UM survival (Slater et al., 2023). Given the evidence that Q8 is a potent anti-angiogenic which can modulate multiple mediators that drive GBM progression, plus in light of the proven and promising efficacy of anti-angiogenics in GBM, the effectiveness of Q8 to dampen pro-angiogenic processes and other tumourigenic mechanisms will be explored in this thesis.

1.3 The emergence of immunotherapies for GBM

1.3.1 Natural killer (NK) cells

Natural killer (NK) cells are a group 1 innate lymphoid cell (ILC), $CD3^-$, $CD56^+$, and act to quickly challenge arising pathologies through potent cytokine production and cytotoxic activities (Shin et al., 2020). Unlike T cells, they do not require antigen specificity and instead work by recognising and integrating signals inferred by activating and inhibitory receptors present on their surface. Activating receptors (including NKG2D, NKP46, NKP30) recognise their cognate ligands expressed by infected or abnormal cells,

effectively ‘turning on’ the NK cell. Complete activation requires two or more of these ligand interactions to occur and can be enhanced with the addition of pro-inflammatory cytokines like IL-2, IL-15, and IL-21 (Fasbender & Watzl, 2018). NK cell function is then regulated by inhibitory receptors such as NKG2A to limit damage done to healthy tissue. Germ-line encoded receptors bind to major histocompatibility class-1 molecules (MHC-I) present on healthy cells inducing an NK cell inhibitory signal preventing their activation (Morvan & Lanier, 2015). There are three classes of inhibitory receptors: killer immunoglobulin-like receptors (KIRs), C-type lectin NKG2A/CD94, and leukocyte immunoglobulin-like receptors (LILRs) (Lanier, 2008). In cancer, MHC-1 is downregulated to evade detection by T-cells, but this prevents NK cell inhibition and activates their killing function. To compensate for this, GBM cells express other inhibitory ligands which supress NK cell function by binding to inhibitory receptors. In particular, human leukocyte antigens (HLA) HLA-E and HLA-F are overexpressed in GBM, and their expression is further increased after exposure to ionizing radiation (Hrbac et al., 2022).

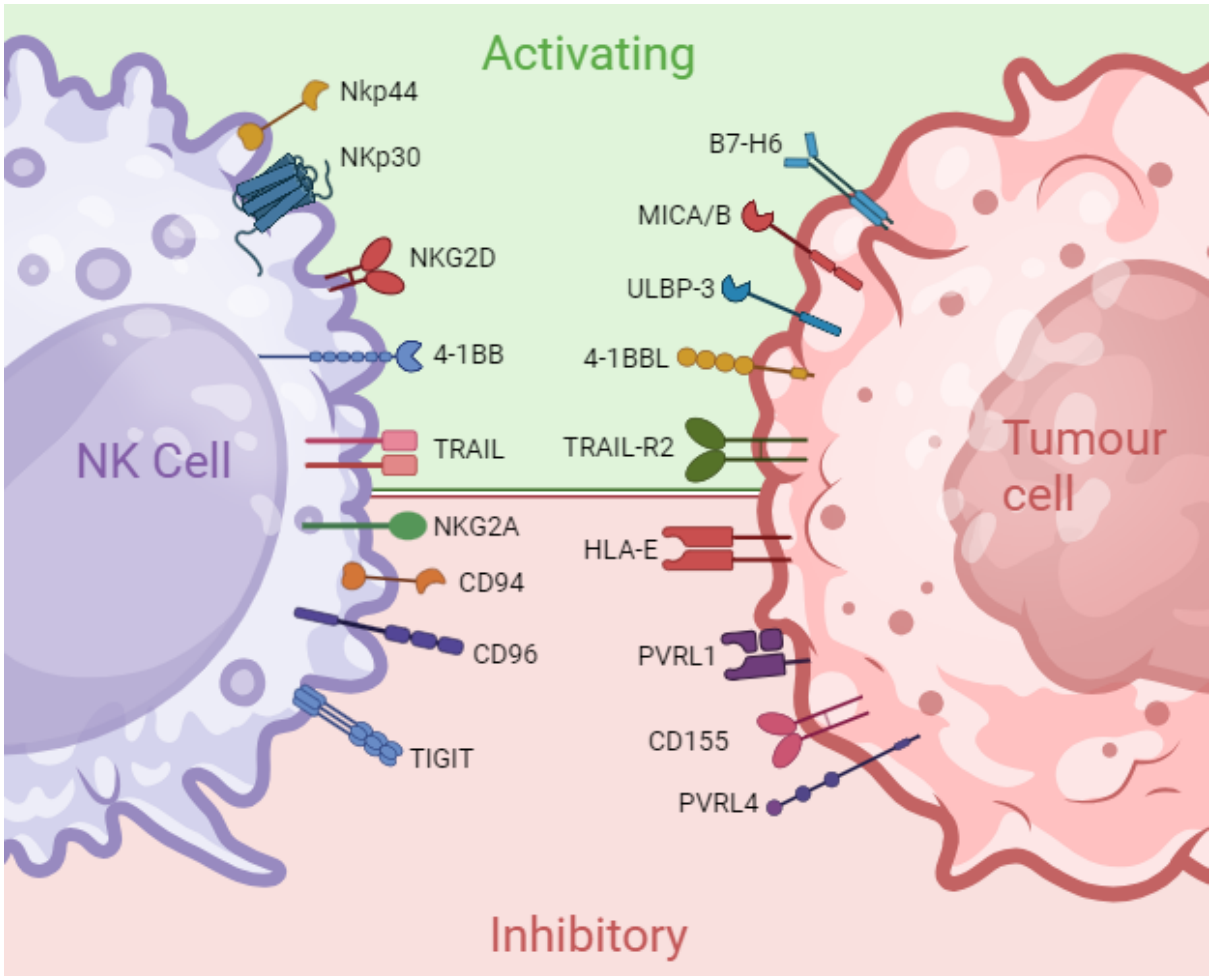

Figure 6: Activating and inhibitory receptors presented by NK cells, and corresponding ligands expressed by tumour cells. Generated using BioRender.com.

Tumour development incurs a level of cellular stress which upregulates activating receptor ligands for NK cells, shifting the balance toward NK cell activation and lysis of target cells (Paul & Lal, 2017). NK cells release perforin, a pore-forming protein, which punctures the target cell membrane allowing an influx of serine proteases (granzymes). This attack induces cell death either by necrosis if the membrane damage cannot be repaired or by caspase cascade activation and apoptosis (Backes et al., 2018). Additionally, NK cells are potent producers of IFN-γ and TNF-α which promote the anti-cancer immune response and aid in the elimination of cancer cells.

1.3.2 NK cell modulation in GBM

As previously described, tumour cell evasion of immune response is vital to their survival and growth and there are multiple strategies they employ to achieve this. In GBM, tumour cells are able to reduce NK cell receptor ligand expression through downregulation or by 'shedding' whereby NKR activating ligands are proteolytically cleaved from the cell surface. Tumour cells can also increase inhibitory ligand expression, such as MHC-I, CD155 and FasL, to increase NK cell inhibitory signalling and suppress their function (Burster et al., 2021).

Tumours may also attract immune cells such as regulatory T cells which produce inhibitory cytokines to disrupt NK cell interactions and impair their function (Sabry & Lowdell, 2017). Immunomodulatory molecules such as IL-10 and TGF-β that are secreted by tumour cells downregulate a major activating receptor, natural killer group 2 member D (NKG2D), on the surface of NK cells which greatly aids immune evasion (Crane et al., 2009).

TGF-β is an extremely powerful immunosuppressive molecule, known to limit tumour cell growth in the initial stages of cancer development (Huang et al., 2021). However, as GBM progresses, overexpression of TGF-β triggers oncogenesis. Furthermore, its expression inhibits function and proliferation of anti-cancer NK and T cells while increasing their secretion of TGF-β. Microglia are also affected by TGF-β expression, which negatively regulates their expression of MHC-II and subsequently reduces their anti-tumour function (Batlle & Massagué, 2019).

1.3.3 NK cell immunotherapy

NK cells are potent cancer killers when functioning at capacity so harnessing their abilities with therapeutic intent is an emerging and promising line of clinical research. NK

cells can directly kill cancer cells and rapidly secrete proinflammatory cytokines to recruit more NK cells and also to prompt an adaptive immune response. They offer an attractive "off-the-shelf" alternative to T cells as they do not require antigen specificity and can be sourced from allogenic blood, cell lines, or stem cells. They are easy to isolate and manipulate and offer less challenges than T cell therapy as the source of NK cell can be autologous or allogenic, removing the need for using a cancer patient's own often dysfunctional immune cells. Recent advancements in bioengineering have led to the development of chimeric antigen receptor (CAR)-engineered NK cells. Through genetic modification, CARs can bind to tumour specific NK cell antigens and stimulate activation and subsequent, thereby killing of tumour cells expression the antigen without the NK cells having to physically interact with them (Hou et al., 2021; Maus, 2015). The KHYG-1 cell line is a highly cytotoxic NK cell line and is a well-established model for the study of enhanced KN cell cytotoxicity (Suck et al., 2005). This particular cell line offers a readily available and easily expandible option for NK cell therapy and their suitability for GBM alone and in conjunction with anti-angiogenic treatment will be further studied in this thesis.

1.3.4 Q8 and NK cell conjunctive therapy

Sequenced combination therapies are coming to the fore as successful pathways for recurrent hard-to-treat cancers. This research will investigate whether Q8 and KHYG-1 cell therapies hold therapeutic promise alone and in combination in the setting of GBM. NK cell therapy has been assessed in conjunction with bevacizumab plus irinotecan, a potent inhibitor of topisomerase-1 with established use as a chemotherapeutic to treat colon and small cell lung cancer . It was demonstrated that irinotecan decreased proliferation and increased NK receptor ligand expression on GBM cells (Tran et al., 2023). Given the proven anti-cancer potential of Q8 in other hard-to-treat cancers, it is hoped that equivalent properties will be observed in GBM. It is crucial to examine the interplay between these therapeutic approaches and elucidate any immunomodulatory properties of Q8 before its extension and combination with immunotherapy in GBM can be considered.

1.4 Hypothesis

Q8 has therapeutic utility in GBM as an anti-angiogenic compound and holds potential as a combination approach with NK cell immunotherapy.

1.5 Study Aims

Aim 1: Elucidate the anti-proliferative effect of Q8 in GBM using the T98G and U251 cell line models.

Aim 2: Investigate the effects of Q8 on angiogenic factor expression by GBM tumour cells using the T98G and U251 cell line models.

Aim 3: Investigate the effects of Q8 on tumour-promoting inflammation and immunosuppressive mechanisms of GBM tumours by studying its effects on pro- and anti-inflammatory cytokine production in T98G and U251 cell line models.

Aim 4: Examine the effects of Q8 on the susceptibility of GBM tumours to NK cells and its impact on the functional capacity of the NK cell therapy KHYG-1.

2. Materials and Methods

2.1 Survival analysis of altered gene expression for proteins that indicate potential effectiveness of Q8 in GBM patients

Associations between altered gene expression and survival outcomes in GBM patients were analysed to determine key factors association with poorer prognosis. The large-scale genomics database cBioPortal (www.cBioPortal.org) provided the necessary datasets for appropriate analysis to be conducted. A total cohort of 2,220 GBM patients across several studies was used (Mayo Clinic, Clin Cancer Res 2020; CPTAC, Cell 2021; Columbia, Nat Med 2019; TCGA, Cell 2013; TCGA, Nature 2008; TCGA, Firehose Legacy; TCGA, PanCancer Atlas). Genes encoding proteins associated with CysLtR signalling (including the receptor itself) or the Tie-2/angiopoietin signalling pathway (a known pro-angiogenic axis in GBM which has been shown to be modulated by Q8 in other cancers) were analysed, and patients with available information regarding altered expression were extracted. Overall and disease-free survival metrics were obtained and analysed using a log-rank test. Significant differences were identified by a log-rank value of <0.05.

2.2 Cell culture of the T98G and U251 cell lines

The T98G cell line was gifted by Dr Maria Valasco, Centro Nacional de Investigaciones Oncológicas, CNIO, Madrid, Spain. The U251 cell line was purchased from Merck. All *in vitro* cell culture was performed using the laminar flow hood (FASTER), with all equipment used being autoclaved and sprayed with 70% ethanol before being introduced into the hood. Cells were cultured in DMEM/F12 1:1 + 2.5mM L-Glutamine + 15mM HEPES Buffer (Catalogue #SH30023.01) supplemented with 10% foetal bovine serum (FBS) (Catalogue #F7524) and 1% penicillin streptomycin (pen-strep) (Catalogue #P4333). Cells were checked using light microscopy (10x objective lens) to assess viability and distributed, and were incubated at 37°C, 95% humidity, and 5% CO_2 concentration in T-75 flasks (pre-established optimal growth conditions by previous lab members). The antifungal agent AquaStabil Julabo (Catalogue # 8940006) was used in all incubators and water baths used to minimise contamination.

Cells were split every 4-5 days based on confluency (>90%) as shown in Figure 7. Old medium was removed, the cells were washed with 5mL phosphate buffered saline (PBS) (Catalogue #SH30256.02), and 3mL of trypsin 1X (Catalogue #59418C) (10X

diluted in PBS to working concentration) added to detach cells from the base of the flask. Cells were incubated at 37°C for 8-9 minutes, after which 10mL of medium was added to neutralise the trypsin. The contents of the flask were transferred to a 15mL tube and centrifuged for 5 minutes at 1300RPM and 25°C. The supernatant was decanted, and the remaining cell pellet was resuspended in 5mL of medium.

A

T98G Cell Line

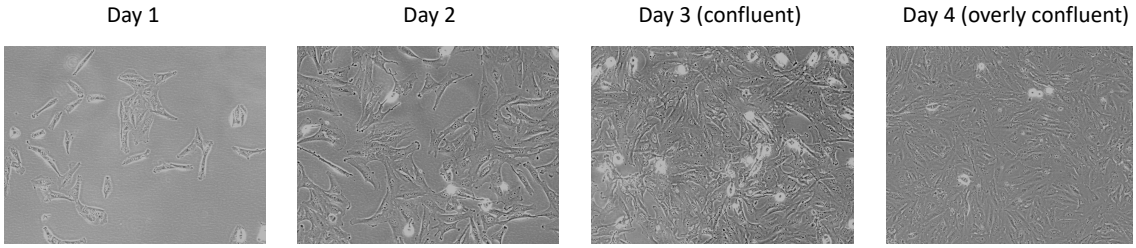

B

U251 Cell Line

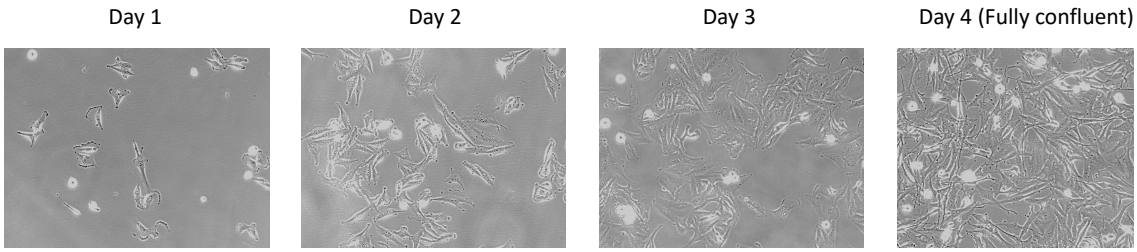

Figure 7: Representative images of GBM cell line growth. Light microscope images (x10 magnification) obtained of **(A)** T98G cells and **(B)** U251 cells in medium in T-75 flasks.

10µL of cells was mixed with 10µL trypan blue (Catalogue #T8154) and 10µL was transferred to a haemocytometer (Neubauer glass haemocytometer 0.1 mm depth, Bright-Live^{R}) for counting. Cells were counted in 5 quadrants (4 corners and centre) The number of cells was calculated using the formula below.

$$\frac{\textbf{Number of cells counted}}{\textbf{Number of chambers (5)}} \textbf{ x dilution factor (2) x } 10^4 \textbf{ = number of cells in 1mL}$$

$$\textbf{Number of cells in 1mL x 5 = total number of cells}$$

Subculture at a 1:8/1:10 ratio was performed by adding the appropriate volume of cells and making up the remaining 10mL volume with fresh medium.

2.3 Drug treatments with Q8

1,4-dihydroxy quininib (Q8) (Catalogue #2738) was purchased from Axon Medchem and reconstituted in dimethyl sulfoxide (Catalogue #D8418) to a stock concentration of 33.4mM from which the working concentrations could be made. Cells were trypsinised, counted as described, and seeded according to the experimental plate plan designed prior to each. Working concentration of Q8 were made by diluting the stock concentration in complete medium.

2.4 MTT assay

Oxidoreductase enzymes involved in cellular metabolism reduce MTT (3-(4,5-dimethylthiazol-2-yl)-2,5-diphenyltetrazolium bromide) to an insoluble formazan which has a purple colour. The amount of formazan produced, and hence the intensity of the purple colour, is proportional to cell viability. Both cell lines were seeded at a density of 5000 cells per well in 100µL of medium in 96-well plates and incubated for 24 hours. The medium was removed and replaced with serum free medium (SFM) and incubated for 4 hours. Cells were treated with Q8 at various concentrations (1µM, 5µM, 10µM, 20µM, 50µM, 100µM, 200µM), a vehicle control (1% DMSO (v/v)), 20% DMSO, and just medium as depicted in Figure 8. The cells were incubated at various timepoints (24-, 48-, and 72-hours). After the required time the cells were assessed using light microscopy, representative pictures were acquired, and 5mg of MTT (Catalogue #M6494) was dissolved in 1mL of PBS. The cell supernatant was removed and stored at -20 for future use and replaced with 100µL of fresh

medium and 10µL of MTT solution. The plates were wrapped in tinfoil and incubated for 4 hours at 37°C. 75µL was removed from each well and 50µL of DMSO was added to lyse the cells and release the formazan crystals. The plate was then read using Gen5 plate reader (Version 2.00.18) at an optical density (OD) of 540nm.

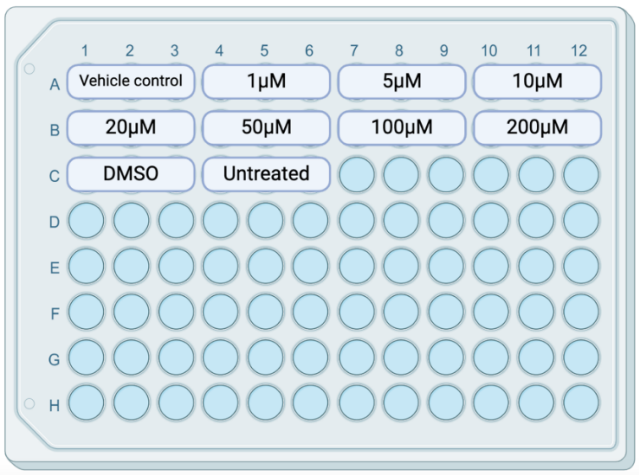

Figure 8: An outline of the MTT assay plate plan detailing the treatments applied to each well. Each condition was repeated in triplicate and averages were taken to produce a dose-response curve for analysis.

2.5 Immunofluorescence staining and microscopy

2.5.1 Staining cells

Immunofluorescence microscopy was used to investigate the effect of Q8 treatment on the expression of pro-angiogenic factors by the T98G and U251 cell lines. 24 well plates were preprepared with circular glass slide inserts. Both cell lines were seeded at a density of 5000 cells per well in 500µL of medium and incubated for 24 hours. The medium was removed and replaced with serum free medium (SFM) and incubated for 4 hours. Cells were then treated according to the plate plans, shown in Figure 9, for 48 hours.

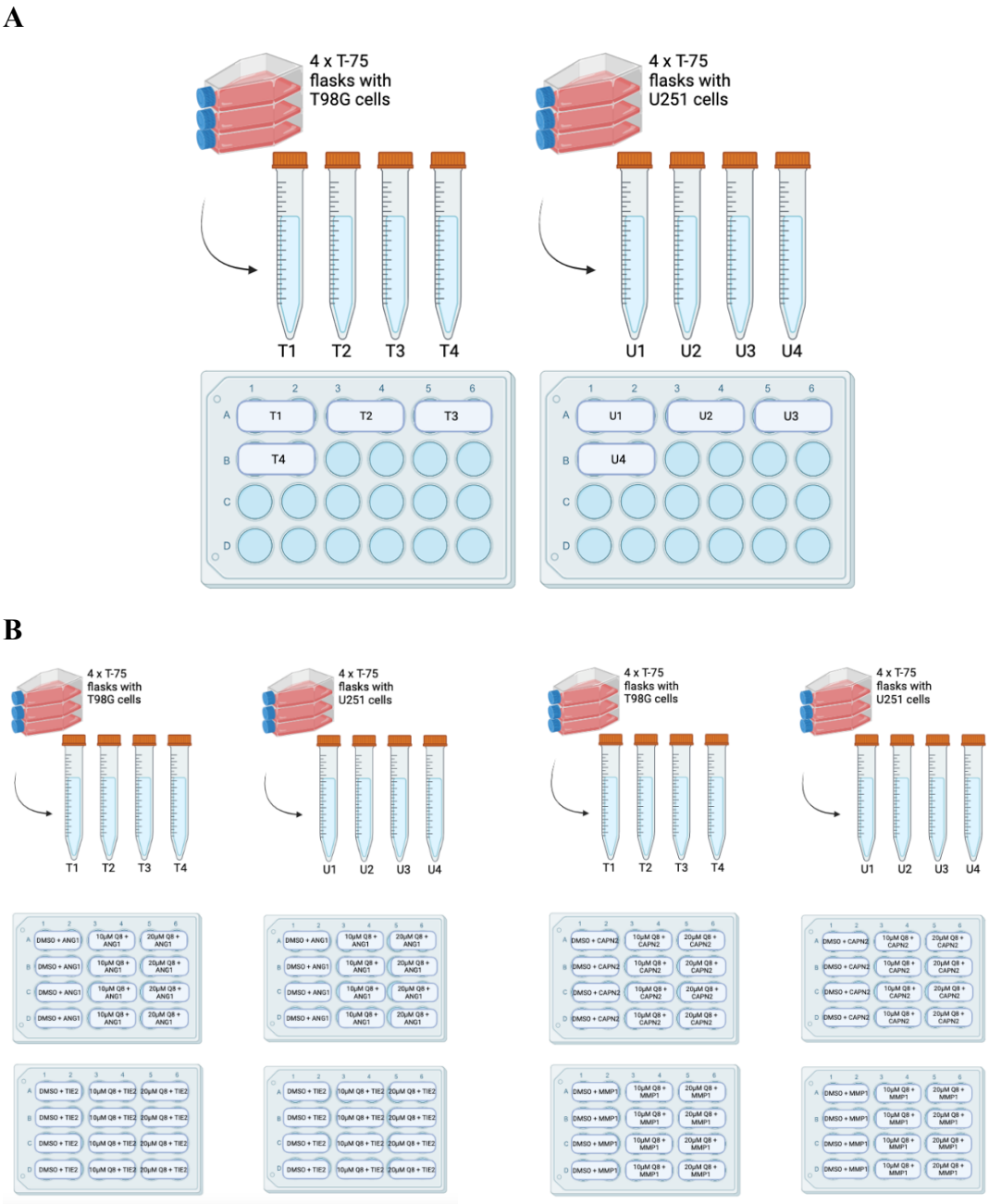

Figure 9: Plate plans for immunofluorescence experiments. (A) Outlines the CysLtR screening experiment plan, whereby both cell lines were seeded and stained with a CysLtR1 receptor antibody for receptor expression analysis. **(B)** Illustrates the plate plans for the respective angiogenic and matrix remodelling mediator expression analysis in response to Q8 concentrations. 1% DMSO (v/v) was used as a vehicle control, with 10µM and 20µM Q8 concentrations being chosen in line with previous experimental data.

The old medium was removed and 400µL of 4% formaldehyde (Catalogue #F8775) was added to each well for 5 minutes to fix the cells. The cells were then washed with PBS 3 times (3 x PBS wash) and treated with 250µL of 0.1% Triton-X (Catalogue #T9284) for 5 minutes. Following another 3 x PBS wash, 250µL of 1% bovine serum albumin (BSA) (Catalogue #A3294) was added for 1 hour. Each primary antibody was diluted in 1% BSA according to the manufacturer's guidelines with 250µL added to each of the wells.

The expression of CysLtR1 (Catalogue #PA5-97751) was investigated to ensure the cell lines expressed the drug target. Two cell membrane protein markers were used to show the morphology of the GBM cell lines including platelet endothelial cell adhesion molecule (PECAM-1 or CD31) (Catalogue #sc-376764) and Collagen IV (Catalogue #PA5-104508). The angiogenic factors studied here include angiopoietin-1 (Catalogue #sc-518157), TIE-2 (Catalogue #sc-518076), calpain-2 (Catalogue #sc-373966), and MMP-1 (Catalogue #sc-21731).

Primary antibodies were left to incubate at 4°C for 48 hours, after which it was removed and stored for further use. The cells underwent a 3 x PBS wash, 250µL of secondary antibody diluted in 1% BSA was added to the appropriate wells and were incubated at 4°C for 1 hour.

The secondary antibodies used include Goat anti-Rabbit IgG (H+L) Cross-Adsorbed Secondary Antibody, Alexa Fluor™ 488 (Catalogue #A11008) and Goat anti-Mouse IgG (H+L) Highly Cross-Adsorbed Secondary Antibody, Alexa Fluor™ 633 (Catalogue #A21052). Their use is further detailed in the results chapters that follow.

The secondary antibody was discarded and 250µL of Hoechst nuclear stain (Catalogue #62249) was added. The cells were incubated for 30 minutes at 4°C and washed in PBS three times for 10 minutes each time and a final time in distilled water (dH_2O).

Two 2µL of mounting buffer (SlowFade™ Gold Antifade Mountant) (Catalogue #S36936) were added to a glass slide. The circular glass inserts were carefully lifted from the plates using a curved forceps, dried off, inverted, and lowered onto the mounting buffer ensuring there were no air bubbles. Slides were stored at 4°C until imaging was performed.

2.5.2 Imaging cells

Leica Application Suite X (LAS X) immunoimaging software was used. The glass slide was mounted and focused using the microscope coarse and fine focus knobs. The microscope was further focused and adjusted using the computer software, and images were captured in 1024 x 1024 resolution at 200 frames per second (fps). Ten images were

acquired per sample to ensure sufficient data for analysis. Image analysis was performed using ImageJ software, detailed further in the results section.

2.6 ELISA assay

Enzyme linked immunosorbent assays (ELISAs) were performed on the cell supernatant acquired during previous experiments. In particular, those supernatants from the 48-hour Q8 treatments were used as this was determined to be the optimal concentration with which to conduct further experimentation. Levels of soluble analytes IL-2 (Catalogue #HUDC0050-96, Assay Genie), IL-4 (Catalogue #DY204, R&D Systems), IL-6 (Catalogue #31670069, ImmunoTools), IL-8 (Catalogue #31670089, ImmunoTools), IL-17 (Catalogue #DY5194, R&D Systems), CRP (Catalogue #DY1707, R&D Systems), TNF-α (Catalogue #DY210, R&D Systems), IFN-γ (Catalogue #HUDC0036-96, Assay Genie), and CD147 (Catalogue #31671479, ImmunoTools) were measured using ELISA kits according to manufactures guidelines.

To begin with, 50µL of capture antibody diluted in distilled PBS (dPBS) (Catalogue #14190-094) was added to the plates according to the plate plans outlined in Figure 10 and stored at 4°C overnight. A washing solution was prepared by dissolving 5g of PBS powder (Catalogue #L182-50) in 2L of dH_2O and adding 1mL of Tween 20 (Catalogue #P1379). Plates were washed and dried thoroughly and 50µL of blocking buffer (1% BSA) was added to each well for 2 hours at room temperature. The plates were washed and dried again and the samples and standards (serial diluted 1:2 from highest concentration according to manufacturer's recommendations) were added and left overnight at 4°C. The plates were washed and dried, 50µL detection antibody was added to each well and left for 2 hours at room temperature. Plates were washed and dried and 50µL of streptavidin-horse radish peroxidase (Strep-HRP) was added to each well followed by a 20-minute incubation. A substrate solution was prepared by dissolving one tablet of Sigma Fast o-phenylenediamine dihydrochloride (OPD) (Catalogue #P8936) and one tablet of Sigma Fast buffer with urea H_2O_2 (Catalogue #P8812) in 200ml of dH2O. The plate was washed and 50µL of the substrate solution was added to each well which was left to react for 30 minutes. The reaction was stopped by adding 25µL of sulfuric acid (H_2SO_4) to each well. The plate was read using Gen5 plate reader at an OD of 490nm.

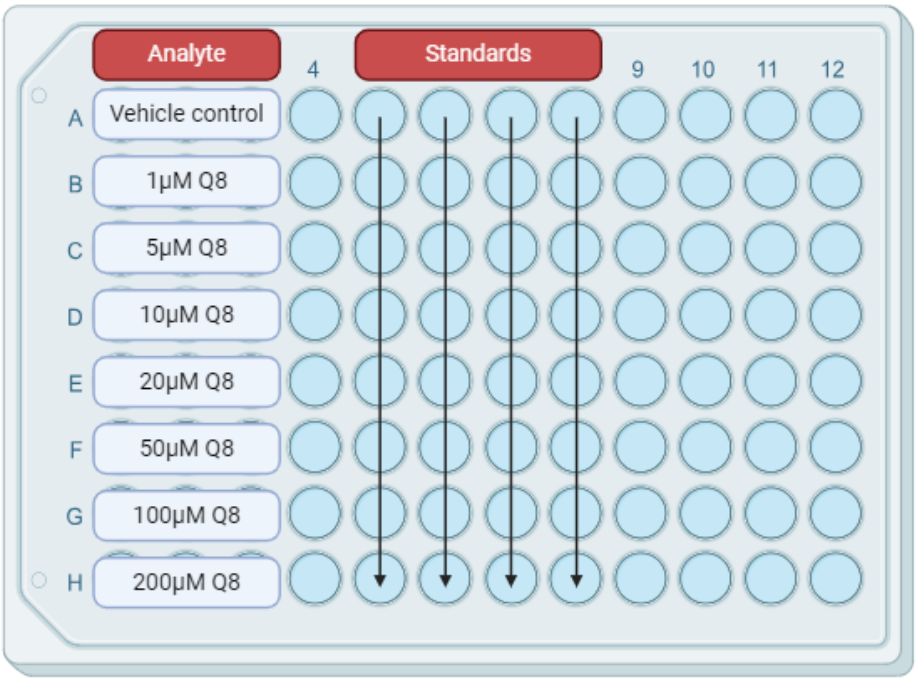

Figure 10: Plate plan for the various ELISA assays performed to assess immune analyte levels after Q8 treatment. Analytes were tested at a range of concentrations in triplicate, and the standards produced by serial dilution, 1:2, from the highest working concentration in duplicate.

2.7 Flow cytometry

Fluorescence-activated cell sorting (FACS) flow cytometry was employed to interrogate the potential of treating GBM cell lines with NK cell immunotherapies. Unstained controls were used and were subject to the same protocols as the stained groups, barring the addition of flow cytometry antibodies.

2.7.1 Flow cytometric analysis of NK receptor and NK receptor ligand surface expression by KHYG-1 and GBM cells

Cells were seeded and treated according to the plate plans outlined in Figure 11. Following 48-hour incubation, the cells were transferred in suspension to a FACS tube (~500000 cells per condition). The tubes were centrifuged, the supernatant discarded, and the cells were washed by centrifugation in 1mL of FACS buffer (PBS supplemented with 2% FBS and 0.1% sodium azide). The supernatant was discarded, and the cells resuspended in 100µl of FACS buffer. The antibody master mixes were prepared according to the panel plan and the required volumes of each flow cytometry antibody. The appropriate volume of each mix was added to their respective FACS tube subjects which were incubated at 4°C for 30 minutes in the dark. The cells were washed twice in 2mL FACS buffer and resuspended in 500µl FACS buffer for acquisition.

Positive and negative controls were prepared using BD positive (Catalogue #51-90-9001229) and negative (Catalogue #51-90-9001291) CompBeads, and Miltenyi Biotec positive (Catalogue #130-104-693) and negative (Catalogue #130-104-693) CompBeads. CompBeads were added to a FACS tube, and an appropriate volume of antibody was added. This was repeated for all fluorochrome channels being used.

A

NKR Ligand Screen on the T98G and U251 GBM cell lines

FITC	PVRL1	2.5µl	HLA-E	0.5µl		
PE	PVRL4	2.5µl	B7-H6	2.5µl	TRAIL-R2	1µl
PE-Cy7	41BBL	0.5µl	MICA/B	2.5µl		
APC	ULBP-3	2.5µl	CD155/PVR	0.5µl		

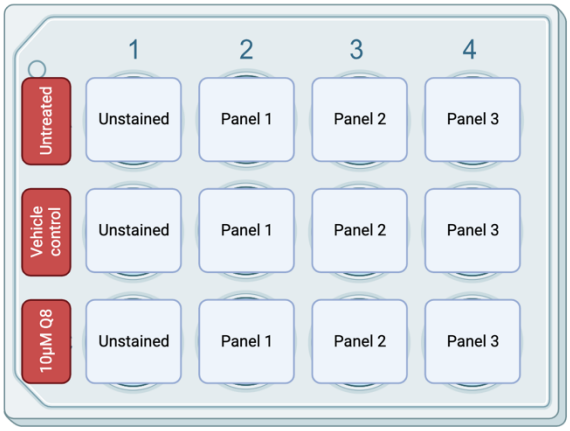

B

NK Receptor Screen on the KHYG-1 cell line

FITC	CD56	1ul		
PE	CX3CR1	1ul		
PE-Cy5	NKG2D	5ul	TIGIT	2ul
PE-Cy7	NKP46,	1ul		
APC	NKG2A,	2ul	TRAIL	1ul
APC-Cy7	CD3	1ul		
BV1	NKP30	1ul	FasL	1ul
BV2	CD69	1ul	CD62L	1ul

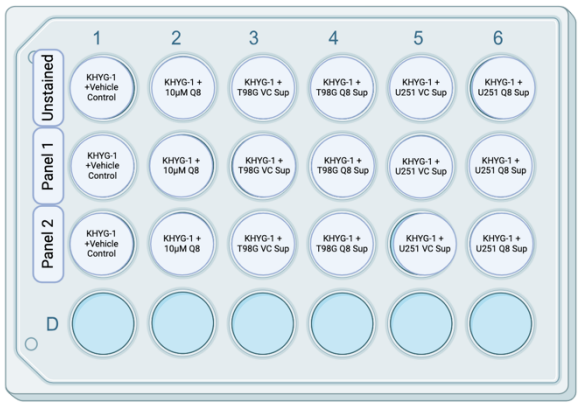

Figure 11: Plate plans for flow cytometry experiments to be performed as part of this research. (A) Schematic outlining the NKR ligand screen of T98G and U251 cells in response to Q8 with the accompanying panel design and fluorochromes used. **(B)** Schematic detailing the KHYG-1 NK receptor screen after direct treatment with the drug or various Q8-treated T98G and U251 cell line supernatants collected to elucidate the direct and indirect impact of Q8 on NK cell receptor expression and function.

Antibody	Type	Volume (µl)	Manufacturer	Catalogue No.
Nectin-1/PVRL1 FITC-conjugated	NKR Ligand	2.5	R&D Systems	FAB2880G
Nectin-4 PE-conjugated	NKR Ligand	2.5	R&D Systems	FAB2659P
CD137 (4-1BBL) PE-Vio 770 REAfinity	NKR Ligand	0.5	Miltenyi Biotec	130-119-153
ULBP-3 APC-conjugated	NKR Ligand	2.5	R&D Systems	FAB1517A
HLA-E FITC REAfinity	NKR Ligand	0.5	Miltenyi Biotec	130-117-549
B7-H6 PE-conjugated	NKR Ligand	2.5	R&D Systems	FAB7144P
MICA/B PE-Vio 770 REAfinity	NKR Ligand	2.5	Miltenyi Biotec	130-100-927
CD155/PVR APC REAfinity	NKR Ligand	0.5	Miltenyi Biotec	130-119-176
CD262 (DR5, TRAIL-R2) PE-conjugated	NKR Ligand	1	BioLegend	307405
CD56 FITC REAfinity	Surface	1	Miltenyi Biotec	130-114-552
CX3CR1 PE REAfinity	Surface	1	Miltenyi Biotec	130-122-912
CD314 (NKG2D) PerCP/Cyanine5.5-conjugated	Surface	5	BioLegend	320817
CD335 (NKp46) PE/Cyanine7-conjugated	Surface	1	BioLegend	331915
CD159a (NKG2A) APC REAfinity	Surface	2	Miltenyi Biotec	130-114-089
CD3 APC/Cyanine7-conjugated	Surface	1	BioLegend	300317

CD337 (NKp30) Brilliant Violet 421-conjugated	Surface	1	BioLegend	325227
CD69 Brilliant Violet 510-conjugated	Surface	1	BioLegend	310935
TIGIT (VSTM3) PerCP/Cyanine5.5-conjugated	Surface	2	BioLegend	372717
CD253 (TRAIL) APC conjugated	Surface	5	BioLegend	308209
CD178 (Fas-L) Brilliant Violet 421-conjugated	Surface	1	BioLegend	306411
CD62L Brilliant Violet 510-conjugated	Surface	1	BioLegend	304843

Table 1: Fluorochrome conjugated antibody panels used for extracellular staining of GBM cell lines and KHYG-1 NK cells for flow cytometric analysis.

2.7.2 Acquisition and analysis

Cells were acquired using the BD FACSCanto II system. The cell population were gated on using SSC-A and FSC-A. Single cells were gated within FSC-H and FSC-A. The compensation beads were used to compensate for spectral overlap. Unstained controls were used to distinguish positive and negative populations once acquisition began. Data was analysed using FlowJo Version 10 software.

2.8 Statistical analysis

Data was gathered and organised using Microsoft Excel. Statistical analysis was performed using GraphPad Prism 9.0. Individual statistical tests are detailed in each figure legend.

3. Results

3.1. Elucidating the anti-cancer potential of Q8 in GBM

3.1.1 Key angiogenic factors which are modulated by Q8 are associated with poorer patient outcomes in GBM.

Q8 is a CysLtR antagonist which elicits anti-angiogenic effects in a VEGF-independent manner. There is evidence to support that Q8 decreases the expression of pro-angiogenic factors in order to fulfil this mechanism (Butler et al., 2017). Using the online cancer database, cBioPortal.com, we performed univariate analysis of this large-scale GBM patient genomics data to elucidate whether key pro-angiogenic factors and signalling proteins downstream of CysLtR (and previously shown to be modulated by Q8 in other cancers) had altered expression in GBM patients with poorer outcomes. Similarly, we investigated if altered expression of CysLtR1 and CysLtR2 was associated with decreased overall and disease-free patient survival. There was no data available for the effect of altered CYSLTR1 gene expression on disease-free progression This analysis revealed that alterations in the gene expression of two such angiogenic factors were associated with lower survival in this GBM cohort.

Specifically, alterations in the ANGPT1 gene (which encodes the angiopoietin-1 ligand), and the CAPN2 gene encoding for calpain-2 (which is a downstream signalling molecule of CysLtR1 and who's upregulation is linked to increase aggressiveness of cancer cell migration and invasion, and chemosensitivity) were linked to poorer survival outcomes in GBM patients. In particular, alterations in the ANGPT1 gene, which plays a vital role in vascular development and angiogenesis, were found to be associated with both poorer overall survival [p=0.013, Figure 12A] and disease-free survival [p=0.0176, Figure 12A]. Mutation of ANGPT1 was primarily gene amplification with a small number of cases with missense mutations. Similarly, amplification and missense mutation of the calpain-2 gene were significantly associated with poorer disease-free survival [p=0.0236, Figure 12B]. No associations were identified between expression of TIE-2, CYSLTR1, or CYSLTR2 and survival in these GBM cohorts. Overall, this data indicates that angiogenic factors modulated by Q8 are linked with poorer survival in GBM and their modulation by Q8 in GBM might elicit anti-angiogenic and therapeutic utility.

A

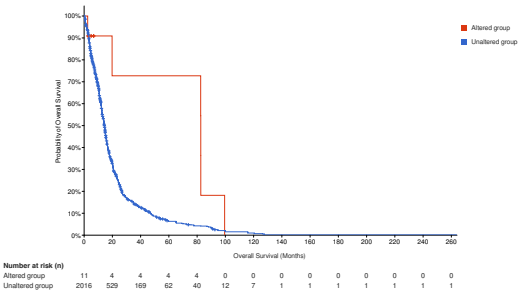

ANGPT1 Overall Survival (log-rank test, p=0.0139)

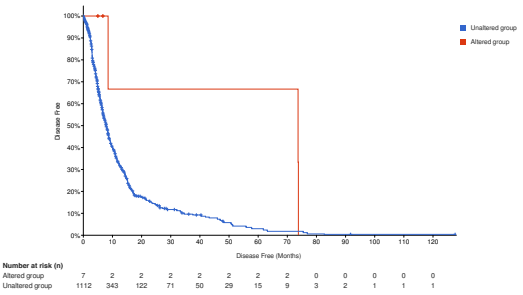

ANGPT1 Disease Free Survival (log-rank test, p=0.0176)

B

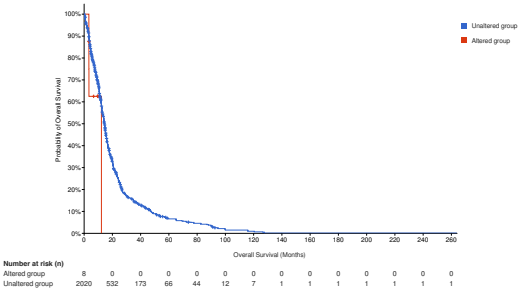

CAPN2 Overall Survival (log-rank test, p=0.238)

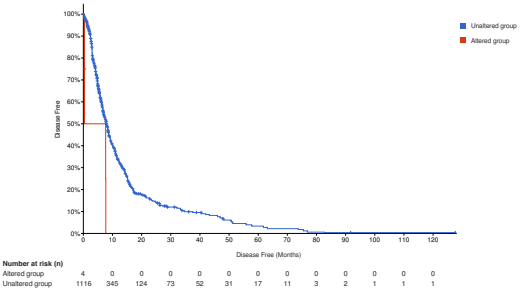

CAPN2 Disease Free Survival (log-rank test, p=0.0236)

C

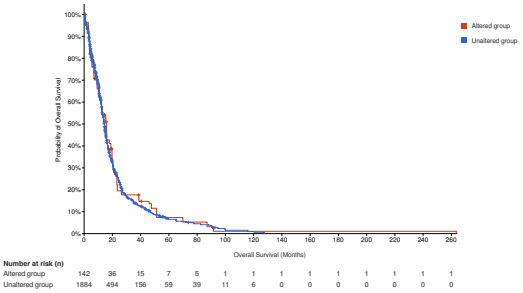

TIE-2/TEK Overall Survival (log-rank test, p=0.685)

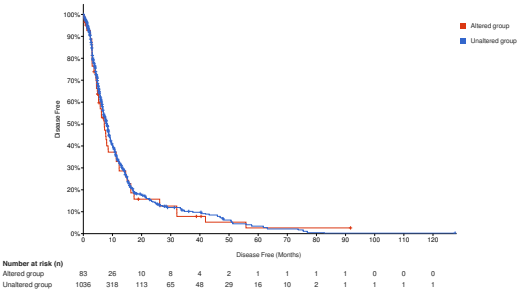

TIE-2/TEK Disease Free Survival (log-rank test, p=0.701)

D

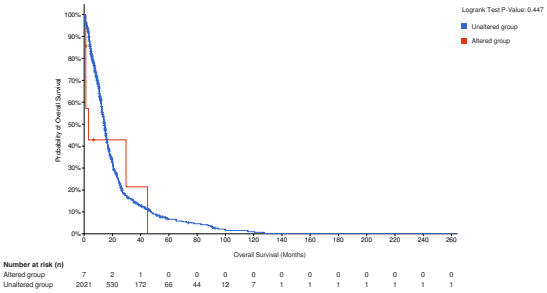

CYSLTR1 Overall Survival (log-rank test, p=0.447)

E

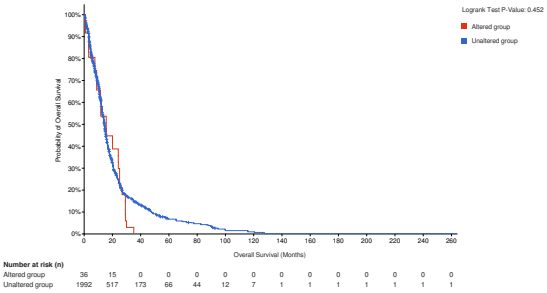

CYSLTR2 Overall Survival (log-rank test, p=0.452)

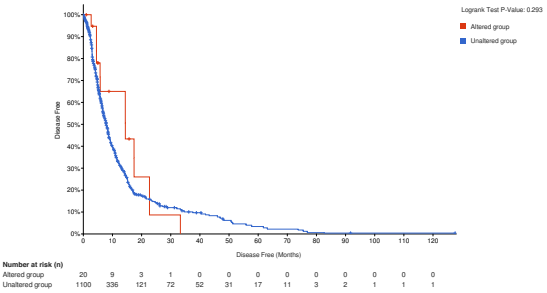

CYSLTR2 Overall Survival (log-rank test, p=0.293)

Figure 12: Alterations in expression of ANG1 and CAPN2 are associated with lower survival in Glioblastoma multiforme patients. Survival analysis with overall survival (left) and disease-free survival (right) data of 2241 samples from 2220 Glioblastoma patients with alterations in Angiopoietin-1 gene **(A)**, Calpain-2 gene **(B)**, TIE-2 gene **(C)**, CysLtR1 gene **(D)**, and CysLtR2 gene **(E)**, Log-rank test, *$p<0.05$.

3.1.2 The T98G and U251 GBM cell lines express the cysteinyl leukotriene receptor 1 (CysLtR1).

Q8 is an antagonist of its target receptor CysLtR1. To ensure that antagonism of CysLtR1 using Q8 was a viable approach for GBM and that we had selected appropriate cell line models, the T98G and U251 cell lines were screened for CysLtR1 using immunofluorescence microscopy. Hoechst was used as a nuclear stain, CD31 was used as a cell membrane marker to show cell morphology, and finally CysLtR1 allowed us to visualise receptor expression. These experiments showed that the receptor is abundantly expressed in both the T98G [57.58%, n=4, 312B] and U251 [54.95%, n=4, Figure 13B] cell lines. In fact, T98G cells express slightly but significantly more CysLtR1 than U251 cells [$p<0.001$, Figure 13B].

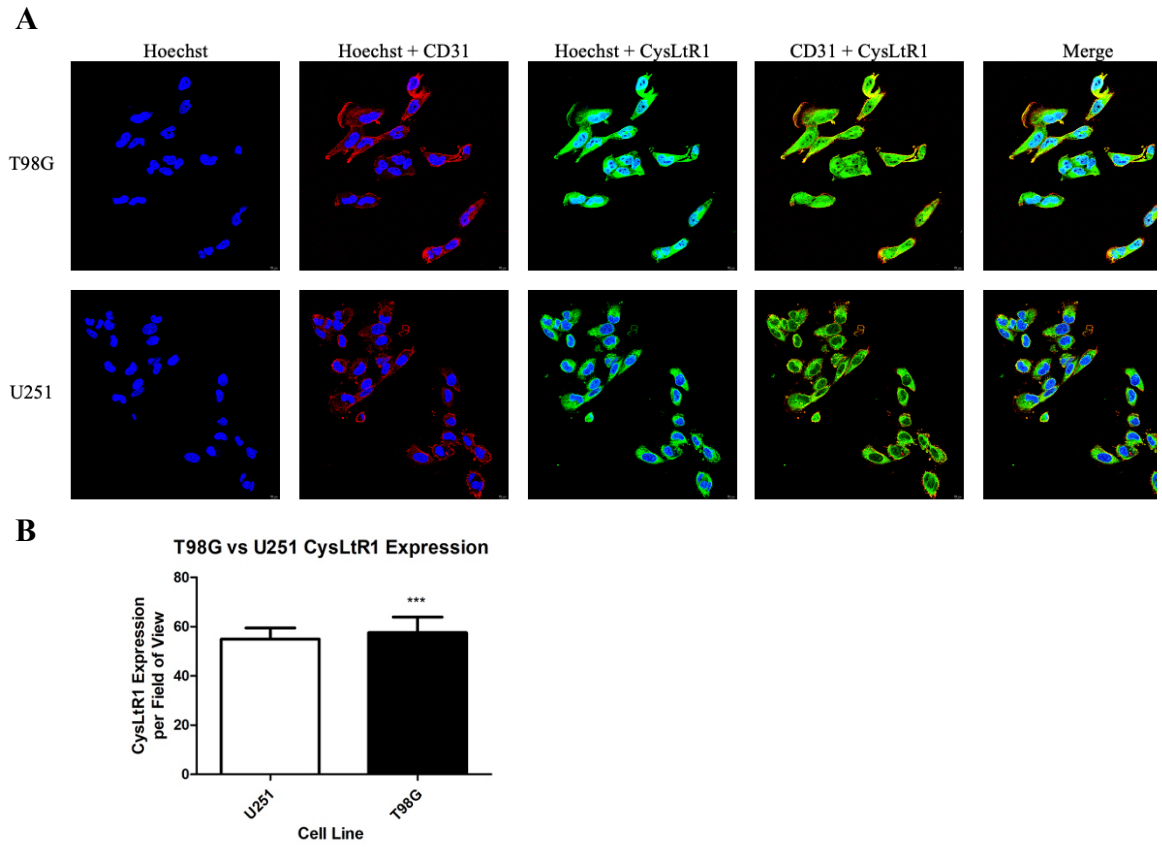

Figure 13: The T98G and U251 GBM cell lines abundantly express the CysLtR1 receptor. (A) Representative confocal images captured at x40 magnification displaying Hoechst (blue), CD31 (red), and CysLtR1 (green) immunostaining in the T98G and U251 cell lines. CysLtR1 is abundantly expressed in both cell lines, providing further rationale to the use of Q8 in GBM. Scale bar 10μm. **(B)** Bar graph representing CysLtR1 expression derived from their mean fluorescence intensity. A total of ten images were analysed per condition, each tested in duplicate. Semi-quantitative analysis of CysLtR1-associated fluorescence in GBM cells was conducted using ImageJ. Data presented as mean ± SEM, n=4, unpaired t-test with Welch's correction, ***$p < 0.001$.

3.1.3 Q8 reduces the viability of the U251 cell line and the T98G cell line following 48- and 72-hour treatments at high drug concentrations.

Following confirmation that CysLtR1 is expressed in the chosen cell lines, we investigated the effects of Q8 treatment on cell viability/survivability of U251 and T98G cells at various drug concentrations (1μM, 5μM, 10μM, 20μM, 50μM, 100μM, 200μM, and a vehicle control of 1% DMSO (v/v) in cell medium) and at various timepoints (24, 48, and 72 hours). MTT assay analysis showed that Q8 treatment elicits a dose-dependent effect on U251 cell viability [Figure 14B] but not T98G cell viability [Figure 15B] following 48- and 72-hour treatments. From this we further determined a clinical working concentration of 10μM-20μM of Q8 for 48 hours which will be used in subsequent experiments.

3.1.3.1 High dose Q8 reduces the viability of the U251 cell line following 48- and 72-hour treatments.

The viability of U251 cells was examined by MTT assay following 24-, 48-, and 72-hour treatments with various doses of Q8. Cell viability at each concentration was compared to the vehicle control. Following treatment for 24 hours there was no significance seen between treatment groups compared to vehicle control other than slight statistical significance at 200μM Q8 [Vehicle control (100%) vs 1μM (125.1%, p=0.2993) vs 5μM (138.14%, p=0.2461) vs 10μM (101.76%, p=0.9606) vs 20μM (123.81%, p=0.5181) vs 50μm (51.79%, p=0.1119) vs 100μM (42.21%, p=0.0995) vs 200μM (38.91%, p=0.0328), n=4, Figure 14B].

Similarly, there were no statistically significant changes in cell viability after 48-hour treatment at non-toxic concentrations, with significance being observed at doses over 50μM [Vehicle control (100%) vs 1μM (123.81%, p=0.3401) vs 5μM (102.14%, p=0.9257) vs 10μM (64.93%, p=0.17) vs 20μM (53.62%, p=0.0614) vs 50μM (8.98%, p=0.0001) vs 100μM (8.52%, p=0.0020) vs 200μM (6.25%, p=0.0017), n=4, Figure 14B].

Finally, after 72-hour treatment with Q8 no statistical significance was observed apart from high concentrations [Vehicle control (100%) vs 1μM (151.54%, p=0.2101) vs 5μM (117.75%, p=0.6889) vs 10μM (99.15%, p=0.9856) vs 20μM (76.36%, p=0.3647) vs 50μM (26.26%, p=0.06) vs 100μM (0.93%, p<0.0001) vs 200μM (0.42%, p<0.0001), n=4, Figure 14B].

When comparing the three timepoints with one another, at high concentrations of Q8, 48- and 72-hour treatments decrease cell viability significantly more than 24-hour

treatments [n=4, $p<0.0001$, Figure 14C]. However as stated these concentrations likely results in non-specific toxicity which is undesirable for therapeutic use.

A

24 hours

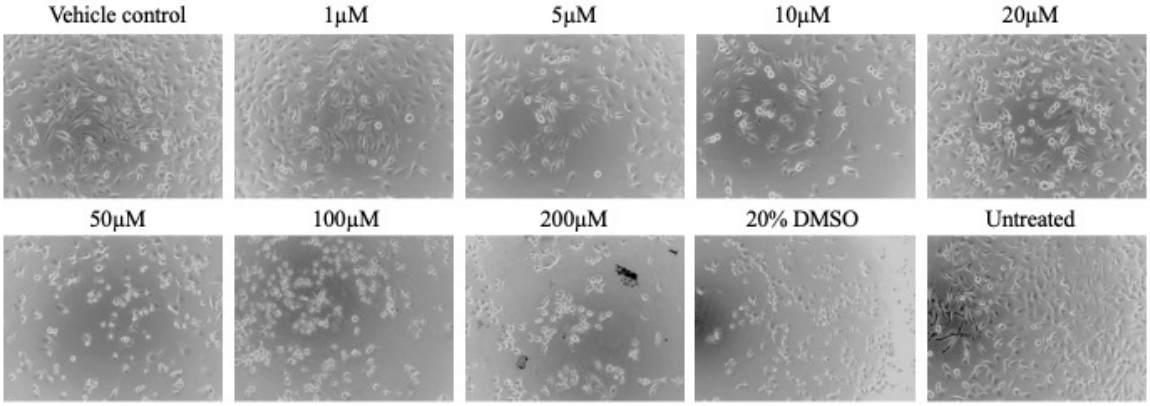

48 hours

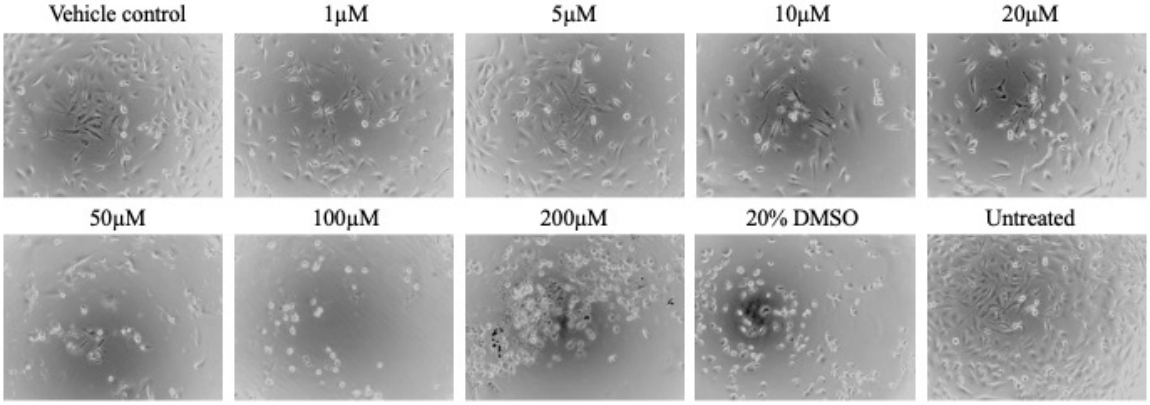

72 hours

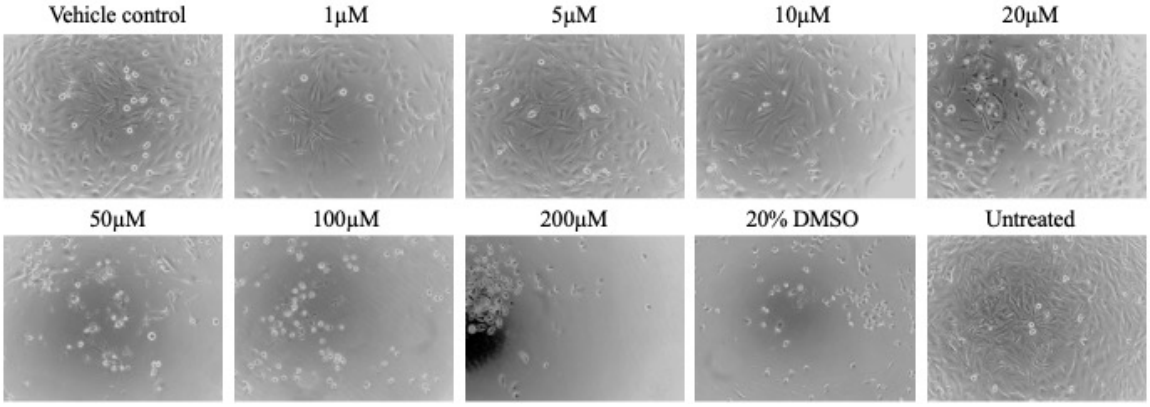

B

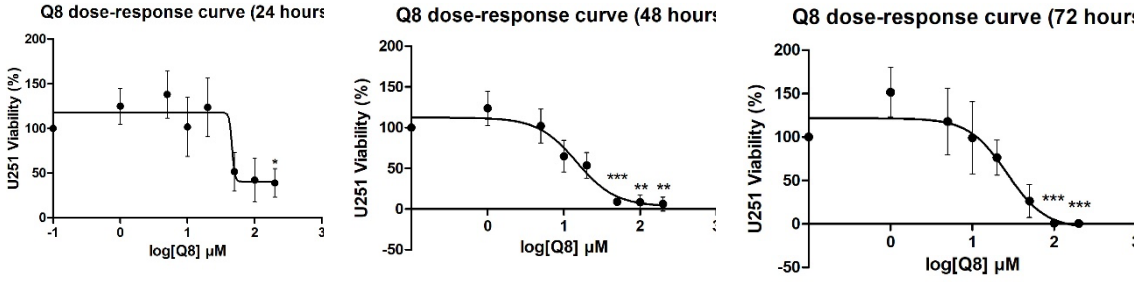

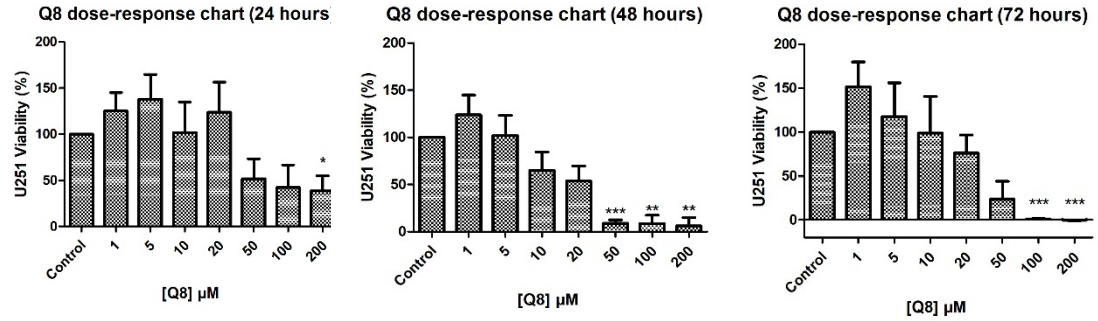

C

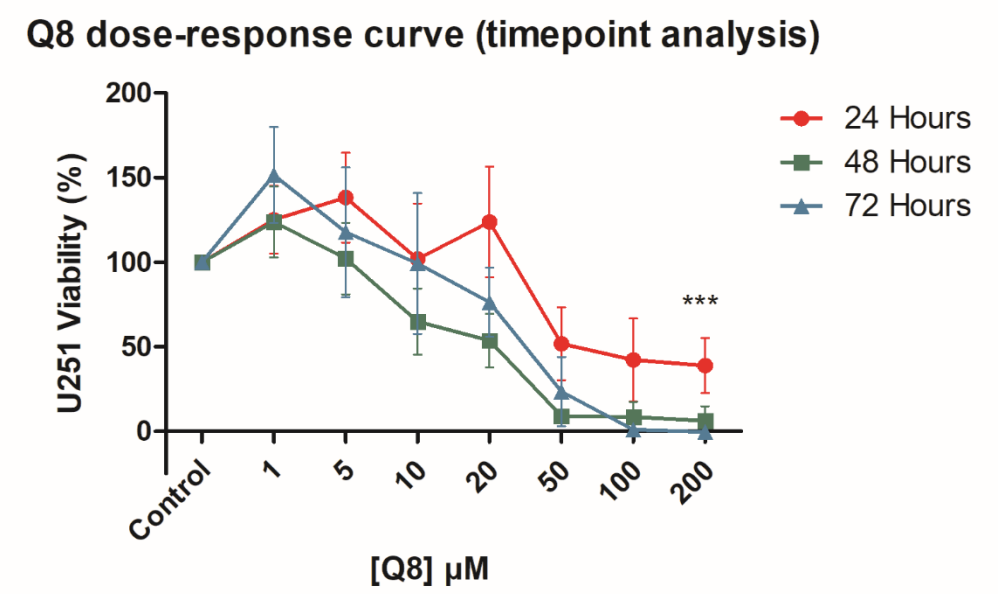

Figure 14: Q8 reduces U251 cell viability after 48- and 72-hour treatment. (A) Light \microscope representative images at x10 magnification of cells in their medium wells at different Q8 treatment concentrations, including a vehicle control and a 20% DMSO treatment. They show increased cell death as Q8 concentration is increased. **(B)** A dose-response curve of Q8 concentration effects on cell viability & bar chart representation of the dose-dependent effect of Q8 on cell viability. Data presented as mean ± SEM, n=4, paired t-test, *p<0.05. **(C)** A graphic representation comparing Q8 treatment at various concentrations across different timepoints. Data presented as mean ± SEM, n=4, two-way analysis of variance (ANOVA) with Bonferroni's ad hoc test, ***. $p < 0.0001$.

3.1.3.2 High dose Q8 reduces the viability of the T98G cell line following 24-, 48-, and 72-hour treatments.

The viability of the T98G cell line was examined by MTT assay following 24-, 48-, and 72-hour treatments with various doses of Q8. Cell viability at each concentration was compared to the vehicle control. Following 24-hour treatment with Q8, the effects on cell viability were not significant [Vehicle control (100%) vs 1μM (149.61%, p=0.2410) vs 5μM (158.31%, p=0.2065) vs 10μM (157.95%, p=0.315) vs 20μM (131.57%, p=0.2514) vs 50μm (94.4%, p=0.8622) vs 100μM (93.58%, p=0.8862) vs 200μM (78.64%, p=0.5008), n=4, Figure 15B].

When cells were treated for 48 hours, significance arose only at high Q8 concentrations over 100μM [Vehicle control (100%) vs 1μM (202.33%, p=0.2042) vs 5μM (177.13%, p=0.1386) vs 10μM (160.08%, p=0.1062) vs 20μM (141.73%, p=0.2521) vs 50μm (69.13%, p=0.1342) vs 100μM (31.21%, p=0.0158) vs 200μM (7.59%, p=0.003), n=4, Figure 15B].

Similar results were observed after 72-hour treatment, whereby effects on cell viability are observed at high doses (10μM is seen here as a statistical outlier) [Vehicle control (100%) vs 1μM (164.43%, p=0.1251) vs 5μM (265.73%, p=0.2483) vs 10μM (153.75%, p=0.0211) vs 20μM (182.41%, p=0.1077) vs 50μm (124.64%, p=0.7006) vs 100μM (18.76%, p=0.0531) vs 200μM (-8.71%, p=0.006), n=4, Figure 15B].

Similar to the U251 cell line results when comparing the three timepoints with one another, at high concentrations of Q8, 48- and 72-hour treatments decrease cell viability significantly more than 24-hour treatments [n=4, $p<0.0001$, Figure 15C].

A

24 hours

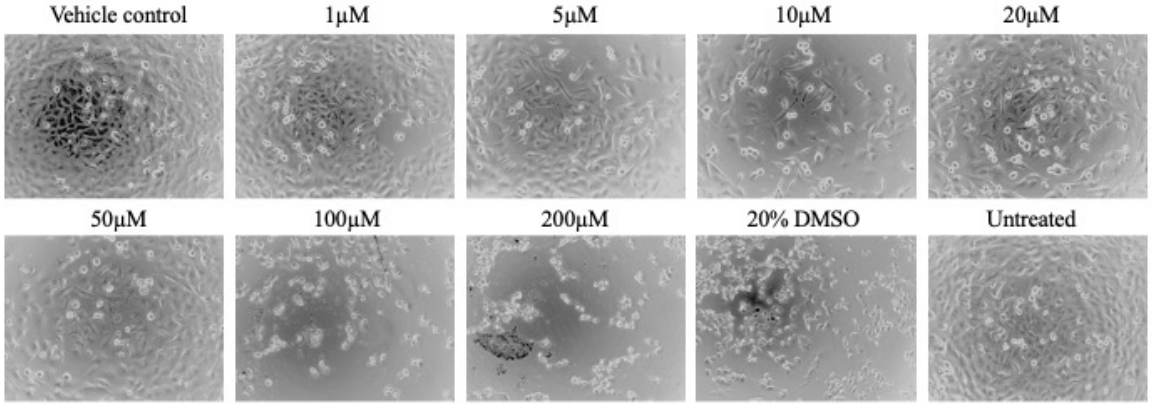

48 hours

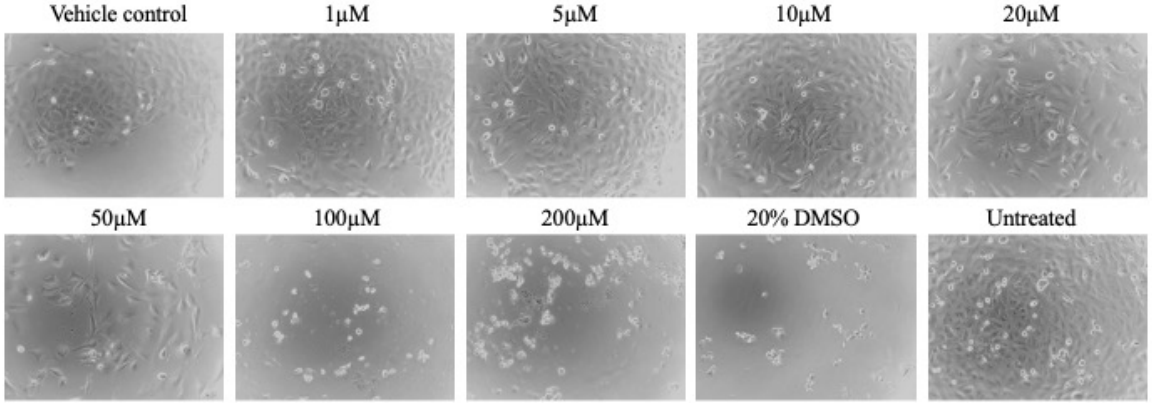

72 hours

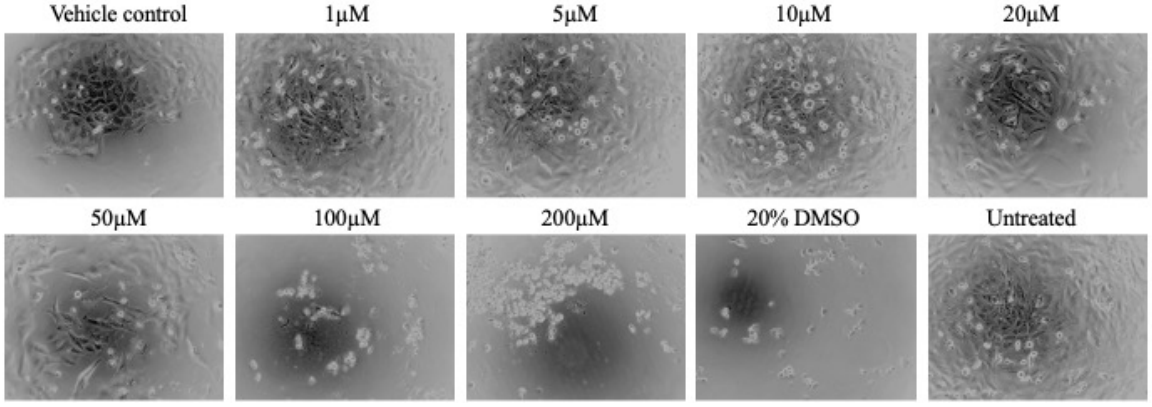

B

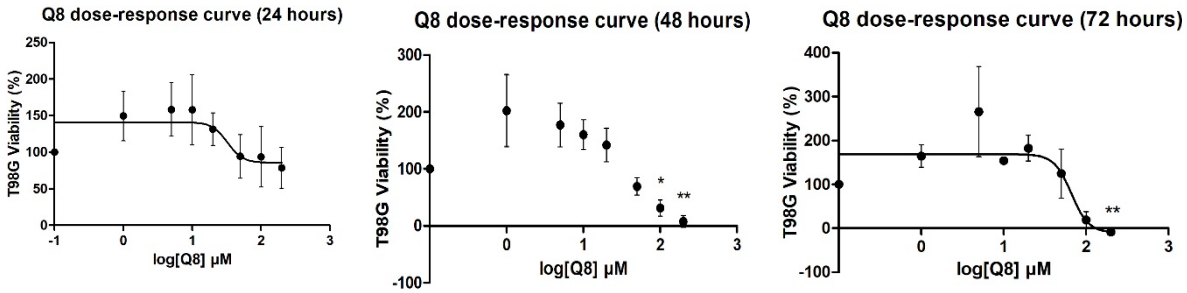

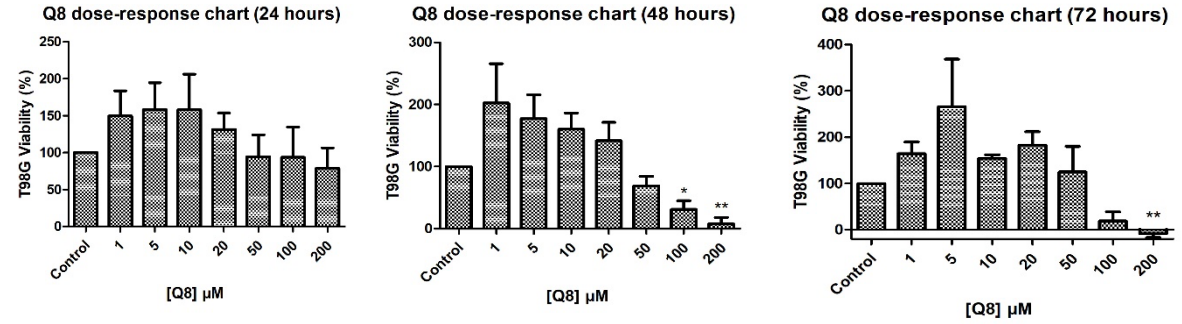

C

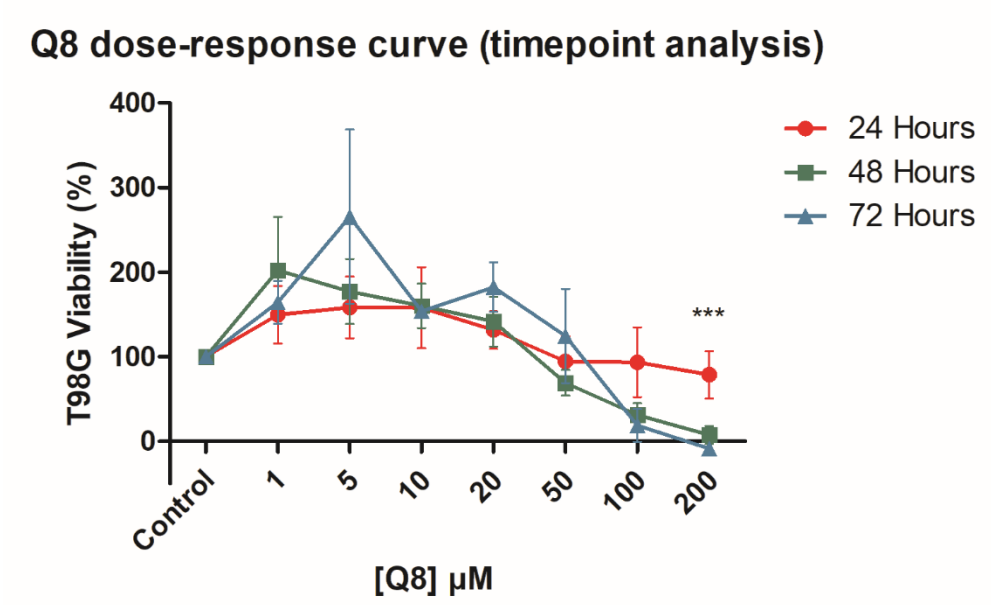

Figure 15: Q8 has little effect on T98G cell viability after any timepoints tested. (A) Light microscope representative images at x10 magnification of cells in their medium wells at different Q8 treatment concentrations, including a vehicle control and a 20% DMSO treatment. They show increased cell death as Q8 concentration is increased. **(B)** A dose-response curve of Q8 concentration effects on cell viability & bar chart representation of the dose-dependent effect of Q8 on cell viability. Data presented as mean ± SEM, n=4, paired t-test, *p<0.05. **(C)** A graphic representation comparing Q8 treatment at various concentrations across different timepoints. Data presented as mean ± SEM, n=4, two-way analysis of variance (ANOVA) with Bonferroni's ad hoc test, ***. $p < 0.0001$.

3.1.3.3 The effect of Q8 on cell viability was more significant in the U251 cell line versus the T98G cell line after 48-hour treatment.

The efficacy of Q8 in reducing cell viability was evident in both the U251 and T98G cell lines, however the results were significantly different between the two. After 24-hour treatment, there were no significant differences between the two cell lines [U251 vs T98G: 1μM (125.1% vs 149.61%, p=0.5577), 5μM (138.14% vs 158.31%, p=0.6694), 10μM (101.76% vs 157.95%, p=0.3725), 20μM (123.81% vs 131.57%, p=0.8506), 50μM (51.76% vs 94.4%, p=0.2897), 100μM (42.21% vs 93.58%, p=0.3255), and 200μM (38.91% vs 78.64%, p=0.2653), n=4, Figure 16A]. Similarly, after 72-hours no significant differences are seen [U251 vs T98G: 1μM (151.54% vs 164.43%, p=0.5577), 5μM (117.75% vs 265.73, p=0.6694), 10μM (99.15% vs 153.75%, p=0.3725), 20μM (76.36% vs 182.41%, p=0.8506), 50μM (26.26% vs 124.64%, p=0.2897), 100μM (0.93% vs 18.76%, p=0.3255), and 200μM (0.42% vs -8.71%, p=0.2653), n=4, Figure 16C]

Significant differences between the effects of Q8 on the two cell lines were observed following 48-hour treatment [U251 vs T98G: 1μM (123.81% vs 202.33%, p=0.2836), 5μM (102.14% vs 177.13%, p=0.1382), 10μM (64.93% vs 160.08%, p=0.0270), 20μM (53.62% vs 141.73%, p=0.0391), 50μM (8.98% vs 69.13%, p=0.0083), 100μM (8.52% vs 31.21%, p =0.2186), and 200μM (6.25% vs 7.59%, p=0.9242), n=4, Figure 16B]. This data indicates that the T98G cell line is less susceptible to the cell killing ability of Q8, which is in-keeping with its pre-known resistant properties when compared to the U251 cell line.

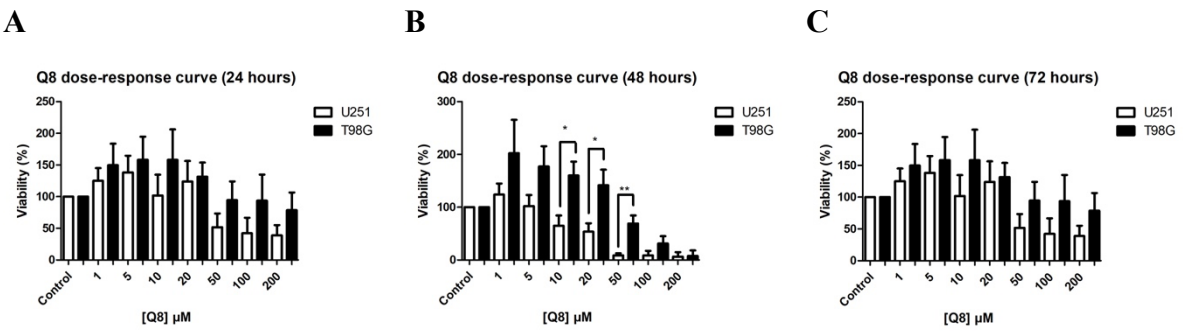

Figure 16: Q8 has a more significant affect in reducing U251 cell viability compared to the T98G cell line. Graphic representations comparing the U251 and T98G GBM cell line viability following treatment with Q8 for **(A)** 24-, **(B)** 48-, and **(C)** 72-hours. Data presented as mean ± SEM, n=4, unpaired t-test, ***p < 0.0001.

Taking all of this data into consideration, it was decided that subsequent experiments with Q8 treatment would focus on 48-hour timepoints at working concentrations of 10μM and 20μM. This decision was made based on visual and statistical evidence (visual reduction in cells and near statistical significance in reducing viability) as well as evidence from previous publications with which our findings are aligned.

3.2 Examining the biological effects of Q8 in GBM

3.2.1 Q8 modulates in vitro expression of key angiogenic and matrix remodelling mediators in the U251 cell line.

Having previously identified two target pro-angiogenic factors using cancer genomics data, immunofluorescence imaging was employed to elucidate changes in protein expression levels in the U251 and T98G cell lines in response to Q8 treatment. In addition to angiopoietin-1 and calpain-2, TIE-2 and MMP-1 were also identified as crucial factors involved in both vascular and extracellular matrix remodelling which greatly aid angiogenesis and invasion in GBM, and hence their protein expression was also examined in response to treatment.

Hoechst was used as a nuclear stain, CD31 and Collagen-IV were used as cell membrane markers to show cell morphology, and finally antibodies for each target mediator were used to visualise their expression. Working concentrations of 10μM and 20μM Q8 were compared to vehicle control expression after 48-hour treatment.

Q8 treatment of U251 cells caused significant changes to angiogenic and remodelling mediators. There was a significant increase of angiopoietin-1 expression in response to both 10μM [6.3443%, n=4, $p<0.0001$, Figure 17A] and 20μM [9.4801%, n=4, $p<0.0001$, Figure 17A] Q8 when compared to vehicle control [4.3122%, n=4]. Similarly, calpain-2 expression was increased in response to Q8 at both 10μM [2.949%, n=4, $p=0.0122$, Figure 17B] and 20μM [2.9163%, n=4, $p=0.014$, Figure 17B] concentrations compared to the vehicle control [2.5163%, n=4]. MMP-1 expression was modulated in response to 10μM [3.3494%, n=4, $p<0.0001$, Figure 17D] Q8 treatment compared to vehicle control [2.3794%, n=4] and 20μM [2.5325%, n=4, $p=0.7037$, Figure 17D]. Finally, 10μM Q8 caused a significant decrease in TIE-2 expression [3.5088%, n=4, $p<0.0001$, Figure 17C] compared to vehicle control [4.2437%, n=4] and 20μM [4.4697%, n=4, $p=0.4548$, Figure 17C] treatments. These data provide further evidence that Q8 increases angiopoietin-1 and MMP-1 in GBM cells and also show an induction of Calpain-2 by the drug in U251 cells, indicating its potential pro-angiogenic and pro-invasive effects on GBM cells and casting doubt on its anti-cancer clinical utility in GBM.

A

Angiopoietin-1

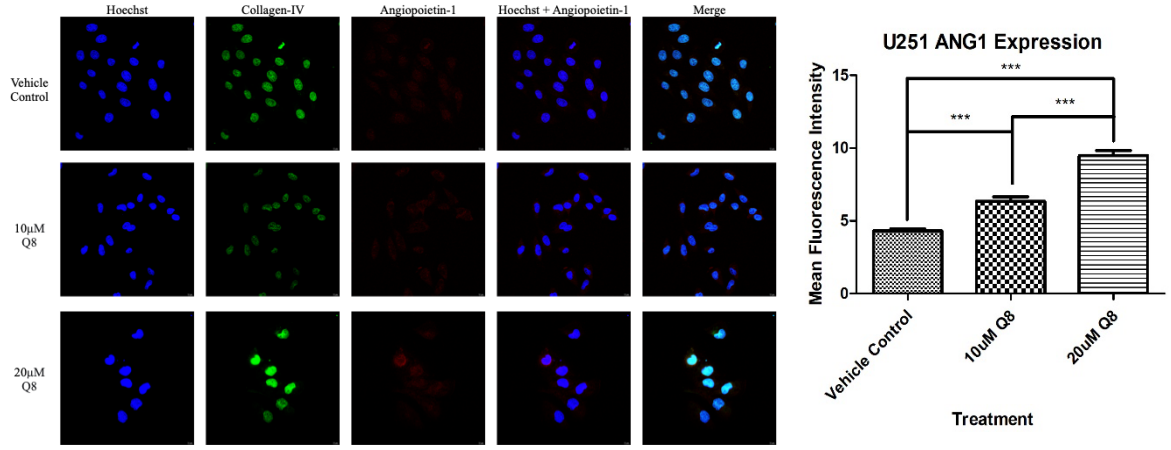

B

Calpain-2

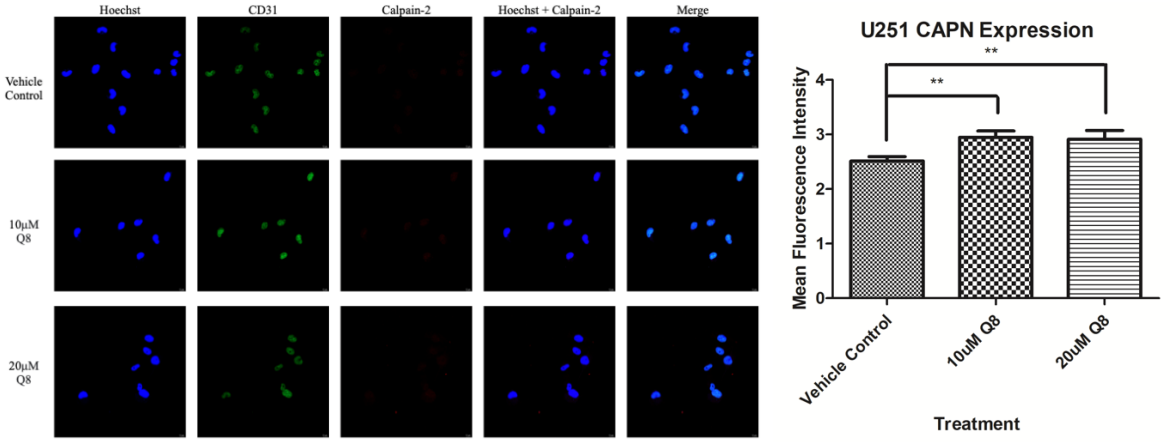

C

Tyrosine-protein kinase receptor TEK

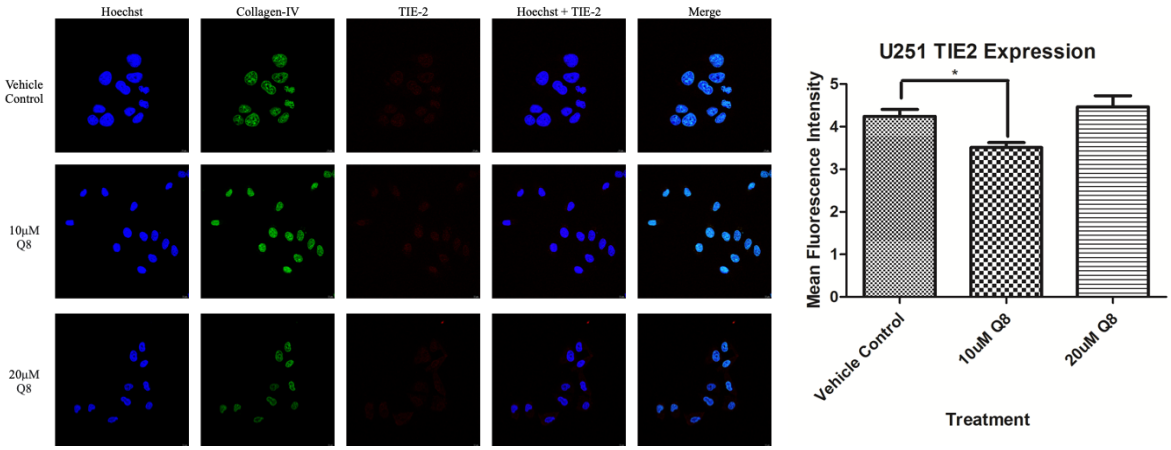

D

Matrix metalloproteinase 1

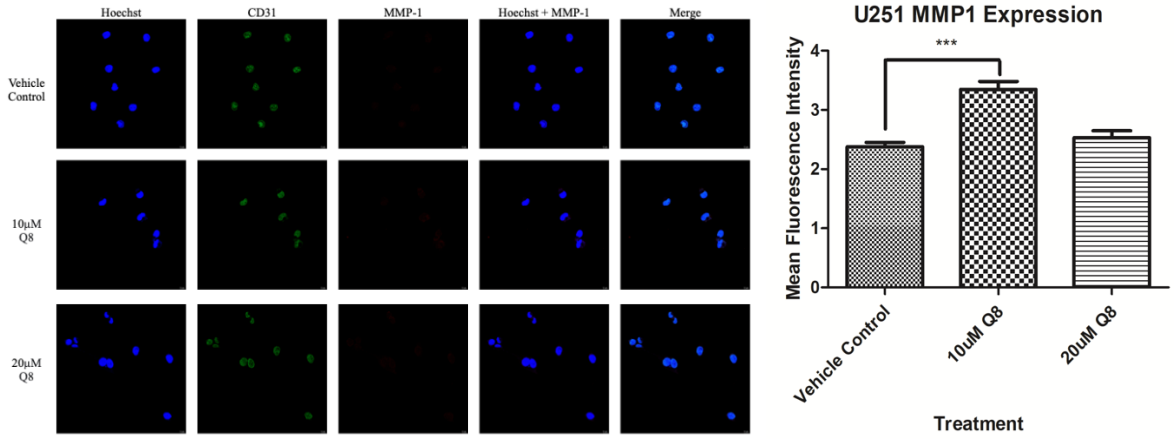

Figure 17: Angiogenic factor modulation in the U251 cell line in response to Q8 treatment. Representative confocal images captured at x40 magnification displaying Hoechst (blue), CD31 or collagen-IV (green), and **(A)** angiopoietin-1, **(B)** calpain-2, **(C)** TIE-2, and **(D)** MMP-1 (red) immunostaining in the U251 cell line. Accompanying bar graphs representing **(A)** angiopoietin-1, **(B)** calpain-2, **(C)** TIE-2, and **(D)** MMP-1 expression derived from their mean fluorescence intensity. A total of ten images were analysed per condition, each tested in duplicate. Semi-quantitative analysis of associated fluorescence in U251 cells was conducted using ImageJ. Data presented as mean ± SEM, n=4, one-way ANOVA with Bonferroni's ad hoc test, ***$p < 0.0001$.

3.2.2 Q8 modulates in vitro expression of key angiogenic and matrix remodelling mediators in the T98G cell line.

Angiogenic factor expression was also examined in the T98G cell line in the same fashion as the experiments described above.

Hoechst was used as a nuclear stain, CD31 and Collagen-IV were used as cell membrane markers to show cell morphology, and finally antibodies for each target mediator were used to visualise their expression. Working concentrations of 10μM and 20μM Q8 were compared to vehicle control expression after 48-hour treatment.

It was found that Q8 significantly modulates angiopoietin-1, calpain-2, and MMP-1 expression in the T98G cell line. There was a marked increase in angiopoietin-1 expression in response to both 10μM [12.4487%, n=4, $p<0.0001$, Figure 18A] and 20μM [11.8661%, n=4, $p<0.0001$, Figure 18A] when compared to vehicle control [7.8385%, n=4]. Similarly, there was a significant increase in MMP-1 at 20μM [2.8964%, n=4, $p=0.0047$, Figure 18D] Q8 treatment compared to both vehicle control [1.5524%, n=4] and 10μM [1.7096%, n=4, $p=0.2058$, Figure 18D] treatment. Finally, Q8 caused a decrease in calpain-2 expression at 20μM [1.8255%, n=4, $p<.0001$, Figure 18B] compared to vehicle control [2.2548%, n=4] and 10μM [2.4231%, n=4, $p=0.1852$, Figure 18B]. There were no significant changes observed to TIE-2 expression in response to Q8 treatment [Vehicle control (4.1729%) vs 10μM (4.0729%, $p=0.0516$) vs 20μM (4.4887%, $p=0.081$), n=4, Figure 18C]). These data suggest that Q8 increases angiopoietin-1 and MMP-1 in T98G while decreasing calpain-2. Such contrasting effects cast doubt on whether Q8 would have clinical utility in GBM owing to its pro-angiogenic and pro-invasive effects on GBM cells by inducing angiopoietin-1 and MMP-1, respectively. However, there is still a possibility that it would elicit some anti-angiogenic effects via decreasing calpain-2. Further studies are warranted to interrogate such effects.

A

Angiopoietin-1

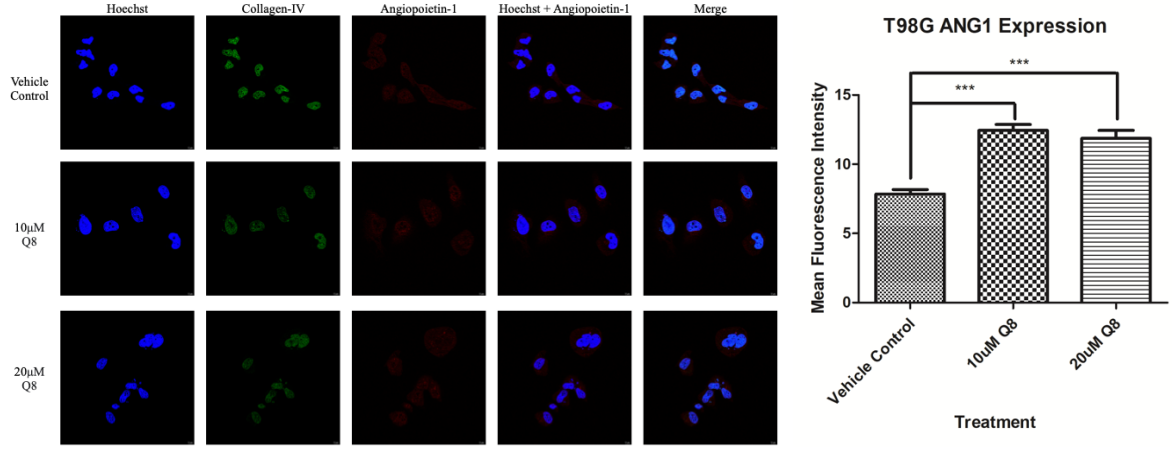

B

Calpain-2

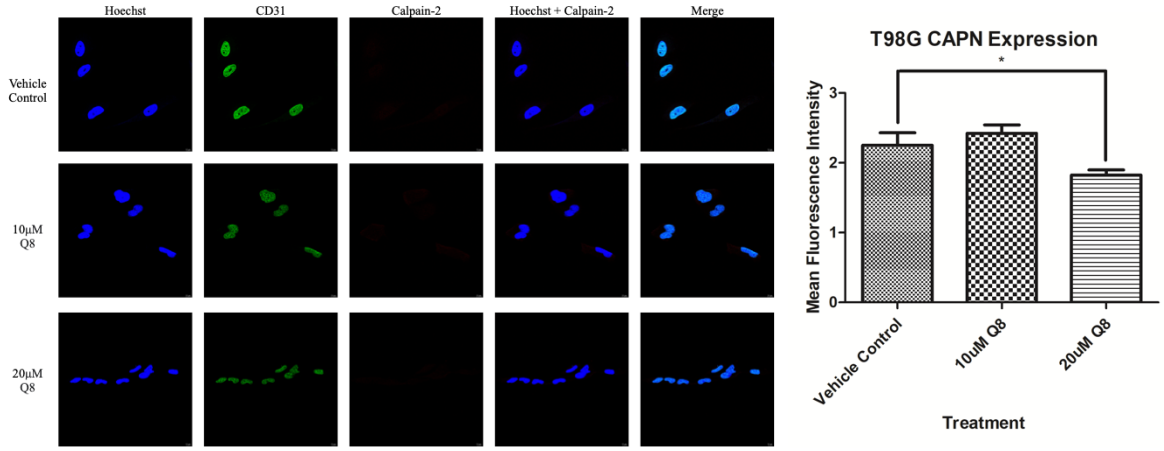

C

Tyrosine-protein kinase receptor TEK

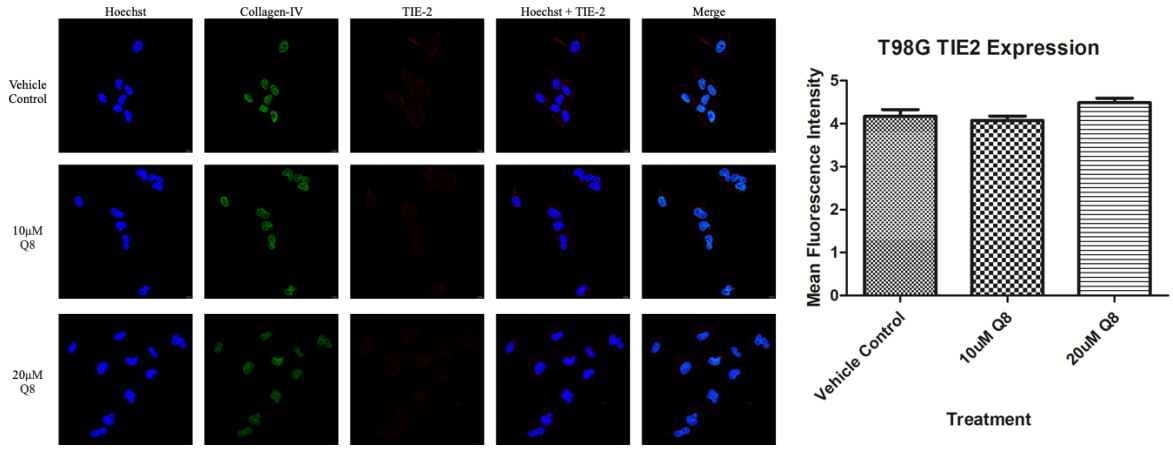

D

Matrix metalloproteinase 1

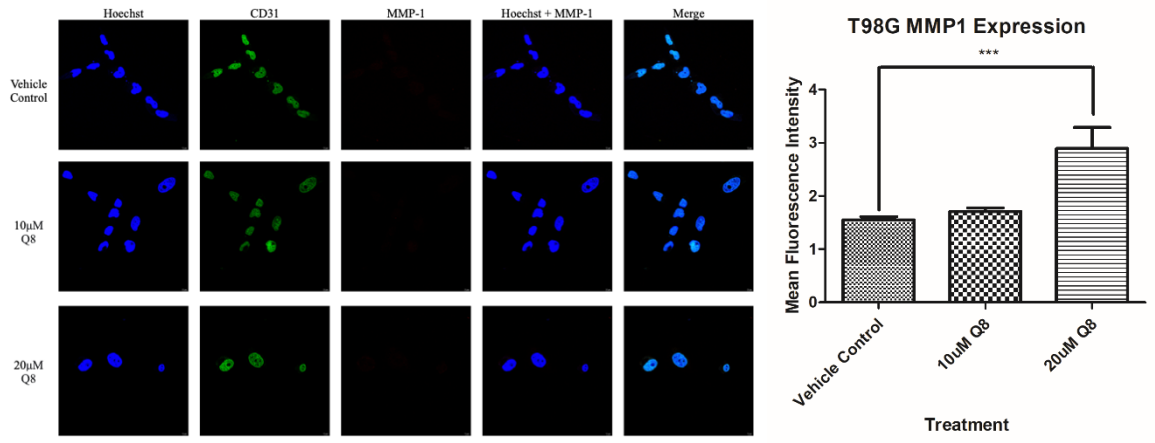

Figure 18: Angiogenic factor secretion is modulated in the T98G cell line in response to Q8 treatment. Representative confocal images captured at x40 magnification displaying Hoechst (blue), CD31 or collagen-IV (green), and **(A)** angiopoietin-1, **(B)** calpain-2, **(C)** TIE-2, and **(D)** MMP-1 (red) immunostaining in the T98G cell line. Accompanying bar graphs representing **(A)** angiopoietin-1, **(B)** calpain-2, **(C)** TIE-2, and **(D)** MMP-1 expression derived from their mean fluorescence intensity. A total of ten images were analysed per condition, each tested in duplicate. Semi-quantitative analysis of associated fluorescence in T98G cells was conducted using ImageJ. Data presented as mean ± SEM, n=4, one-way ANOVA with Bonferroni's ad hoc test, ***$p < 0.0001$.

3.2.3 Angiogenic and matrix remodelling factor expression differs significantly between the U251 and T98G lines prior to, and after, Q8 treatment.

As previously discussed, Q8 displays significant modulatory effects on the expression of key angiogenic factors in both the U251 and T98G cell lines. Comparatively, there is marked differences in the magnitude of this effect between our chosen cell lines. All comparisons presented as U251 vs T98G in the subsequent analysis.

Angiopoeitin-1 expression was shown to increase in response to Q8 across both cell lines, however these expression levels where much higher in the T98G model at baseline (4.3122% vs 7.8385%, $p<0.0001$), 10μM (6.3443% vs 12.4487%, $p<0.0001$), and 20μM (9.4801% vs 11.8661%, $p=0.0004$) of Q8 [n=4, Figure 19A]. Similarly, the expression of TIE-2 was significantly higher in the T98G model after treatment with 10μM Q8 compared to the U251 cell line (3.5088% vs %, $p=0.0004$). There was no significant difference between our chosen cell lines at baseline (4.2437% vs 4.1729%, $p=0.7510$) or 20μM Q8 (4.4697% vs 4.4887%, $p=0.9426$) [n=4, Figure 19B].

In contrast, expression levels of calpain-2 was markedly increased in the U251 cell line when compared to the T98G population at 10μM (2.949% vs 2.4231%, $p=0.0025$) and 20μM (2.9163% vs 1.8255%, $p<0.0001$), with no significance observed between the baseline of either group (2.5163% vs 2.2548%, $p=0.1298$) [n=4, Figure 19C]. Similarly, MMP-1 expression was significantly higher in the U251 cell line at baseline (2.3794% vs 1.5524%, $p<0.0001$) and 10μM (3.3494% vs 1.7096%, $p<0.0001$) treatment, but not at 20μM Q8 (2.5325% vs 2.8964%, $p=0.4141$) [n=4, Figure 19D]. This data strongly suggests a heterogeneity in the expression of angiogenic and remodelling mediators between our models, and eludes to differing levels of blood vessel formation which may infer some resistance to Q8 treatment.

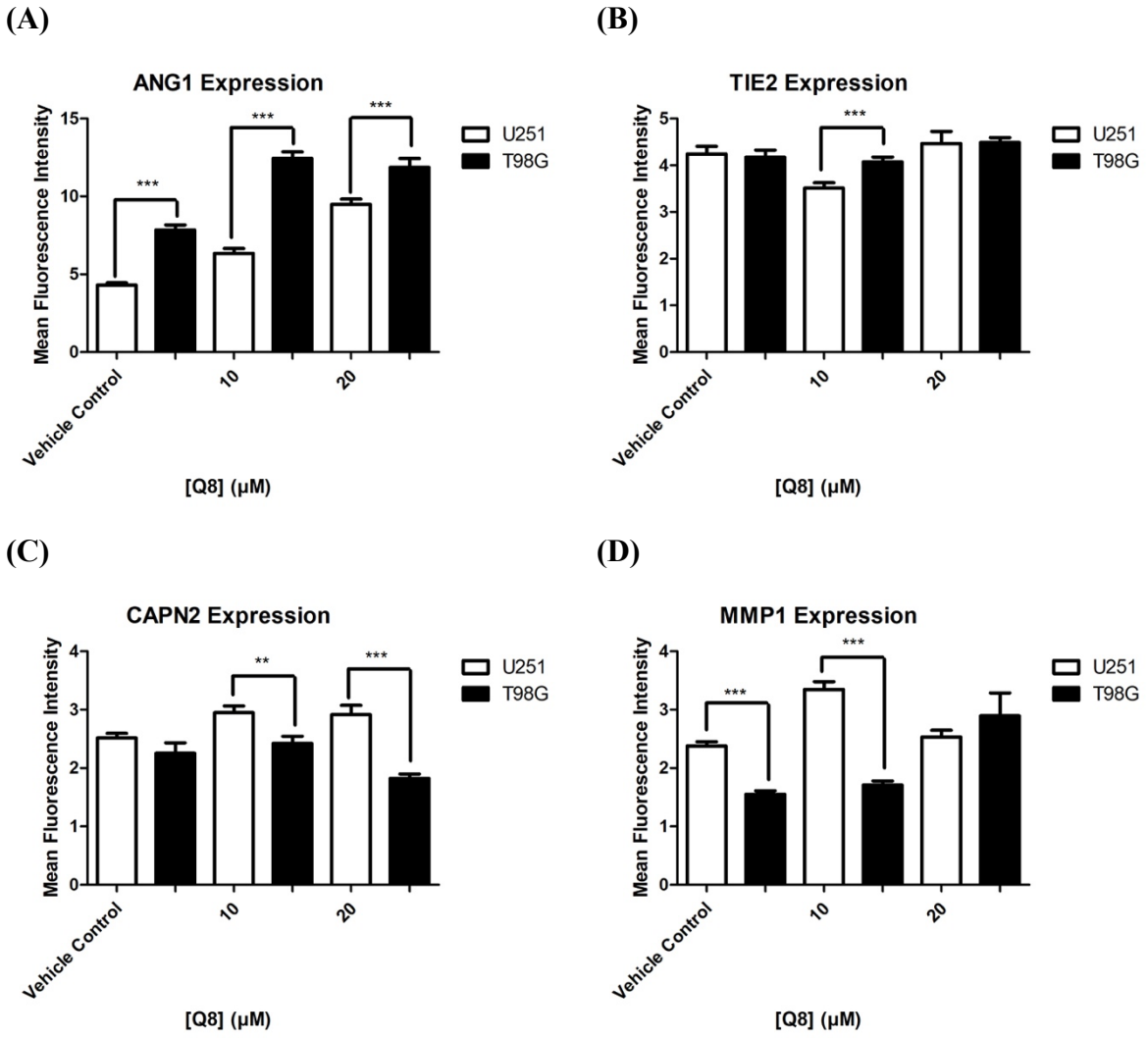

Figure 19: Q8 differentially modulates key angiogenic factors in the U251 and T98G GBM cell lines. Graphic representation comparing the expression of **(A)** angiopoietin-1, **(B)** TIE-2, **(C)** calpain-2, and **(D)** MMP-1 between the U251 and T98G cell lines, and the differing effects Q8 has on modulating such factors between these models. Data presented as mean ± SEM, n=4, unpaired t-test, ***$p < 0.0001$.

3.2.4 Q8 significantly modulates IL-2 and IFN-γ secretion in the U251 and T98G GBM cell lines.

The GBM microenvironment is functionally immunosuppressive, leading to altered immune activity and levels of major pro- and anti-inflammatory mediators. Marked increases in the production of cytokines like IL-6, IL-8, IL-10, and TGF-β hamper anti-tumour responses, including inhibition of IL-2 secretion and subsequent activation of T-cells and suppression of immune signalling markers such as IFN-γ and TNF-α (Razavi et al., 2016). Here, we measured relative cytokine/chemokine concentrations of Q8 treated U251 and T98G cell line supernatants to determine its modulatory effects. ELISA analysis of nine key analytes was conducted including IL-4, IL-6, IL-8, IL-17, CRP, TNF-α, and CD147. IL-2 concentrations were investigated as it is a key regulator in T cell infiltration and proliferation, and in induces potent NK cell anti-tumour activity (Chen et al., 2020). IFN-γ secretion was also interrogated as this mediator plays a crucial role in adaptive cellular immunity and stimulating host anti-tumour responses (Razavi et al., 2016). Due to technical issues, the standard curves for the IL-4, IL-8, IL-17, and CD147 ELISAs could not be used and hence data could not be analysed and were inconclusive.

Analysis of the U251 cell line showed an increase of IL-2 in response to 20μM [1.46pg/mL, $p<0.0001$, Figure 20A] Q8 compared to vehicle control [0.82pg/mL, n=4] and 10μM [0.0875pg/mL, n=4], and a marked decrease of IFN-γ at 10μM and 20μM [2.4pg/mL and 3.245pg/mL, n=4, $p<0.0001$, Figure 20A] Q8 treatments compared to the vehicle [8.062pg/mL, n=4]. There were no significant effects observed in secretion levels of IL-6 [Vehicle control (282.667pg/mL) vs 1μM (288.5pg/mL, p=0.8399) vs 5μM (272.667pg/mL, p=0.7418) vs 10μM (278.5pg/mL, p=0.9123) vs 20μM (273.5pg/mL, p=0.5766) vs 50μm (277.667pg/mL, p=0.8159) vs 100μM (267.667pg/mL, p=0.4626) vs 200μM (254.333pg/mL, p=0.1168), n=4, Figure 20A], CRP [Vehicle control (85pg/mL) vs 1μM (83.6667pg/mL, p=0.8325) vs 5μM (69.6667pg/mL, p=0.0575) vs 10μM (81.6667pg/mL, p=0.8111) vs 20μM (68pg/mL, p=0.0234) vs 50μm (72.6667pg/mL, p=0.0260) vs 100μM (89.3333pg/mL, p=0.7746) vs 200μM (75.6667pg/mL, p=0.3717), n=4, Figure 20A], or TNF-α [Vehicle control (248.75pg/mL) vs 1μM (253.75pg/mL, p=0.8367) vs 5μM (253.75pg/mL, p=0.8635) vs 10μM (298.75pg/mL, p=0.184) vs 20μM (237.083pg/mL, p=0.4422) vs 50μm (246.25pg/mL, p=0.9258) vs 100μM (253.75pg/mL, p=0.6697) vs 200μM (302.917pg/mL, p=0.33), n=4, Figure 20A].

Similarly, in the T98G cell line supernatants, IL-2 concentration was significantly increased at 20μM [56.93pg/mL, n=4, $p<0.0001$, Figure 20B] Q8 treatment compared to

vehicle control [4.465pg/mL, n=4] and 10μM [0.975pg/mL, n=4, Figure 20B] treatment. In contrast, IFN-γ production was diminished at both 10μM and 20μM [5.3pg/mL and 3.58pg/mL, n=4, $p<0.0001$, Figure 20B] treatments compared to vehicle control [6.495pg/mL, n=4]. There was no significant modulation seen in the concentrations of IL-6 [Vehicle control (320.167pg/mL) vs 1μM (331.833pg/mL, p=0.6496) vs 5μM (356pg/mL, p=0.2644) vs 10μM (325.167pg/mL, p=0.8337) vs 20μM (319.333pg/mL, p=0.986) vs 50μm (304.333pg/mL, p=0.6329) vs 100μM (316pg/mL, p=0.9506) vs 200μM (304.333pg/mL, p=0.79), n=4, Figure 20B], CRP [Vehicle control (68.6667pg/mL) vs 1μM (67.6667pg/mL, p=0.4778) vs 5μM (76.3333pg/mL, p=0.0341) vs 10μM (70pg/mL, p=0.4226) vs 20μM (75pg/mL, p=0.3261) vs 50μm (68pg/mL, p=0.8995) vs 100μM (76.6667pg/mL, p=0.0464) vs 200μM (76pg/mL, p=0.0785), n=4, Figure 20B], or TNF-α [Vehicle control (237.917pg/mL) vs 1μM (247.083pg/mL, p=0.3681) vs 5μM (237.083pg/mL, p=0.9139) vs 10μM (265.417pg/mL, p=0.0027) vs 20μM (267.083pg/mL, p=0.2607) vs 50μm (249.583pg/mL, p=0.3487) vs 100μM (272.917pg/mL, p=0.1122) vs 200μM (261.25pg/mL, p=0.1814), n=4, Figure 20B].

Overall, these data show that Q8 significantly increases IL-2 production by GBM cells which might elicit positive effects on immune cells such as NK cells, albeit there might also be activation of regulatory T cells by this cytokine. In contrast, the reduction of IFN-γ is likely to have deleterious effects on the anti-tumour immune response and this warrants further investigation to determine the overall immune-modulatory or immune activating properties of Q8.

A

U251

IL-2

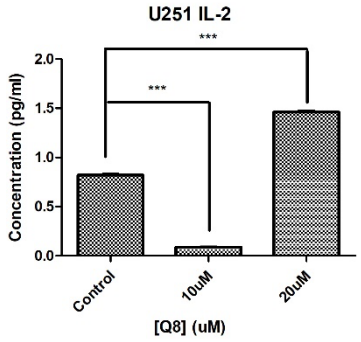

IFN-γ

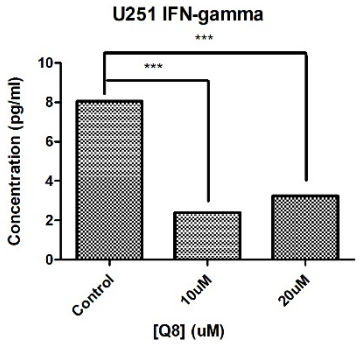

IL-6

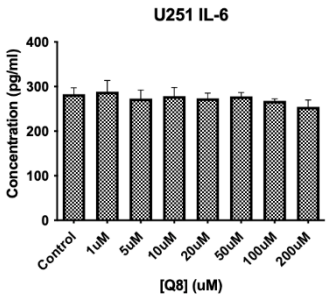

CRP

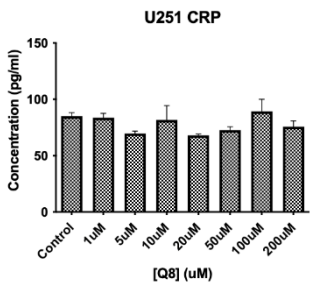

TNF-α

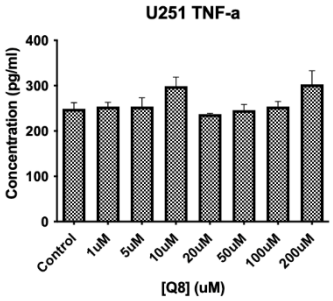

B

T98G

IL-2

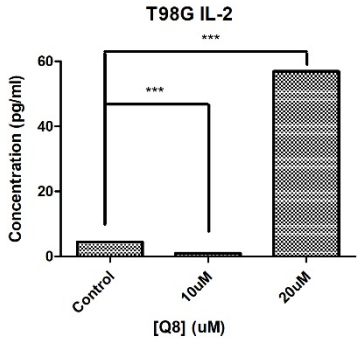

IFN-γ

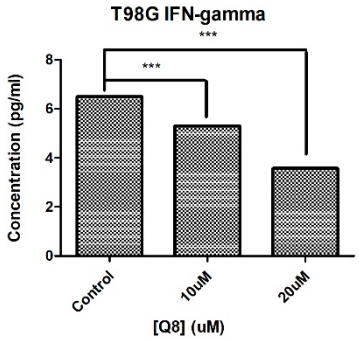

IL-6

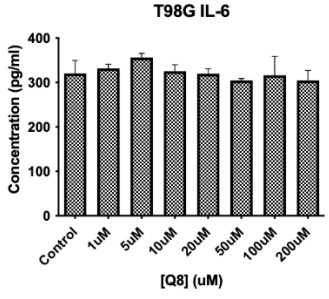

CRP

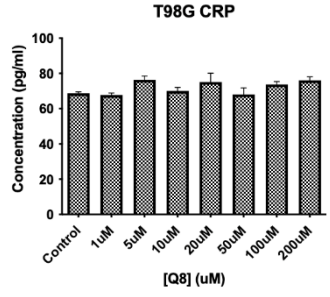

TNF-α

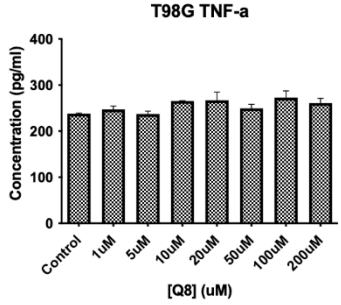

Figure 20: Q8 modulates IL-2 and IFN-γ release from U251 and T98G cells. Measuring cytokine and chemokine release from Q8 treated U251 and T98G cell line supernatants show significant immunomodulatory effects. The above graphs represent ELISA analysis performed on Q8 treated **(A)** U251 cell supernatants, and **(B)** T98G cell supernatants. Each condition was tested in duplicate, pooled supernatant n=4. Data presented as mean ± SEM, pooled supernatants n=4, one-way ANOVA with Bonferroni's ad hoc test, ***$p < 0.0001$.

3.2.5 The immunomodulatory effects of Q8 differ significantly between the U251 and T98G GBM cell lines.

Comparative analysis between the U251 and T98G cell lines revealed significant differences in cytokine and chemokine levels in their supernatant at baseline and in response to Q8 treatment. Most notably, IL-2 secretion was significantly higher in the T98G cell line at baseline (0.82pg/mL vs 4.465pg/mL, p=0.0001), 10μM (0.0875pg/mL vs 0.975pg/mL, p=0.001), and 20μM (1.46pg/mL vs 56.93pg/mL, p<0.0001) [n=4, Figure 21]. The concentration of IFN-γ varied slightly, with increased levels in the U251 cell line at baseline (8.062pg/mL vs 6.495pg/mL, p=0.0009), but higher levels were then observed in the T98G model at 10μM (2.4pg/mL vs 5.3pg/mL, p=0.0002) and 20μM (3.245pg/mL vs 3.58pg/mL, p=0.0064) treatment groups [n=4, Figure 21].

There were slight differences observed at specific concentrations between the cell lines in the expression of IL-6 [Vehicle control (282.667pg/mL vs 320.167pg/mL, p=0.3152), 1μM (288.5pg/mL vs 331.833pg/mL, p=0.1805), 5μM (272.667pg/mL vs 356pg/mL, p=0.0181), 10μM (278.5pg/mL vs 325.167pg/mL, p=0.1267), 20μM (273.5pg/mL vs 319.333pg/mL, p=0.0492), 50μm (277.667pg/mL vs 304.333pg/mL, p=0.0538), 100μM (267.667pg/mL vs 316pg/mL, p=0.3222), 200μM (254.333pg/mL vs 304.333pg/mL, p=0.1455), n=4, Figure 21] and CRP [Vehicle control (85pg/mL vs 68.6667pg/mL, p=0.0080), 1μM (83.6667pg/mL vs 67.6667pg/mL, p=0.0165), 5μM (69.6667pg/mL vs 76.3333pg/mL, p=0.0973), 10μM (81.6667pg/mL vs 70pg/mL, p=0.4187), 20μM (68pg/mL vs 75pg/mL, p=0.2442), 50μm (72.6667pg/mL vs 68pg/mL, p=0.39867), 100μM (89.3333pg/mL vs 76.6667pg/mL, p=0.2209), 200μM (75.6667pg/mL vs 76pg/mL, p=0.9557), n=4, Figure 21], There was no significant differences in TNF-α expression across either group [Vehicle control (248.75pg/mL vs 237.917pg/mL, p=0.4784), 1μM (253.75pg/mL vs 247.083pg/mL, p=0.6087), 5μM (253.75pg/mL vs 237.083pg/mL, p=0.4614), 10μM (298.75pg/mL vs 265.417pg/mL, p=0.1747), 20μM (237.083pg/mL vs 267.083pg/mL, p=0.1613), 50μm (246.25pg/mL vs 249.583pg/mL, p=0.8345), 100μM (253.75pg/mL vs 272.917pg/mL, p=0.3575), 200μM (302.917pg/mL vs 261.25pg/mL, p=0.2561), n=4, Figure 21].

IL-2 IFN-γ

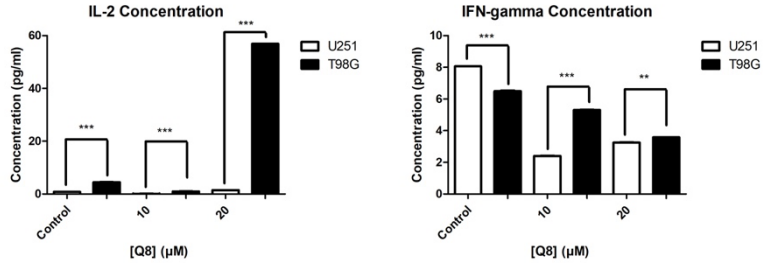

IL-6 CRP TNF-α

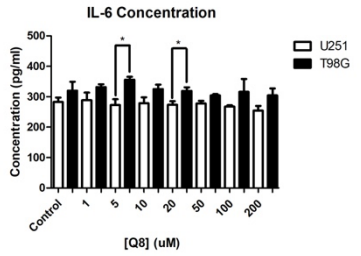

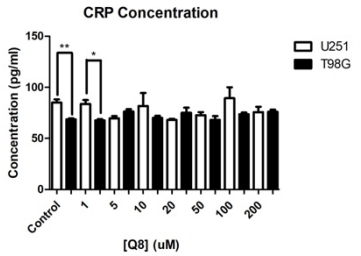

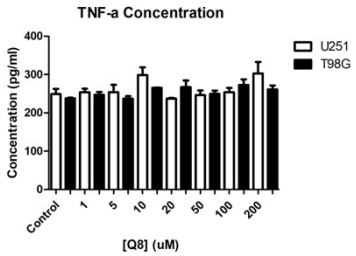

Figure 21: Q8 treatment significantly alters IL-2 and IFN-γ expression in the U251 and T98G cell lines, which differ significantly from one another. Comparing cytokine and chemokine release from U251 and T98G cell line supernatants show significant differences in **(A)** IL-2 and **(B)** IFN-γ between the two. Each condition was tested in duplicate, pooled supernatant n=4. Data presented as mean ± SEM, pooled supernatants n=4, unpaired t-test, ***$p < 0.0001$.

3.3 Investigating the effects of Q8 on susceptibility of GBM tumours to NK cells and NK cell therapy.

Here the effects of Q8 on NKR ligand surface expression by U251 and T98G cells was examined as a measure of how it might increase their susceptibility to NK cells and NK cell therapy. The direct and indirect effects of Q8 on NK cell phenotype was also examined using the NK cell therapy KHYG-1 to elucidate how this drug might directly impact the efficacy or function of NK cell therapy and how it might affect it within the context of the GBM tumour microenvironment. Gating strategies were generated to carry out flow cytometry experiments and are detailed in Figure 22.

1) U251 NKR Ligand Screen (Gating Strategy)

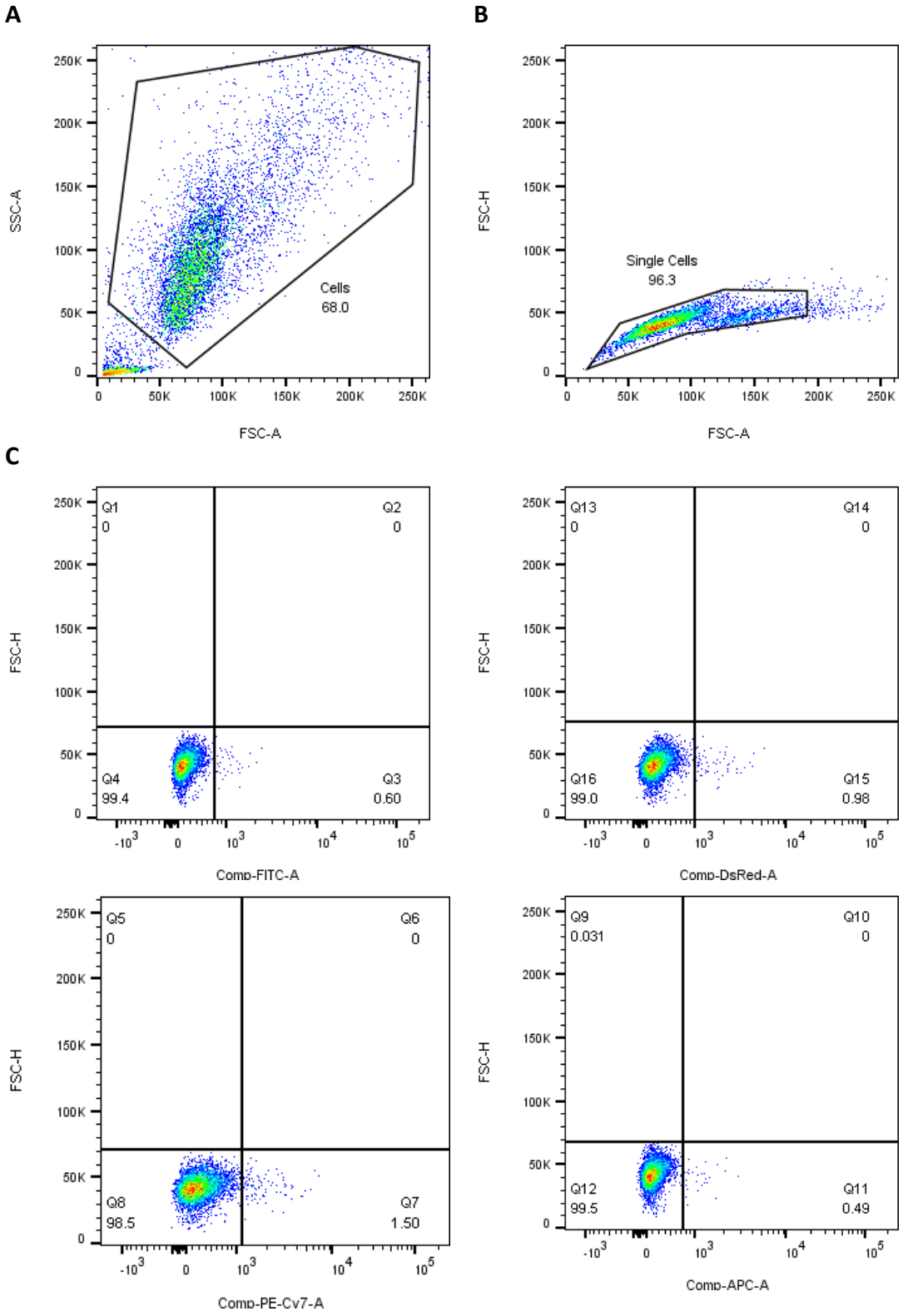

2) T98G and U251 NKR Ligand Response to Q8 (Gating Strategy)

A

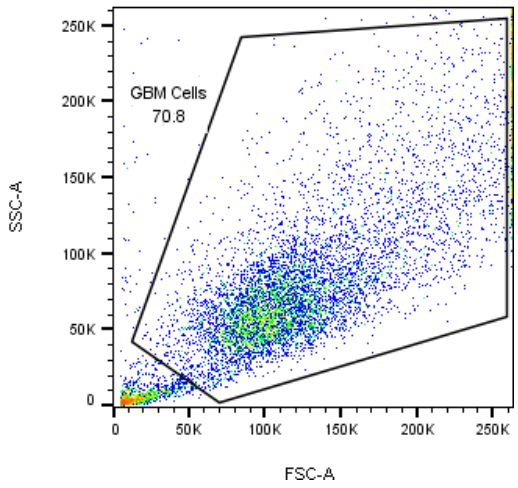

B

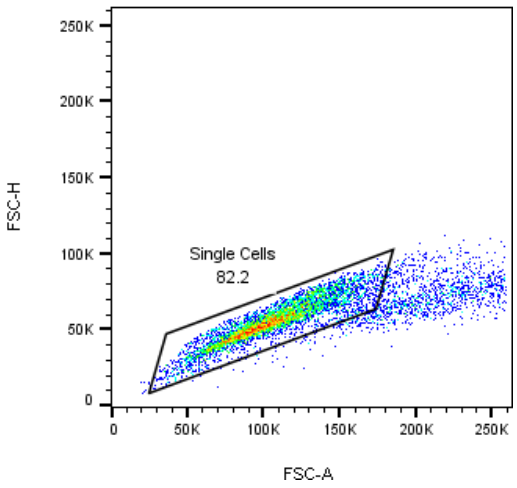

C

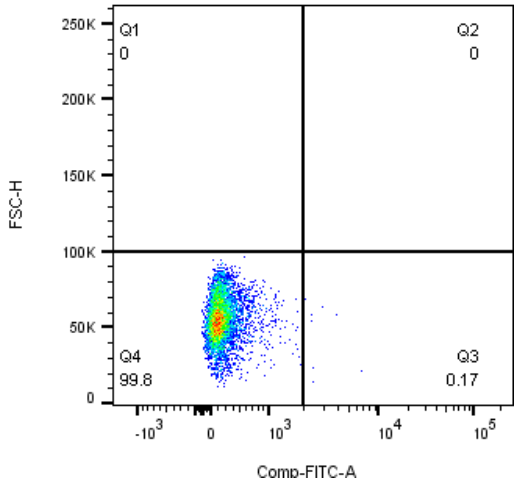

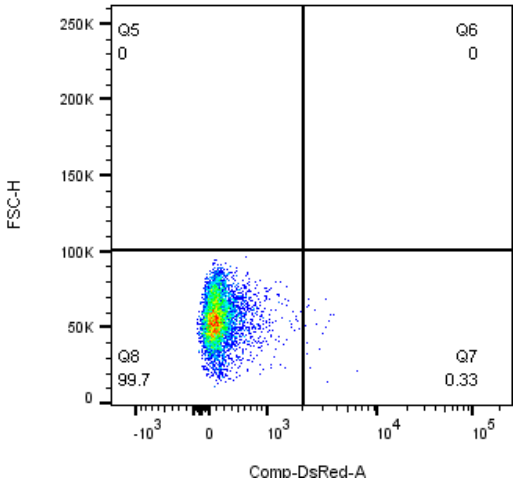

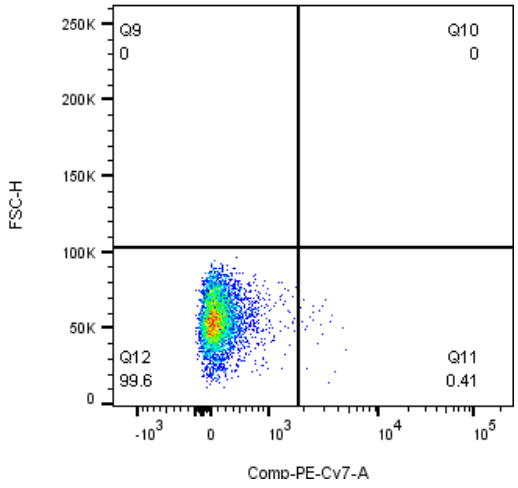

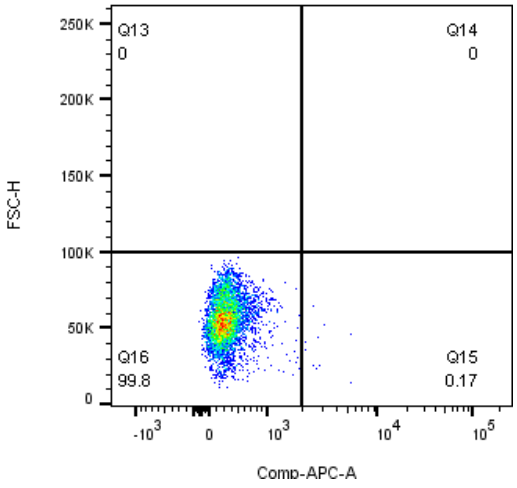

3) KHYG-1 NKR Screen (Gating Strategy)

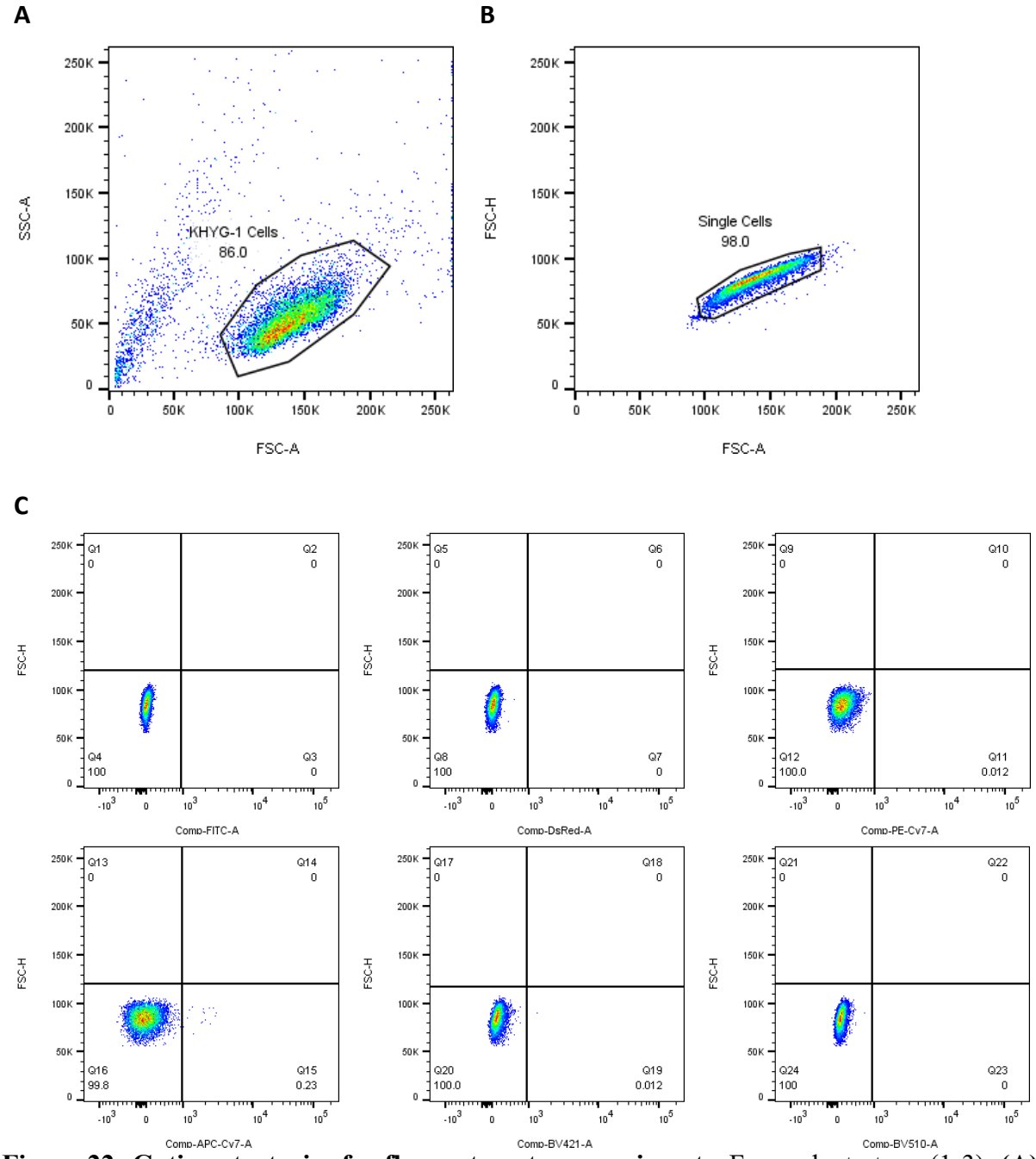

Figure 22: Gating strategies for flow cytometry experiments. For each strategy (1-3): **(A)** The target cell population was gated using the SSC-A and FSC-A: **(B)** Single cells were gated on FSC-H and FSC-A to eliminate doublet populations: **(C)** Unstained single cell populations (together with single stain compensation beads) were gated on for each fluorochrome, allowing identification of positive cells. Fluorochromes represent markers of interest are described in Figure 11A and Figure 11B.

3.3.1 U251 and T98G cell lines display heterogenicity in their NK receptor ligand surface expression profiles and Q8 elicits significant effects on these profiles.

In order to elucidate the potential effects of Q8 on NK cell function, both U251 and T98G cell lines were screened for their baseline expression of activating and inhibitory NK receptor (NKR) ligands. This would give us an idea of the balance of activating and inhibitory signals being elicited by these cancer cells and whether they are targetable by Q8. Furthermore, this would allow us to deduce the prominent pathways through which these cells activate NK cells and whether they are particularly inhibitory to NK cell function.

Here, we screened the U251 cell line to investigate the expression of the activating ligands 4-1BBL (90.8%), ULBP-3 (33.118%), B7-H6 (1.29%), MICA/B (9.3102%), and TRAIL-R2 (99.5%), and inhibitory ligands including PVRL1 (1.172%), PVRL4 (2.984%), HLA-E (3.942%), and CD155 (98.24%) [n=5, Figure 23B].

NK receptor ligand screen of the T98G cell line was performed previously for activating ligands including 4-1BBL (49%), ULBP-3 (19.525), B7-H6 (4.4%), MICA/B (54%), and TRAIL-R2 (92.575%), and inhibitory ligands including HLA-E (41.85%), and CD155 (85.625%) [n=5, Figure 23A].

Having characterised the NK receptor ligand profile for both cell lines, Q8 treatment was performed, and the expression profiles re-tested to quantify the modulatory effects of drug treatment on the ligands present on GBM cells, outlined in subsequent sections of this chapter.

A

U251

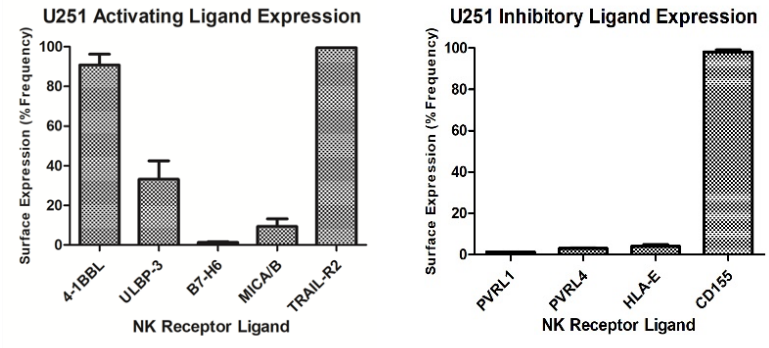

B

T98G

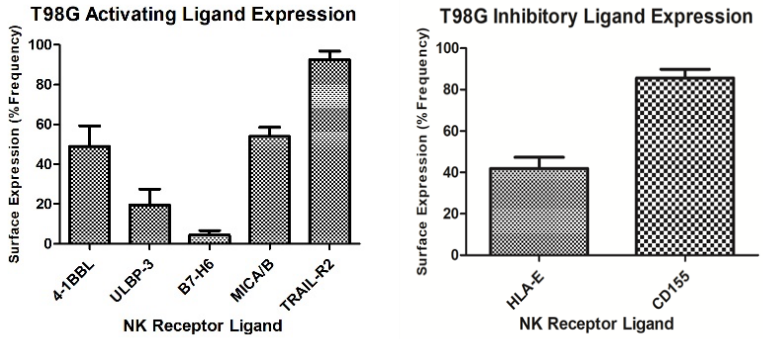

Figure 23: U251 and T98G GBM cell lines have differing NK receptor ligand profiles. Bar charts of % frequency by flow cytometric analysis representing the activating and inhibitory NKR ligands presented on the cell surfaces of the **(A)** U251 and **(B)** T98G GBM cell lines. Data presented as mean ± SEM, n=5.

3.3.2 Q8 treatment increases expression of the activating receptor ligands MICA/B and B7-H6 in the U251 cell line.

The surface expression of activating NKR ligands present on U251 cells was assessed after 48-hour treatment with 10μM of Q8. Flow cytometry analysis of % frequency showed that treatment with 10μM Q8, when compared to untreated and vehicle control groups, caused a significant increase in MICA/B [75.4% vs 19.0667% and 23.8333%, n=4, p= 0.0007, Figure 24A] and B7-H6 [16.9% vs 0.8475% and 0.89%, n=4, p<0.0001, Figure 24B] expression. There was no significant effect seen in expression of 4-1BBL [99.1% vs 92.6333% and 96.7667%, n=4, p=0.1018, Figure 24C], ULBP-3 [99.3667% vs 99.3333% and 99.3667%, n=4, p=0.9827, Figure 24C], or TRAIL-R2 [99.475% vs 99.35% and 99.275%, n=4, p=0.9706, Figure 24C].

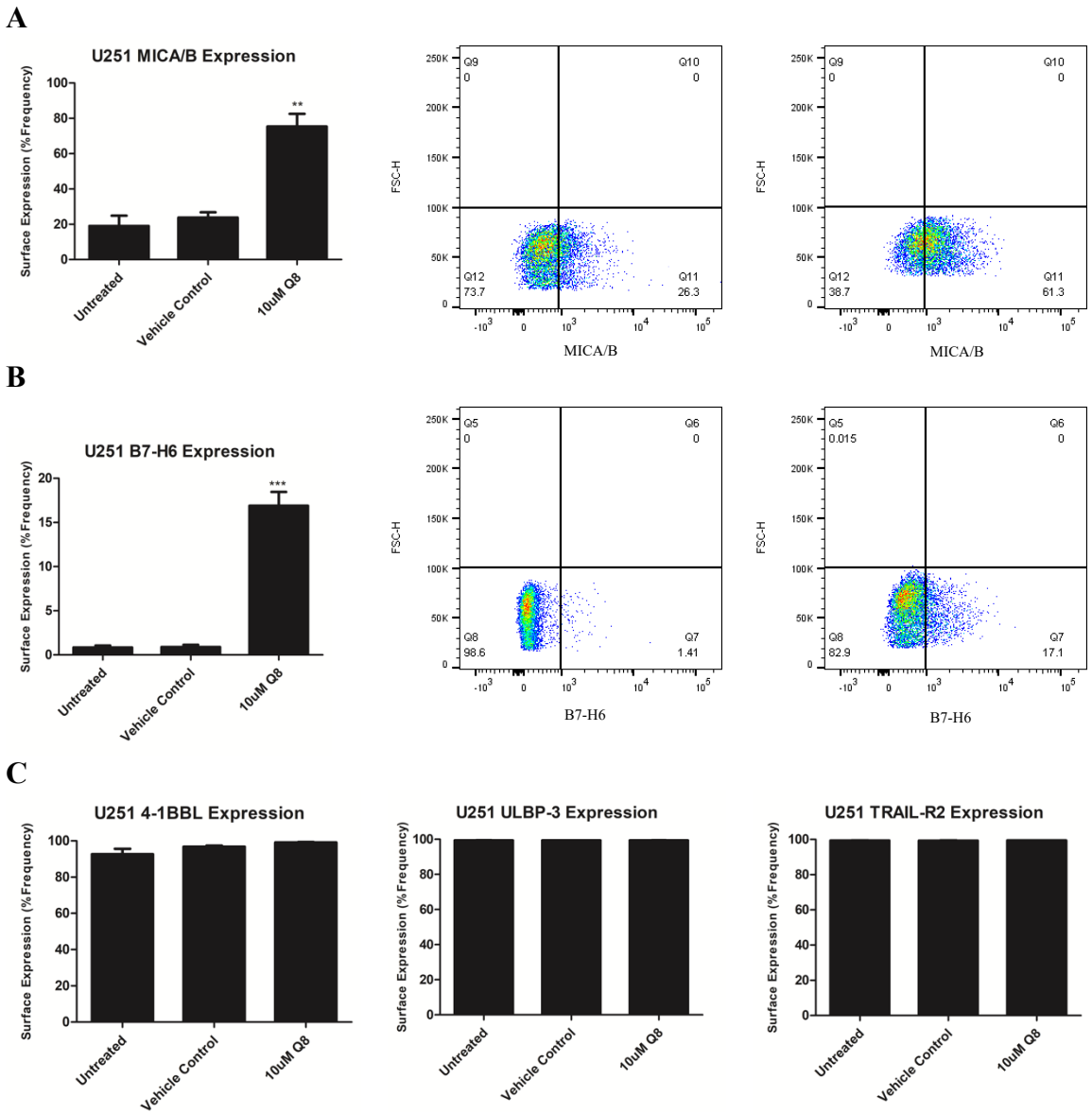

Figure 24: Q8 significantly altered the expression of activating ligands in U251 cells. Bar charts **(left)** of % frequencies representing relative NKR ligand expression of **(A)** MICA/B and **(B)** B7-H6 comparing untreated, vehicle control, and Q8 treated conditions with representative dot plots **(right)** of vehicle control and Q8 treatment groups. **(C)** Bar charts representing 4-1BBL, ULBP-3, and TRAIL-R2 expression which showed no significant change in response to Q8. Data presented as mean ± SEM, n=4, one-way ANOVA with Bonferroni's ad hoc test, ***$p < 0.0001$.

3.3.3 Q8 significantly modulates the expression of inhibitory NKR ligands in U251 cells.

The surface expression of inhibitory NKR ligands present on U251 cells was assessed after 48-hour treatment with 10μM of Q8. Flow cytometry analysis of % frequency showed that treatment with 10μM Q8 caused a significant increase in PVRL1 [24.3% vs 1.5825% and 2.1065%, n=4, $p<0.0001$, Figure 25A], PVRL4 [76.667% vs 30.7333% and 29.0333%, n=4, $p<0.0001$, Figure 25B], and HLA-E [11.35% vs 0.824% and 0.9575%, n=4, $p<0.0001$, Figure 25C] expression when compared to untreated and vehicle control groups. There was no significant effect seen in expression of CD155 [99.875% vs 99.925% and 99.95%, n=4, $p=0.8348$, Figure 25D].

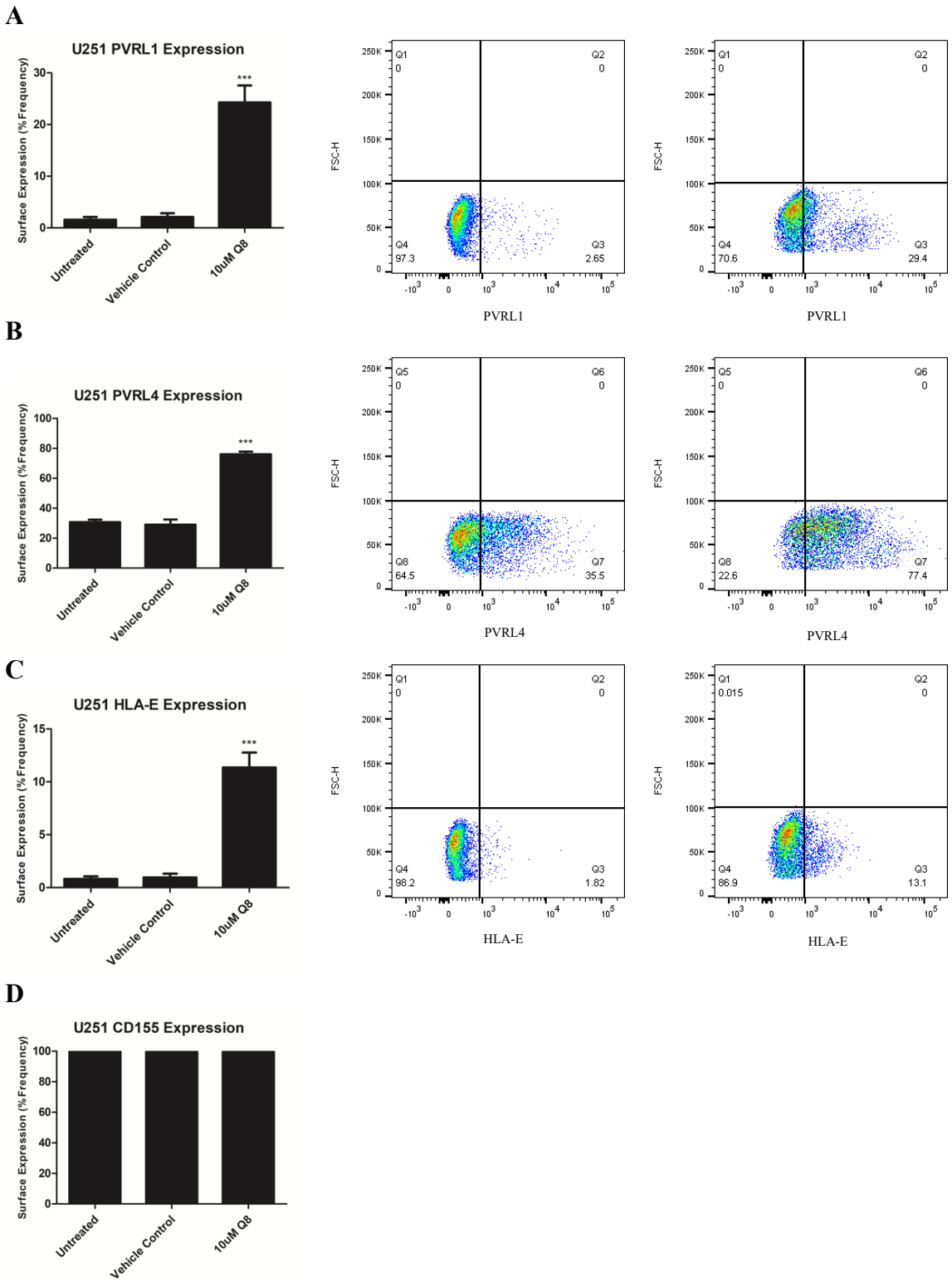

Figure 25: Q8 significantly alters inhibitory ligand expression in the U251 cell line. Bar charts **(left)** of % frequencies representing relative NKR ligand expression of **(A)** PVRL1, **(B)** PVRL4, and **(C)** HLA-E comparing untreated, vehicle control, and Q8 treated conditions with representative dot plots **(right)** of vehicle control and Q8 treatment groups. **(D)** Bar chart representing CD155 expression which showed no significant changes after treatment. Data presented as mean ± SEM, n=4, one-way ANOVA with Bonferroni's ad hoc test, ***$p < 0.0001$.

3.3.4 Q8 significantly increases expression of the activating NK receptor ligands 4-1BBL, B7-H6, and MICA/B in T98G cells.

The surface expression of activating NKR ligands present on T98G cells was assessed after 48-hour treatment with 10µM of Q8. Flow cytometry analysis of % frequency showed that treatment with 10µM Q8, when compared to untreated and vehicle control groups, caused a significant increase in 4-1BBl [95.9% vs 64.1% and 64.7667%, n=4, p=0.0213, Figure 26A], B7-H6 [24.2667% vs 1.665% and 3.9533%, n=4, p=0.0015, Figure 26B], and MICA/B [73.7333% vs 1.665% and 3.9533%, n=4, p<0.0001, Figure 26C]. There was no significant effect seen in expression of ULBP-3 [76.5% vs 71.5% and 60%, n=4, p=0.7117, Figure 26D] or TRAIL-R2 [99.075% vs 99.275% and 99.2%, n=4, p=0.9682, Figure 26D].

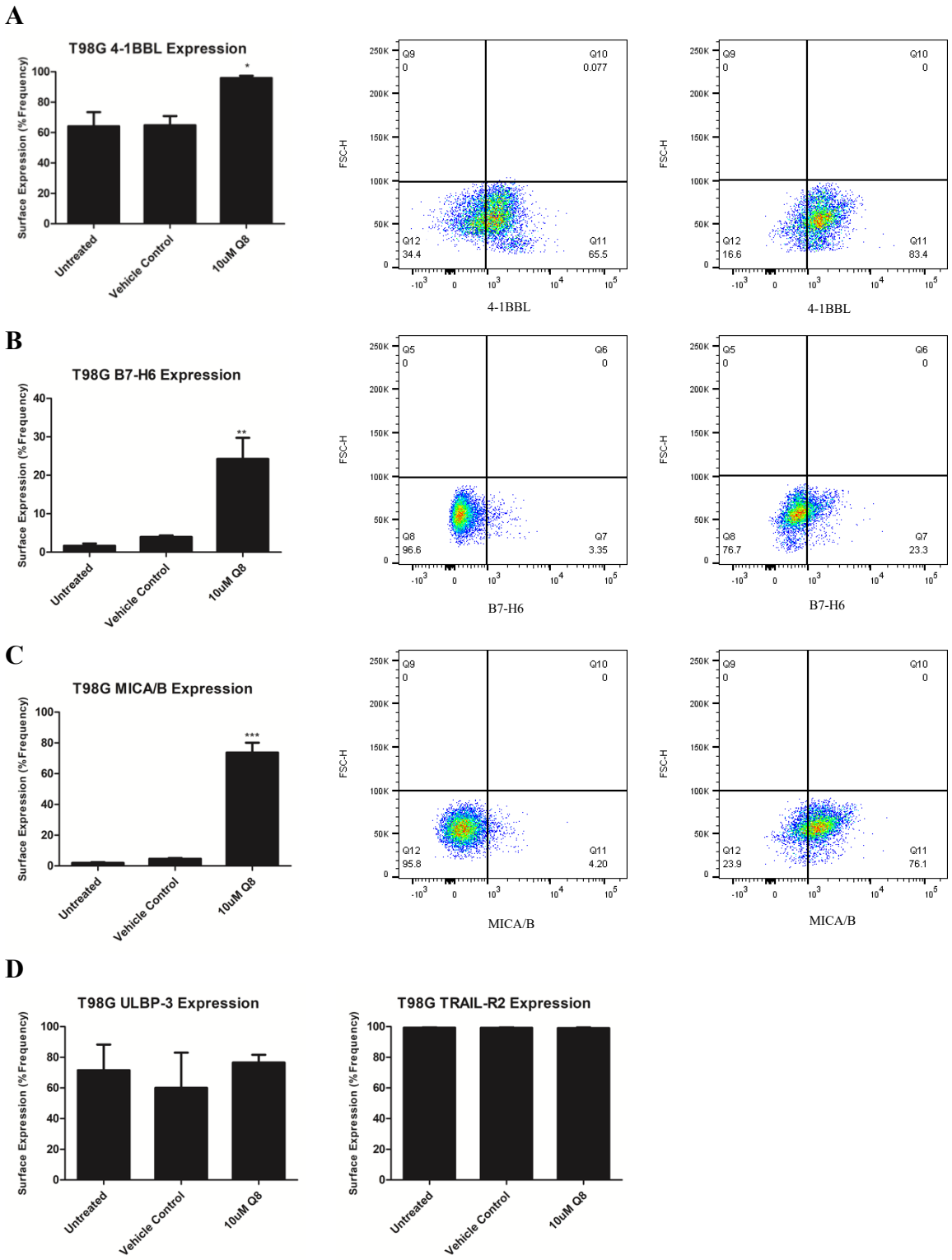

Figure 26: Q8 significantly altered the expression of NKR activating ligands in T98G cells. Bar charts **(left)** of % frequencies representing relative NKR ligand expression of **(A)** 4-1BBL, **(B)** B7-H6, and **(C)** MICA/B comparing untreated, vehicle control, and Q8 treated conditions with representative dot plots **(right)** of vehicle control and Q8 treatment groups. **(D)** Bar charts representing ULBP-3 and TRAIL-R2 % frequencies which showed no notable change in expression. Data presented as mean ± SEM, n=4, one-way ANOVA with Bonferroni's ad hoc test, ***$p < 0.0001$.

3.3.5 Q8 significantly increases the expression of the inhibitory NKR ligand Nectin-4 (PVRL4) in the T98G cell line.

The surface expression of inhibitory NKR ligands present on T98G cells was assessed after 48-hour treatment with 10μM of Q8. Flow cytometry analysis of % frequency showed that treatment with 10μM Q8 caused a significant increase in PVRL4 expression when compared to untreated and vehicle control groups [27.6333% vs 2.0275% and 3.24%, n=4, p=0.0008, Figure 27A]. There was no significant effect seen in expression of PVRL1 [12.25% vs 6.36% and 5.3967%, n=4, p=0.0958, Figure 27B], HLA-E [6.0033% vs 1.8925% and 3.1675%, n=4, p=0.2014, Figure 27B], or CD155 [99.675% vs 99.75% and 99.825%, n=4, p=0.40094, Figure 27B].

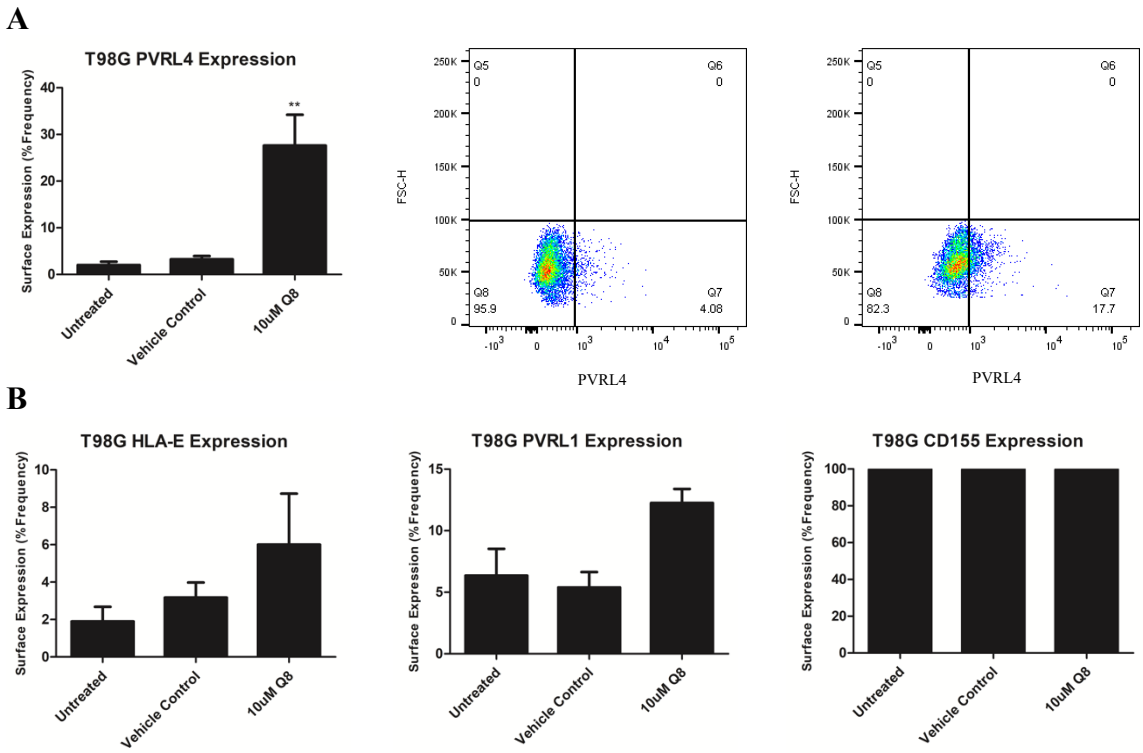

Figure 27: Q8 significantly increases PVRL4 expression in the T98G cell line. (A) Bar chart **(left)** of % frequencies representing relative NKR ligand expression of PVRL4 comparing untreated, vehicle control, and Q8 treated conditions with representative dot plots **(right)** of vehicle control and Q8 treatment groups. **(B)** Bar charts representing HLA-E, PVRL1, and CD155 expression which showed no significant changes. Data presented as mean ± SEM, n=4, one-way ANOVA with Bonferroni's ad hoc test, ***$p < 0.0001$.

3.3.6 Surface NKR ligand expression differs between the U251 and T98G cell lines both at baseline and after treatment with Q8.

The surface expression of both activating and inhibitory NKR ligands is significantly different between the U251 and T98G cell lines, and the modulation of these profiles in response to Q8 treatment also reveals differing expression patterns.

There are marked differences in the expression of activating ligands between the two cell lines. The U251 model shows an increased expression of receptor ligands 4-1BBL [Vehicle control (96.7667% vs 64.1%, p=0.0063), n=4, Figure 28A], B7-H6 [Vehicle control (0.89% vs 3.9533%, p=0.0009), n=4, Figure 28C] and MICA/B [Vehicle control (23.8333% vs 3.9533%, p=0.0031), n=4, Figure 28D] at baseline but not following Q8 treatment [4-1BBL (99.1% vs 95.9%, p=0.0968, Figure 28A), B7-H6 (16.9% vs 24.2667%, p=0.2655, Figure 28C), MICA/B (75.4% vs 73.7333%, p=0.8705, Figure 28D]. Interestingly, the U251 cell line showed no difference in expression at baseline of ULBP-3 [Vehicle control (99.3667% vs 60%, p=0.1053), n=4, Figure 28B] but had a significantly higher expression following treatment with 10μM Q8 [99.3667% vs 76.5%, p=0.0114, n=4, Figure 28B]. There was no significance seen when comparing TRAIL-R2 expression [Vehicle control (99.275% vs 99.2%, p=0.9357) and 10μM Q8 (99.475% vs 99.075%, p=0.5820), n=4, Figure 28E].

Similarly, the expression of inhibitory NKR ligands was varied between our chosen cell lines. There was a marked increased expression of PVRL4 in the U251 line when compared to T98G cells both at baseline [Vehicle control (29.0333% vs 3.24%, p=0.0003), n=4, Figure 28G] and following 10μM Q8 [76.667% vs 27.6333%, p=0.0021, n-4, Figure 28G]. In contrast, the T98G cell line showed a significantly higher expression of HLA-E at baseline [Vehicle control (0.9575% vs 3.1675%, p=0.0468), n=4, Figure 28H] but not following treatment [11.35% vs 6.0033%, p=0.1569, n=4, Figure 28H]. There were no disparities observed in the expression of PVRL1 [Vehicle control (2.1065% vs 5.3967%, p=0.0590) and 10μM Q8 (24.3% vs 12.25%, p=0.0681), n=4, Figure 28F] or CD155 [Vehicle control (99.95% vs 99.825%, p=0.1210) and 10μM Q8 (99.875% vs 99.675%, p=0.2029), n=4, Figure 28I].

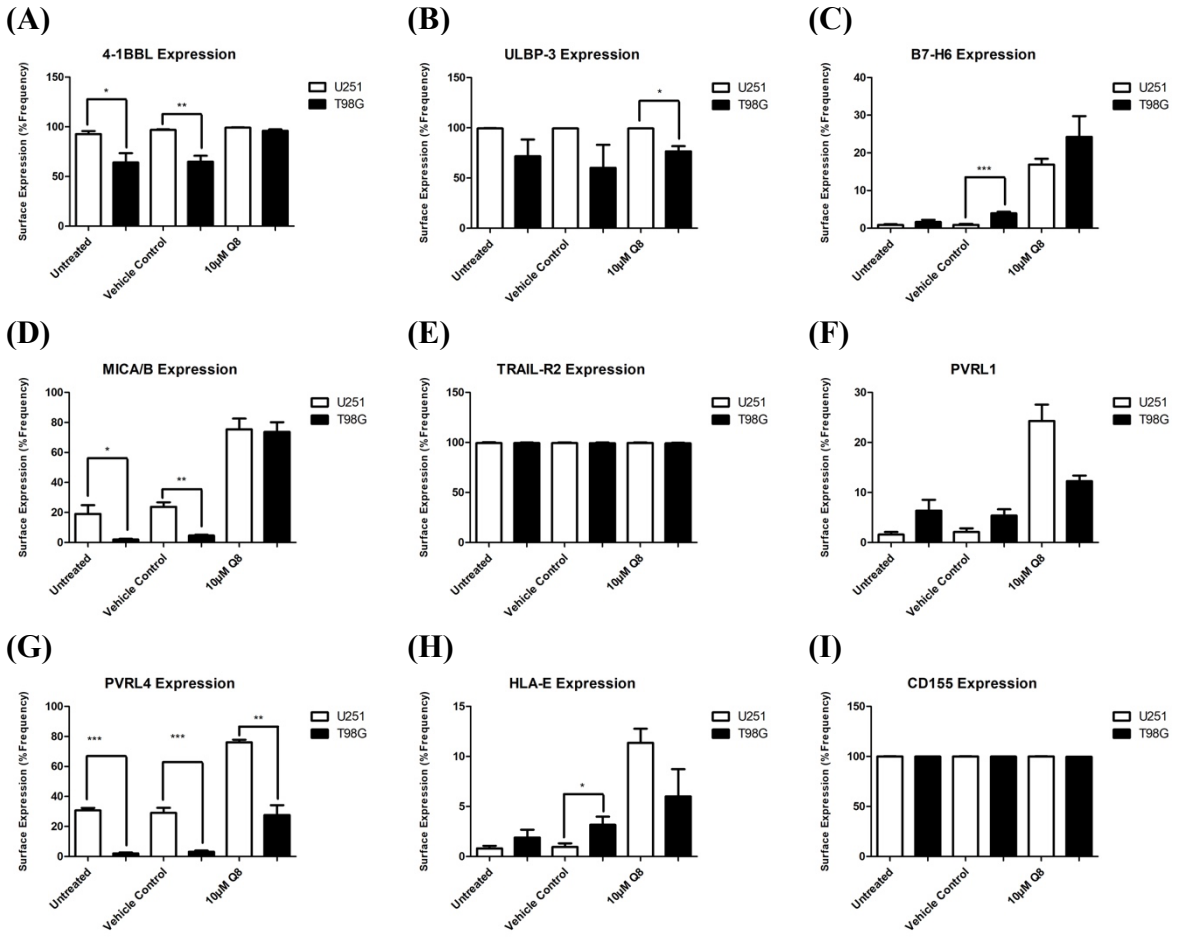

Figure 28: There are significant differences in the expression of NKR ligands between the U251 and T98G cell lines both before and after Q8 treatment. Bar charts of % frequencies comparing U251 and T98G cell lines relative NKR ligand expression for activating ligands **(A)** 4-1BBL, **(B)** ULBP-3, **(C)** B7-H6, **(D)** MICA/B, **(E)** TRAIL-R2 and inhibitory ligands **(F)** PVRL1, **(G)** PVRL4, **(H)** HLA-E, **(I)** CD155. Data presented as mean ± SEM, n=4, unpaired t-test, ***$p < 0.0001$.

3.3.7 Q8 and supernatants from Q8-treated U251 cells has no significant impact on NK receptor expression and function.

KHYG-1 NK cells were treated with a vehicle control and 10μM Q8 and were cultured with supernatant collected from previous experiments to assess the effect of Q8 and Q8 treated cell supernatants on NK cell receptor expression and by proxy NK cell function. Among the receptors being screened was Nkp46. Nkp46 has the ability to promote NK cell adhesion and enhance NK cell lysis of target cells (Hadad et al., 2015). There was a statistically significant alteration of Nkp46 expression on the KHYG-1 cell line in response to U251 Q8 treated supernatant compared to the U251 vehicle control supernatant [43.7667% vs 11.2%, n=4, p=0.0234, Figure 29A]. Interestingly, the U251 control supernatant supressed Nkp46 expression compared to the vehicle control and Q8 treatment groups, and the Q8-treated supernatant recovered this decrease to baseline. There were no significant effects of Q8 treatment alone on receptor expression [33.7333% vs 29.6333%, n=4, p=0.7272, Figure 29A].

There were no significant alterations observed in the expression of the other seven receptors being analysed (Vehicle control vs 10μM Q8; U251 VC treated supernatant vs U251 10μM Q8 treated supernatant) including CD56 [99.9333% vs 99.9667%, p=0.7418; 99.9333% vs 99.9333%, p>0.05], NKp30 [99.2333% vs 99.3333%, p=0.907; 98.7 % vs 99.4%, p=0.2254], CX3CR1 [0.98% vs 1.1633%, p=0.7162; 3.27% vs 5.2067%, p=0.0978], CD3 [0.3267% vs 0.4633%, p=0.1798; 0.29% vs 0.5033%, p=0.3788], CD69 [0.2273% vs 2.5333%, p=0.3462; 0.2567% vs 7.19%, p=0.1252], FasL [0.0083% vs 0.1827%, p=0.3002; 0.1153% vs 0.0287%, p=0.1711], and CD62L [0% vs 0.009%, p=0.2222; 0% vs 0.0293%, p=0.0246] (n=4, Figure 29B).

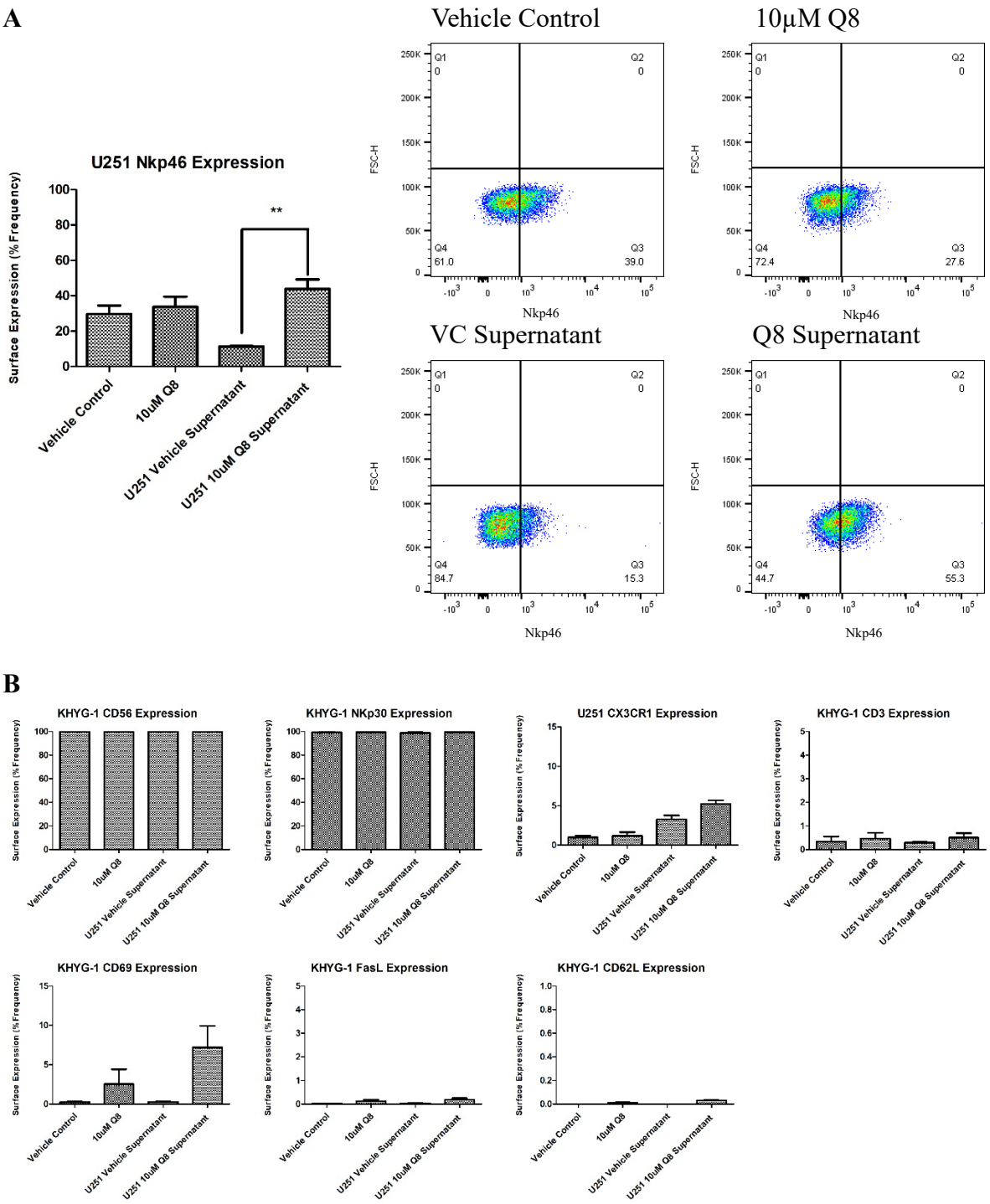

Figure 29: Q8 treated U251 cell supernatant slightly but not significantly alters NK receptor expression in the KHGY-1 NK cell line. (A) Bar chart **(left)** of % frequencies representing relative KHYG-1 receptor expression of Nkp46 comparing vehicle control, Q8 control, U251 vehicle supernatant, and U251 Q8 supernatant treated groups with representative dot plots **(right)**. **(B)** Bar charts representing receptors whose expression showed no significant changes after treatment. Data presented as mean ± SEM, n=4, one-way ANOVA with Bonferroni's ad hoc test, ***$p < 0.0001$.

3.3.8 Q8 and Q8 treated T98G supernatant does not negatively affect NK receptor expression.

The same experiment outlined in the section above was performed using T98G supernatants. Among the receptors analysed was CD69, which serves an important role in NK cell cytotoxicity, proliferation, and TNF-α production (Borrego et al., 1999). There was a statistically significant alteration of CD69 expression on the KHYG-1 cell line in response to T98G Q8 treated supernatant compared to the T98G vehicle control supernatant [14.2367% vs 2.5333%, n=4, p=0.0368, Figure 30A]. Furthermore, there was an increase in the expression of Nkp46 in response to the T98G Q8-treated supernatants compared to the vehicle control supernatant [18.9% vs 52.4333%, n=4, p=0.0016, Figure 30B].

There were no significant alterations observed in the expression of the other seven receptors interrogated (Vehicle control vs 10μM Q8; T98G VC treated supernatant vs T98G 10μM Q8 treated supernatant) including CD56 [99.9333% vs 99.9667%, p=0.7418; 99.8667% vs 99.9333%, p=0.6348], NKp30 [99.2333% vs 99.3333%, p=0.907; 99.7333% vs 99.8667%, p=0.2697], CX3CR1 [0.98% vs 1.1633%, p=0.7162; 2.11% vs 5.23%, p=0.2347], CD3 [0.3267% vs 0.4633%, p=0.1798; 0.19% vs 0.4467%, p=0.1326], FasL [0.0083% vs 0.1153%, p=0.3002; 0.004% vs 0.154%, p=0.1014], and CD62L [0% vs 0.009%, p=0.1841; 0% vs 0.0293%, p=0.0572] (n=4, Figure 30C).

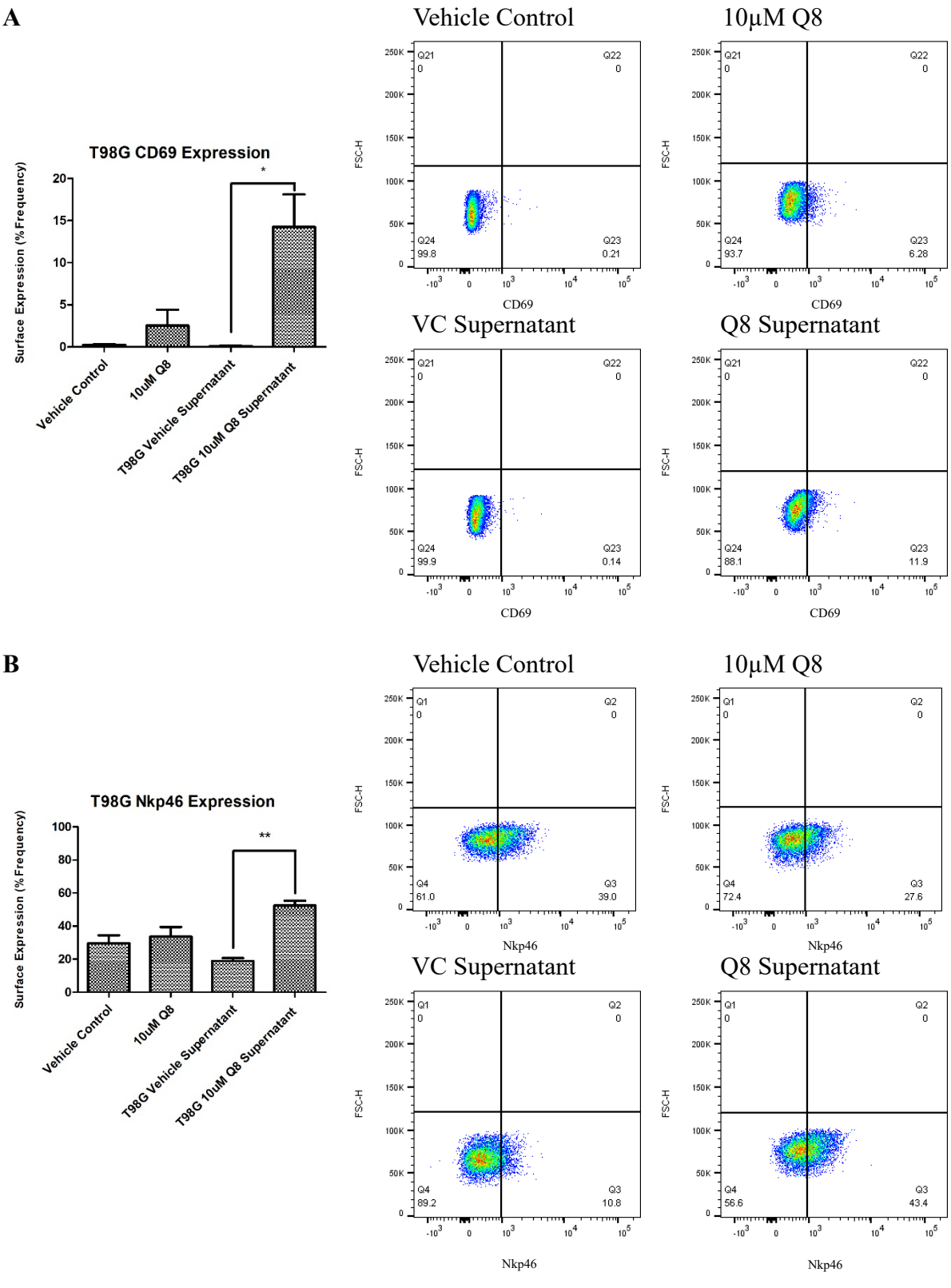
A
Vehicle Control
10µM Q8
T98G CD69 Expression
Surface Expression (%Frequency)
Vehicle Control
10uM Q8
T98G Vehicle Supernatant
T98G 10uM Q8 Supernatant
VC Supernatant
Q8 Supernatant
FSC-H
CD69
B
T98G Nkp46 Expression
Nkp46

C

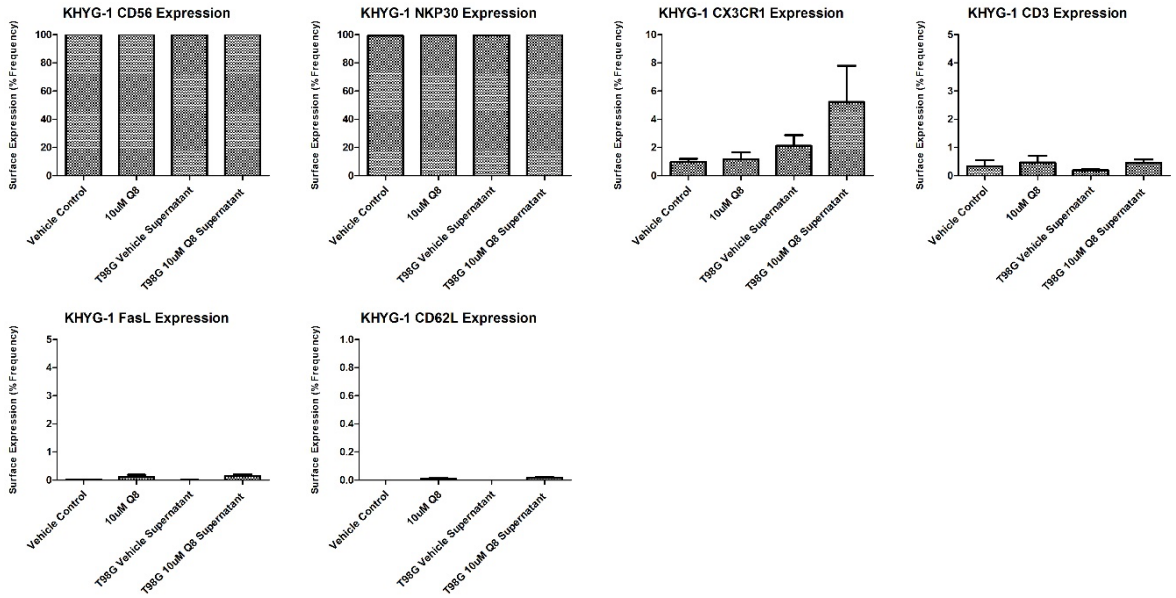

Figure 30: Q8 treated T98G cell supernatant slightly but not significantly alters NK receptor expression in the KHGY-1 NK cell line. (A) Bar chart **(left)** of % frequencies representing relative KHYG-1 receptor expression of CD69 comparing vehicle control, Q8 control, T98G vehicle supernatant, and T98G Q8 supernatant treated groups with representative dot plots **(right)**. **(B)** Bar chart **(left)** of % frequencies representing relative KHYG-1 receptor expression of Nkp46 comparing vehicle control, Q8 control, T98G vehicle supernatant, and T98G Q8 supernatant treated groups with representative dot plots **(right)**. **(C)** Bar charts representing receptors whose expression showed no significant changes after treatment. Data presented as mean ± SEM, n=4, one-way ANOVA with Bonferroni's ad hoc test, ***$p < 0.0001$.

3.3.9 There are no significant differences in NK receptor expression or function when exposed to either vehicle control or Q8-treated U251 supernatant versus T98G supernatant.

When comparing the effects of Q8-treated supernatant from our chosen cell lines, analysis revealed one slight statistically significant result between the U251 and T98G vehicle supernatants and the modulation of Nkp46 expression in the KHYG-1 cell line [11.2% vs 18.9%, p=0.0132, n=4, Figure 31A] but not when comparing Q8-treated supernatant groups [43.7667% vs 52.4333%, p=0.2356, n=4, Figure 31A]. Beyond this there were no statistically significant results found across any of the receptors whose expression was being interrogated (U251 Vehicle Control vs T98G Vehicle Control; U251 Q8-treated vs T98G Q8-treated) including CD56 [99.9333% vs 99.8667%, p=0.6530; 99.9333% vs 99.9333%, p=1, n=4, Figure 31B], NKp30 [98.7% vs 99.7333%, p=0.1961; 99.4% vs 99.667%, p=0.2222, n=4, Figure 31C], CX3CR1 [3.27% vs 2.11%, p=0.2709; 5.2067% vs 5.23%, p=0.9933, n=4, Figure 31D], CD3 [0.29% vs 0.19%, p=0.0963; 0.5033% vs 0.4467%, p=0.8176, n=4, Figure 31E], CD69 [0.2567% vs 2.5333%, p=0.1079; 7.19% vs 14.2367%, p=0.2116, n=4, Figure 31F], FasL [0.1153% vs 0.004%, p=0.0888; 0.0287% vs 0.154%, p=0.7603, n=4, Figure 31G], and CD62L [0% vs 0%; 0.0293% vs 0.0293%, n=4, Figure 31H].

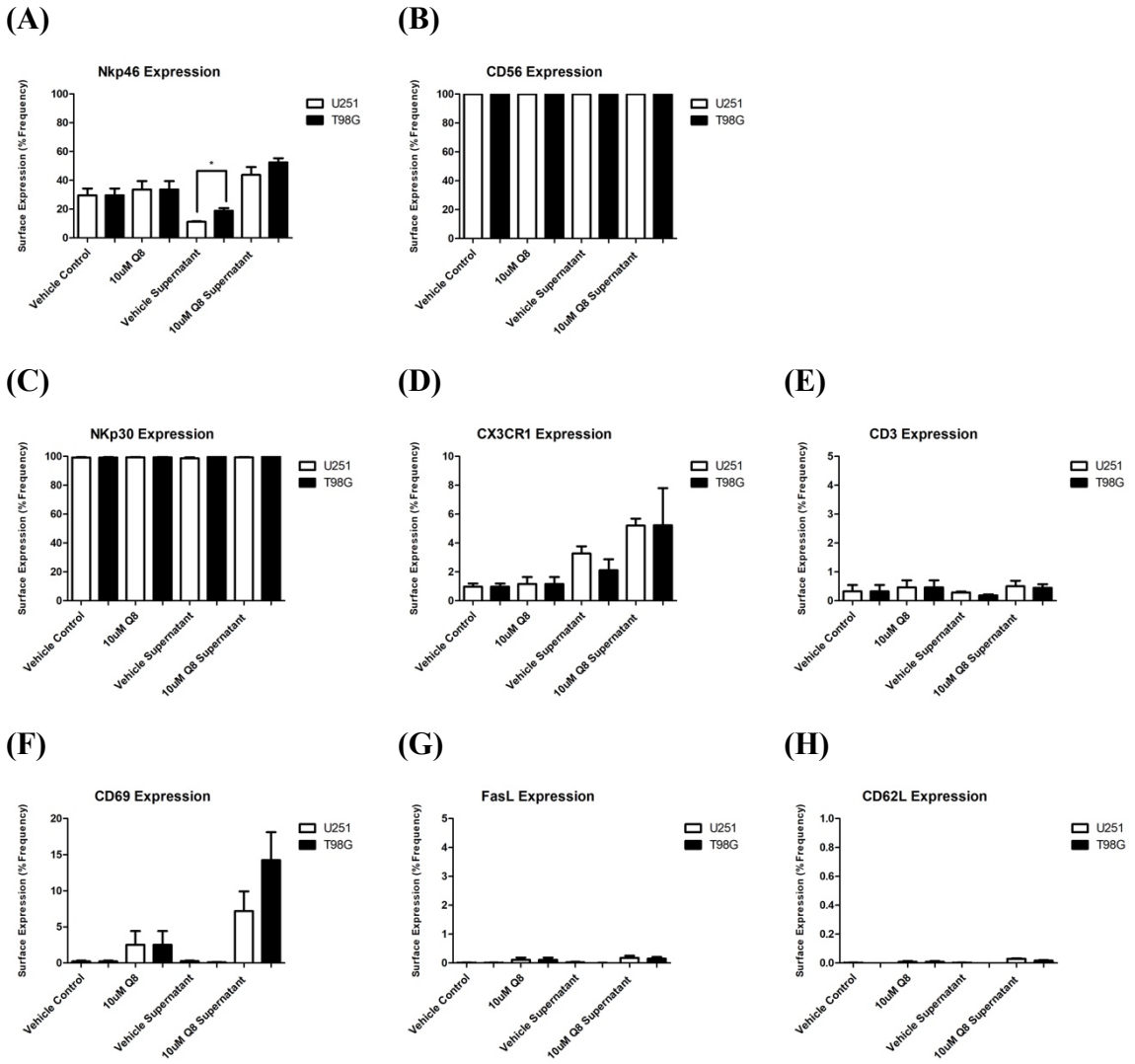

Figure 31: There are no significant differences in the expression of NK receptor expression in the KHYG-1 NK cell line when treated with either U251 or T98G Q8-treateed cell supernatant. Bar charts of % frequencies comparing U251 and T98G cell lines effects on relative KHYG-1 receptor expression for **(A)** Nkp46, **(B)** CD56, **(C)** NKp30, **(D)** CX3CR1, **(E)** CD3, **(F)** CD69, **(G)** FasL, and **(H)** CD62L. Data presented as mean ± SEM, n=4, unpaired t-test, ***$p < 0.0001$.

4. Discussion

Here, we examined the utility of Q8 for its anti-angiogenic and anti-proliferative potential along with its potential immune-stimulatory and immunomodulatory effects in GBM using the T98G and U251 cell lines as a model of GBM and the KHYG-1 cell line as an exemplar model of NK cell therapy.

Our data show that Q8 has little to no effect on T98G cell viability, however, shows some efficacy in the U251 cell line after 48-hour treatment. These effects were seen most clearly at concentrations of 10μM and 20μM, and further research would be required to elucidate statistical significance at these concentrations. Concentrations higher than these resulted in near total cell death which is most likely toxic and would not be therapeutically advantageous. From our research it is clear that Q8 holds some potential in decreasing U251 cell viability. Further studies combining Q8 with other anti-angiogenics such as Bevacizumab may reveal some efficacy in enhancing their proven capabilities and this has been shown to elicit synergistic effects in a well-established zebrafish model of angiogenesis (Butler et al., 2017). It is worth noting that anti-angiogenic testing would be ideally suited to a more multicellular model system as Q8 has prior anti-cancer efficacy in mouse xenograft models (Butler et al., 2019). However, this original screen of the drug was limited by time constraints and resources and more definitive studies would utilise both *in vivo* models such as zebrafish and *ex vivo* brain slice models.

As was previously established, two known angiogenic proteins were shown to be modulated by Q8 and are associated with poor survival in GBM. We took these molecules forward to our next set of experiments along with pro-invasion factor MMP-1 and pro-angiogenic TIE-2. Our results indicate that Q8 treatment of the T98G cell line induces a significant increase in angiopoietin-1 and MMP-1 at increasing drug concentrations, while there was a marked decrease in calpain-2. In the U251 cell line, again there was a significant increase in angiopoietin-1 and MMP-1 expression, as well as a slight increase in calpain-2. These data indicate a potential, undesirable pro-angiogenic and pro-invasive effect of Q8 on GBM cells and suggests that it may in fact promote angiogenesis and facilitate invasion into surrounding tissue, which is not the desired effect. The decrease in calpain-2 in the T98G model though statistically significant is altogether a slight change, however, decrease of calpain-2 in a zebrafish GBM model saw marked decreases in MMP-2 and tumour flexibility/ability to

invade surrounding tissue (Lal et al. 2011). These results require further testing to elucidate a larger panel of angiogenic factors and validation in *in vivo* and *ex vivo* models to elucidate the true impact of such increases/decreases on angiogenesis and invasion. In spite of the seemingly negative data on Q8's anti-angiogenic activity, it may still hold potential as a combination therapy with a more effective anti-angiogenic such as bevacizumab to enhance its proven capabilities further and may impart some immunomodulatory benefits.

Previous studies have shown that Q8 can alter inflammatory mediator release (Butler et al., 2019; Slater et al., 2023). Furthermore, our group's preliminary data indicate that Q8 alters the chemotactic cues of GBM tumour cells to enhance chemoattraction of NK cells [unpublished data]. Here, we sought to examine Q8's effects on a number of cytokines and inflammatory mediators by GBM tumour cell lines to examine if it can enhance atypical anti-tumour soluble mediators and suppress immunosuppressive factors. Due to technical issues beyond our control, a complete analysis of our soluble mediator screen could not be performed. However, from the ELISA data that could be accurately analysed, a significant increase in IL-2 in both U251 and T98G cell lines was observed after Q8 treatment.

IL-2 production is significantly downregulated by the GBM tumour microenvironment, hence the ability to increase its secretion is a significant therapeutic target (Chen et al., 2020). Here we see Q8 has the ability to cause such an increase, which would aid immune infiltration and function, increase T-cell activation and proliferation, and enhance NK cell killing activity. It must be noted that IL-2 activates regulatory T cells (Ross & Cantrell, 2018) and future studies are needed to fully elucidate the net effects of its induction in the GBM tumour microenvironment by Q8.

In contrast, there was a marked decrease in IFN-γ release by both GBM cell lines. IFN-γ is a key immune signalling molecule that promotes the innate inflammatory response and is already inhibited by increased IL-10 production in the GBM microenvironment (Razavi et al., 2016). As previously discussed, increased levels of IL-6 are indicative of advanced tumour development and dampen the anti-tumour response by blocking T-cell activation and limiting NK cell activity (Chen et al., 2020), while TNF-α is a potent mediator of tumour eradication (Wang & Lin, 2008). Here, Q8 showed no evidence of modulating the pro-tumour cytokine IL-6 or the anti-tumour cytokine TNF-α. While it was beyond the time and resources of this MSc project, further analysis of pro- and anti-inflammatory cytokines together with key chemokines is warranted in these cell line models and multicellular *in vivo* and *ex vivo* models to fully

characterise the immunomodulatory effect of Q8, however its positive impact on IL-2 is a significant result.

Complete activation of NK cells requires two or more receptors to be activated by their accompanying ligand (Fasbender & Watzl, 2018). Screening both cell lines for activating and inhibitory NKR ligands gave insight into how GBM cells interact with NK cells and the balance between activating and inhibitory signals. It is desirable to increase activating responses in NK cell immunotherapy to enhance its efficacy in GBM. Flow analysis of GBM cells following Q8 treatment revealed a significant modulation of the NKR ligand profile of both cell lines. In the T98G cell line, 4-1BBL, B7-H6, and MICA/B were increased which in theory would enhance NK cell activation and GBM cell killing. Similarly, B7-H6 and MICA/B showed increased expression on the U251 cell line, however inhibitory ligand expression also increased including PVRL1, PVRL4, and HLA-E. Our results provide compelling evidence that Q8 has potential to increase NK cell activation in emergent immunotherapeutic strategies. Future studies will also elicit the effects of Q8 on NKR ligand shedding by examining the levels of soluble NKR ligands in the cell line supernatants by ELISA. This would be an indicator of whether the increased B7-H6 surface expression, for instance, is accompanied by increased B7-H6 shedding, which is a major NK cell evasion strategy employed by solid tumours and a key challenge for NK cell therapies.

For the purposes of this study, we sought to examine how the effects Q8 elicits on NKR ligand expression by GBM cells translates to its effects on NK cell therapy, i.e., does the modulation of NKR ligands culminate in enhanced or suppressed activation of NK cell therapies. Flow cytometric analysis of the KHYG-1 NK cell line showed that both direct Q8 treatment and culture in Q8-treated U251 and T98G cell line supernatant do not significantly alter the NKR profile of KHYG-1 cells, which is a positive indicator for effective NK cell function. However, it did appear to increase CD69 and Nkp46 expression by the NK cell therapy, which would be a preferable effect and is a likely consequence of the increased IL-2 production (Hood et al., 2019). The apparent lack of immunosuppressive effects of Q8 on KHYG-1 cells is also positive but this must be further scrutinized using functional assays such as killing assays, chemotaxis assays, cytokine production assays and degranulation assays, in order to fully determine the net effects of Q8 on NK cell therapy efficacy and to delineate any synergistic effects. This is particularly pertinent since Q8 reduces IFN-γ by GBM cells and this is such a key effector molecule in NK cell-mediated responses. Furthermore, the overall

consequences of Q8's differential effects on IL-2 and IFN-γ would be better determined if the impact on both NK and T cells were interrogated. These effects have not previously been studied in other cancers, so this would be a novel avenue of research that could broaden our understanding of immune regulation in the tumour microenvironment.

Our data indicates significant heterogeneity between our chosen cell lines across all of the experiments undertaken. The T98G cell line is known to be resistant to both radiation therapy and some chemotherapies like temozolomide (Lee, 2016) and cisplatin (Jt & Kim, 2002). This characteristic makes it an ideal model in treatment sensitising research. The U251 cell line is relatively new in its inclusion in GBM research, and its inclusion in this study gave us an opportunity to explore and define some of the characteristics of this cell line model. Most notably, the U251 cell line was found to have significantly low proliferative activity compared to other established cell lines like the T98G cell line (Torsvik et al., 2014). Our data indicates that there is strong heterogeneity between these cell lines, most notably in Q8s ability to decrease U251 cell viability more effectively than the T98G cell line. The conclusion can be drawn that both the T98G cell line robustness and the U251 cell line's reduced proliferative activity mean that the U251 cells were more susceptible to Q8 while the T98G cells displayed characteristic resistance to drug intervention. Differences in Q8s immunomodulatory and angiogenic mediator altering activity across the cell lines highlights the challenge that is heterogeneity across patients with GBM. Further research is required to determine whether Q8 can perform its therapeutic role consistently in a wide ranging GBM population. NKR ligand profiles are extremely varied in GBM populations (Da Silva et al., 2022). This was observed in the profiles of our chosen cell lines and poses a threat to the efficacy of Q8 as an effective NK cell therapy enhancer (Hosseinalizadeh et al., 2022).

5. Study Limitations

Angiogenesis is the formation of new blood vessels, a process employed by GBM and other solid tumours to create a vasculature to provide blood and essential nutrients for growth and development (Lugano et al., 2019). It is a highly specialised process mediated by a range of external signalling factors that create cascade events through various intermediary signalling molecules. *In vitro* cell line models are not the ideal when studying such a complex, physical process. This research chose to use cell lines as a preliminary model to test Q8s anti-cancer abilities and proceeded with anti-angiogenic studies with this goal in mind. If it could first be shown in such a simple model that Q8 has efficacy it would provide strong evidence to seek ethical approval and funding for more sophisticated models. These models include *ex vivo* GBM models such as an organotypic brain slice model or perhaps a whole brain model with intact vasculature. Better again an *in vivo* model of GBM like murine models or zebrafish would allow more advanced experimentation and research, however escalating to these models would require more time, budget and additional ethical approval which was not possible within the scope of this MSc project. Moreover, the physiological conditions of the solid tumour microenvironment including hypoxia, acidosis and nutrient deprivation are challenging factors for therapeutic efficacy and anti-angiogenics can worsen such conditions which itself can limit immunotherapy access to the tumour (Osawa & Shibuya, 2013). Future studies would incorporate how these factors affect Q8's effects and how Q8 affects these conditions. Q8's effects on these conditions and on the tumour vasculature would indeed impact the sequence timing if it was used in combination with an NK cell therapy.

Quantifying protein expression using immunostaining is a common practice in disease studies, however a major limitation of this study is a lack of alternate means to quantify or support these findings. For example, a positive control could have been used to elucidate a more accurate baseline from which statistical analysis could be performed. Stimulation of cells using known angiogenic factors like VEGF would have increased cellular production of our target signalling molecules for such purposes. There are also alternate methods beyond immunofluorescence imaging by which protein expression can be studied like reverse transcription polymerase chain reaction (RT-PCR) or Western blotting. These techniques would have helped to validate our findings.

Heterogeneity in our chosen cell lines posed the major issue of heterogeneity across all GBM patients. It is a key characteristic of GBM and is a contributing factor to the poor patient outcomes and low survival rates. Every case is different, so drug intervention will not work the

same across the board. Specifically, heterogeneity in NKR ligand profiles will be a major barrier to overcome in future immunotherapeutic strategies (Becker et al., 2021). Therefore, the results generated from these experiments together with any future data must be validated in GBM patient tumour explant samples and potentially in patient-derived xenograft mouse models to maximise pre-clinical accuracy.

Although we were able to elucidate some immunological effects of Q8, the technical issues with ELISA standards and the limited time and money meant that an incomplete panel of soluble mediators were screened here as well as a limitation of phenotypic NK cell studies and not functional studies. To fully ascertain the immunological effects of Q8 more completely, a screen of a more exhaustive panel of cytokines and chemokines, together with a more thorough investigation of KHYG-1 function would be required.

6. Future studies into Q8 efficacy in GBM

Short term: In the immediate short term, research on Q8 efficacy should focus on a number of experiments to further elucidate its anti-cancer potential. Firstly, comprehensive ELISA analysis of cytokine/chemokine expression beyond those analytes studied here should be conducted to better understand the immunomodulatory effects of Q8. In particular, focus should be paid to major interleukins such as IL-8 and IL-10 whose expression is known to dysregulate immune function, in particular T-cell and NK cell activation. Further to these, major neurological immune analytes such as TGF-β, PGE2, and IL-1β should be analysed as they are also implicated in immune dysfunction. Combination therapies with other chemotherapies such as temozolomide and bevacizumab would provide insight into Q8s ability as a CRT enhancer. It has already been shown that combination drug intervention yields better overall outcomes in GBM patients, and the same may be true for Q8. Further to this, Q8s capability as a sensitizer to standard-of-care could be examined by various sensitisation assays. Resistance to both standard-of-care chemotherapies and radiation therapy remains a tough barrier to overcome, and so testing Q8 in this regard would prove useful.

Long term: In the long term, as previously mentioned, more sophisticated models would be necessary to fully understand the efficacy of Q8 in GBM. This could be achieved using novel *ex vivo* models or more established *in vivo* models. Regardless of choice, advancing to this stage in the drug development process, after further studies as outlined above, is pertinent. Following on from GBM models, all results must be validated using clinical patient samples. This would provide insight into the true efficacy of Q8 as a candidate drug treatment and provide an understanding of its capabilities when faced with the diversity of GBM tumours.

7. Conclusions

Our data indicates that Q8 may have potential to reduce cell viability in GBM, but it does not appear to elicit significant anti-angiogenic effects in the cell line model used. Further comprehensive testing, perhaps in an *ex vivo* or *in vivo* model may shed further light on this. In addition, Q8 has the ability to promote IL-2 secretion, which may prove useful in the context of strengthening the immune response and efficacy in the GBM tumour microenvironment. However, its decrease of IFN-γ activity may be problematic.

An exciting prospect emerging from this study is Q8's potential as a combination immunotherapeutic. Our results show Q8 has an ability to modulate the expression of NK receptor ligands presented on GBM cells, both activating and inhibitory, which may help increase NK cell functionality and efficacy in targeting cancer cells. Q8 does not appear to have immunomodulatory effects on the NK cell therapy KHYG-1 and may elicit immunostimulatory effects through its induction of IL-2 and increases in NK cell activation marker CD69. However, its functional effects on NK cells, as a consequence of its alterations of NKR ligands on GBM cells, are yet to be elucidated. The emergence of NK cell immunotherapies is an exciting new prospect, and the ability to bolster their efficacy with combination drug treatments could provide a novel strategy which will improve patient outcomes overall. This study scratches the surface of Q8's potential, and further research will be needed to reveal its true efficacy.

The validation of these results requires novel *ex vivo* and *in vivo* models of GBM to fully understand both the anti-cancer and immunotherapeutic potential of Q8. Furthermore, the ability of Q8 as a candidate for GBM must be validated in patient samples before being brought forward in the drug development chain. Overall, our results indicate that Q8 may have some anti-cancer effects in GBM.

8. Bibliography

Ali, Y., Oliva, C. R., Noman, A. S. M., Allen, B. G., Goswami, P. C., Zakharia, Y., . . . Griguer, C. E. (2020). Radioresistance in glioblastoma and the development of radiosensitizers. *Cancers*, *12*(9), 2511. https://doi.org/10.3390/cancers12092511

Ameratunga, M., Pavlakis, N., Wheeler, H., Grant, R., Simes, J., & Khasraw, M. (2018). Anti-angiogenic therapy for high-grade glioma. *The Cochrane Library*, *2018*(11). https://doi.org/10.1002/14651858.cd008218.pub4

Backes, C., Friedmann, K. S., Mang, S., Knörck, A., Hoth, M., & Kummerow, C. (2018). Natural killer cells induce distinct modes of cancer cell death: Discrimination, quantification, and modulation of apoptosis, necrosis, and mixed forms. *Journal of Biological Chemistry*, *293*(42), 16348–16363. https://doi.org/10.1074/jbc.ra118.004549

Bascur, J. P., Alegría-Arcos, M., Araya-Durán, I., Juritz, E. I., González-Nilo, F. D., & Almonacid, D. E. (2018). IDH1 and IDH2 mutants identified in cancer lose inhibition by isocitrate because of a change in their binding sites. *bioRxiv (Cold Spring Harbor Laboratory)*. https://doi.org/10.1101/425025

Batlle, E., & Massagué, J. (2019). Transforming growth factor-B signaling in immunity and cancer. *Immunity*, *50*(4), 924–940. https://doi.org/10.1016/j.immuni.2019.03.024

Becker, A. P., Sells, B. E., Haque, S. J., & Chakravarti, A. (2021). Tumor heterogeneity in glioblastomas: From light microscopy to molecular pathology. *Cancers*, *13*(4), 761. https://doi.org/10.3390/cancers13040761

Borrego, F., Robertson, M. J., Ritz, J., Peña, J., & Solana, R. (1999). CD69 is a stimulatory receptor for natural killer cell and its cytotoxic effect is blocked by CD94 inhibitory receptor. *Immunology*, *97*(1), 159–165. https://doi.org/10.1046/j.1365-2567.1999.00738.x

Bu, X., Qu, X., Guo, K., Meng, X., Yang, X., Huang, Q., . . . Wang, L. (2021). CD147 confers temozolomide resistance of glioma cells via the regulation of β-TrCP/Nrf2 pathway. *International Journal of Biological Sciences*, *17*(12), 3013–3023. https://doi.org/10.7150/ijbs.60894

Burke, L., Butler, C. T., Murphy, A., Moran, B., Gallagher, W. M., O'Sullivan, J., & Kennedy, B. N. (2016). Evaluation of cysteinyl leukotriene signaling as a therapeutic target for colorectal cancer. *Frontiers in Cell and Developmental Biology*, *4*. https://doi.org/10.3389/fcell.2016.00103

Burster, T., Gärtner, F., Bulach, C., Zhanapiya, A., Gihring, A., & Knippschild, U. (2021). Regulation of MHC I molecules in glioblastoma cells and the sensitizing of NK cells. *Pharmaceuticals*, *14*(3), 236. https://doi.org/10.3390/ph14030236

Butler, C. T., Kennedy, S., Buckley, A., Doyle, R., Conroy, E., Gallagher, W. M., . . . Kennedy, B. N. (2019). 1,4-dihydroxy quininib attenuates growth of colorectal cancer cells and xenografts and regulates the TIE-2 signaling pathway in patient tumours. *Oncotarget*, *10*(38), 3725–3744. https://doi.org/10.18632/oncotarget.26966

Butler, C. T., Reynolds, A., Tosetto, M., Dillon, E., Guiry, P. J., Cagney, G., . . . Kennedy, B. N. (2017). A Quininib Analogue and Cysteinyl Leukotriene Receptor Antagonist Inhibits Vascular Endothelial Growth Factor (VEGF)-independent Angiogenesis and Exerts an Additive Antiangiogenic Response with Bevacizumab. *Journal of Biological Chemistry*, *292*(9), 3552–3567. https://doi.org/10.1074/jbc.m116.747766

Chen, H., Li, M., Guo, Y., Zhong, Y., He, Z., Xu, Y., & Zou, J. (2020). Immune response in glioma's microenvironment. *Innovative Surgical Science*, *5*(3–4), 115–125. https://doi.org/10.1515/iss-2019-0001

Cheng, L., Huang, Z., Zhou, W., Wu, Q., Donnola, S., Liu, J. K., . . . Bao, S. (2013). Glioblastoma stem cells generate vascular pericytes to support vessel function and tumor growth. *Cell*, *153*(1), 139–152. https://doi.org/10.1016/j.cell.2013.02.021

Chu, J., Gao, F., Yan, M., Zhao, S., Zheng, Y., Shi, B., & Liu, Y. (2022). Natural killer cells: a promising immunotherapy for cancer. *Journal of Translational Medicine*, *20*(1). https://doi.org/10.1186/s12967-022-03437-0

Crane, C. A., Han, S. J., Barry, J. J., Ahn, B., Lanier, L. L., & Parsa, A. T. (2009). TGF- downregulates the activating receptor NKG2D on NK cells and CD8+ T cells in glioma patients. *Neuro Oncology*, *12*(1), 7–13. https://doi.org/10.1093/neuonc/nop009

Crivellato, E. (2011). The role of angiogenic growth factors in organogenesis. *The International Journal of Developmental Biology*, *55*(4–5), 365–375. https://doi.org/10.1387/ijdb.103214ec

Da Silva, L. H. R., Catharino, L. C. C., Da Silva, V. J., Evangelista, G. C. M., & Barbuto, J. a. M. (2022). The War Is on: The Immune System against Glioblastoma—How Can NK Cells Drive This Battle? *Biomedicines*, *10*(2), 400. https://doi.org/10.3390/biomedicines10020400

Daneman, R., & Prat, A. (2015). The Blood–Brain barrier. *Cold Spring Harbor Perspectives in Biology*, *7*(1), a020412. https://doi.org/10.1101/cshperspect.a020412

Demuth, T., & Berens, M. E. (2004). Molecular Mechanisms of Glioma Cell Migration and Invasion. *Journal of Neuro-Oncology*, *70*(2), 217–228. https://doi.org/10.1007/s11060-004-2751-6

Deshors, P., Toulas, C., Arnauduc, F., Malric, L., Siegfried, A., Nicaise, Y., . . . Evrard, S. (2019). Ionizing radiation induces endothelial transdifferentiation of glioblastoma stem-like cells through the Tie2 signaling pathway. *Cell Death and Disease*, *10*(11). https://doi.org/10.1038/s41419-019-2055-6

Dhermain, F. (2014). Radiotherapy of high-grade gliomas: current standards and new concepts, innovations in imaging and radiotherapy, and new therapeutic approaches. *Aizheng*, *33*(1), 16–24. https://doi.org/10.5732/cjc.013.10217

Diaz, R. J., Ali, S. C., Qadir, M. G., De La Fuente, M. I., Ivan, M. E., & Komotar, R. J. (2017). The role of bevacizumab in the treatment of glioblastoma. *Journal of Neuro-Oncology*, *133*(3), 455–467. https://doi.org/10.1007/s11060-017-2477-x

Dimitrov, L., Hong, C. S., Yang, C., Zhuang, Z., & Heiss, J. D. (2015). New developments in the pathogenesis and therapeutic targeting of the IDH1 mutation in Glioma. *International Journal of Medical Sciences*, *12*(3), 201–213. https://doi.org/10.7150/ijms.11047

Dong, X. (2018). Current strategies for brain drug delivery. *Theranostics*, *8*(6), 1481–1493. https://doi.org/10.7150/thno.21254

Fasbender, F., & Watzl, C. (2018). Impedance-based analysis of Natural Killer cell stimulation. *Scientific Reports*, *8*(1). https://doi.org/10.1038/s41598-018-23368-5

Filippi-Chiela, E. C., Thomé, M. P. M., Silva, M. M. B. E., Pelegrini, A. L., Ledur, P. F., Garicochea, B., . . . Lenz, G. (2013). Resveratrol abrogates the Temozolomide-induced G2 arrest leading to mitotic catastrophe and reinforces the Temozolomide-induced senescence in glioma cells. *BMC Cancer*, *13*(1). https://doi.org/10.1186/1471-2407-13-147

Fougner, V., Hasselbalch, B., Lassen, U., Weischenfeldt, J., Poulsen, H. S., & Urup, T. (2022). Implementing targeted therapies in the treatment of glioblastoma: Previous shortcomings, future promises, and a multimodal strategy recommendation. *Neuro-oncology Advances*, *4*(1). https://doi.org/10.1093/noajnl/vdac157

Friedman, H. S., Prados, M. D., Wen, P. Y., Mikkelsen, T., Schiff, D., Abrey, L. E., . . . Cloughesy, T. F. (2009). Bevacizumab alone and in combination with irinotecan in

recurrent glioblastoma. *Journal of Clinical Oncology*, *27*(28), 4733–4740. https://doi.org/10.1200/jco.2008.19.8721

Garcia, J., Hurwitz, H., Sandler, A., Miles, D., Coleman, R., Deurloo, R., & Chinot, O. (2020). Bevacizumab (Avastin®) in cancer treatment: A review of 15 years of clinical experience and future outlook. *Cancer Treatment Reviews*, *86*, 102017. https://doi.org/10.1016/j.ctrv.2020.102017

Golán, I., De La Fuente, L. R., & Costoya, J. A. (2018). NK Cell-Based Glioblastoma immunotherapy. *Cancers*, *10*(12), 522. https://doi.org/10.3390/cancers10120522

Gross, P. M. (1992). Chapter 31: Circumventricular organ capillaries. In *Progress in Brain Research* (pp. 219–233). https://doi.org/10.1016/s0079-6123(08)62338-9

Hadad, U., Thauland, T. J., Martinez, O. M., Butte, M. J., Porgador, A., & Krams, S. M. (2015). NKP46 clusters at the immune synapse and regulates NK cell polarization. *Frontiers in Immunology*, *6*. https://doi.org/10.3389/fimmu.2015.00495

Hanahan, D. (2022). Hallmarks of Cancer: New dimensions. *Cancer Discovery*, *12*(1), 31–46. https://doi.org/10.1158/2159-8290.cd-21-1059

Hanahan, D., & Monje, M. (2023). Cancer hallmarks intersect with neuroscience in the tumor microenvironment. *Cancer Cell*, *41*(3), 573–580. https://doi.org/10.1016/j.ccell.2023.02.012

Hanahan, D., & Weinberg, R. A. (2000). The hallmarks of cancer. *Cell*, *100*(1), 57–70. https://doi.org/10.1016/s0092-8674(00)81683-9

Hanahan, D., & Weinberg, R. A. (2011). Hallmarks of Cancer: The next generation. *Cell*, *144*(5), 646–674. https://doi.org/10.1016/j.cell.2011.02.013

Hanif, F., Muzaffar, K., Perveen, K., Malhi, S. M., & Simjee, S. U. (2017). Glioblastoma Multiforme: A Review of its Epidemiology and Pathogenesis through Clinical

Presentation and Treatment. *PubMed*, *18*(1), 3–9. https://doi.org/10.22034/apjcp.2017.18.1.3

Herrlinger, U., Tzaridis, T., Mack, F., Steinbach, J. P., Schlegel, U., Sabel, M., . . . Glas, M. (2019). Lomustine-temozolomide combination therapy versus standard temozolomide therapy in patients with newly diagnosed glioblastoma with methylated MGMT promoter (CeTeG/NOA–09): a randomised, open-label, phase 3 trial. *Lancet*, *393*(10172), 678–688. https://doi.org/10.1016/s0140-6736(18)31791-4

Hood, S., Foulds, G. A., Imrie, H., Reeder, S., McArdle, S. E., Khan, M. A., & Pockley, A. G. (2019). Phenotype and function of activated natural killer cells from patients with prostate cancer: Patient-Dependent responses to priming and IL-2 activation. *Frontiers in Immunology*, *9*. https://doi.org/10.3389/fimmu.2018.03169

Hosseinalizadeh, H., Roudkenar, M. H., Roushandeh, A. M., Kuwahara, Y., Tomita, K., & Sato, T. (2022). Natural killer cell immunotherapy in glioblastoma. *Discover Oncology*, *13*(1). https://doi.org/10.1007/s12672-022-00567-1

Hou, A. J., Chen, L. C., & Chen, Y. Y. (2021). Navigating CAR-T cells through the solid-tumour microenvironment. *Nature Reviews Drug Discovery*, *20*(7), 531–550. https://doi.org/10.1038/s41573-021-00189-2

Hrbac, T., Kopkova, A., Siegl, F., Vecera, M., Ruckova, M., Kazda, T., . . . Sana, J. (2022). HLA-E and HLA-F are overexpressed in glioblastoma and HLA-E increased after exposure to ionizing radiation. *Cancer Genomics & Proteomics*, *19*(2), 151–162. https://doi.org/10.21873/cgp.20311

Huang, Z., Chung, C. L., Hu, T. H., Chen, J. J., Liu, P., & Chen, C. (2021). Recent progress in TGF-β inhibitors for cancer therapy. *Biomedicine & Pharmacotherapy*, *134*, 111046. https://doi.org/10.1016/j.biopha.2020.111046

Humphries, W., Wei, J., Sampson, J. H., & Heimberger, A. B. (2010). The role of TREGs in Glioma-Mediated Immunosuppression: Potential target for intervention. *Neurosurgery Clinics of North America*, *21*(1), 125–137. https://doi.org/10.1016/j.nec.2009.08.012

Jt, P., & Kim, T. Y. (2002). Cisplatin-Induced apoptosis by cisplatin in human glioblastoma cell line. *Journal of Korean Neurosurgical Society*, *31*(6), 574–584. Retrieved from http://wprim.whocc.org.cn/local/detail.jsp?channelid=75002&searchword=WPRIMID%3D205128

Kennedy, S., Morrissey, M. E., Dunne, M. R., O'Connell, F., Butler, C. T., Cathcart, M., . . . O'Sullivan, J. (2020). Combining 1,4-dihydroxy quininib with Bevacizumab/FOLFOX alters angiogenic and inflammatory secretions in ex vivo colorectal tumors. *BMC Cancer*, *20*(1). https://doi.org/10.1186/s12885-020-07430-y

Kirstein, A., Schilling, D., Combs, S. E., & Schmid, T. E. (2021). Lomeguatrib increases the radiosensitivity of MGMT unmethylated human glioblastoma multiforme cell lines. *International Journal of Molecular Sciences*, *22*(13), 6781. https://doi.org/10.3390/ijms22136781

Kondělková, K., Vokurková, D., Krejsek, J., Borská, L., Fiala, Z., & Andrýs, C. (2010). Regulatory T cells (Treg) and Their Roles in Immune System with Respect to Immunopathological Disorders. *Acta Medica*, *53*(2), 73–77. https://doi.org/10.14712/18059694.2016.63

Krakstad, C., & Chekenya, M. (2010). Survival signalling and apoptosis resistance in glioblastomas: opportunities for targeted therapeutics. *Molecular Cancer*, *9*(1), 135. https://doi.org/10.1186/1476-4598-9-135

Kumari, S., Ahsan, S. M., Kumar, J. M., Kondapi, A. K., & Rao, N. M. (2017). Overcoming blood brain barrier with a dual purpose Temozolomide loaded Lactoferrin

nanoparticles for combating glioma (SERP-17-12433). *Scientific Reports*, *7*(1). https://doi.org/10.1038/s41598-017-06888-4

Lal, S., Du, J., Tanguay, R. L., & Greenwood, J. A. (2011). Calpain 2 is required for the invasion of glioblastoma cells in the zebrafish brain microenvironment. *Journal of Neuroscience Research*, *90*(4), 769–781. https://doi.org/10.1002/jnr.22794

Lanier, L. L. (2008). Up on the tightrope: natural killer cell activation and inhibition. *Nature Immunology*, *9*(5), 495–502. https://doi.org/10.1038/ni1581

Lee, S. Y. (2016). Temozolomide resistance in glioblastoma multiforme. *Genes and Diseases*, *3*(3), 198–210. https://doi.org/10.1016/j.gendis.2016.04.007

Lugano, R., Ramachandran, M., & Dimberg, A. (2019). Tumor angiogenesis: causes, consequences, challenges and opportunities. *Cellular and Molecular Life Sciences*, *77*(9), 1745–1770. https://doi.org/10.1007/s00018-019-03351-7

Ma, Q. (2013). Role of NRF2 in oxidative stress and toxicity. *Annual Review of Pharmacology and Toxicology*, *53*(1), 401–426. https://doi.org/10.1146/annurev-pharmtox-011112-140320

Maus, M. V. (2015). Designing CAR T cells for glioblastoma. *OncoImmunology*, *4*(12), e1048956. https://doi.org/10.1080/2162402x.2015.1048956

Melaiu, O., Lucarini, V., Cifaldi, L., & Fruci, D. (2020). Influence of the tumor microenvironment on NK cell function in solid tumors. *Frontiers in Immunology*, *10*. https://doi.org/10.3389/fimmu.2019.03038

Molenaar, R. J., Verbaan, D., Lamba, S., Zanon, C., Jeuken, J., Boots-Sprenger, S., . . . Bleeker, F. E. (2014). The combination of IDH1 mutations and MGMT methylation status predicts survival in glioblastoma better than either IDH1 or MGMT alone. *Neuro-Oncology*, *16*(9), 1263–1273. https://doi.org/10.1093/neuonc/nou005

Morvan, M., & Lanier, L. L. (2015). NK cells and cancer: you can teach innate cells new tricks. *Nature Reviews Cancer*, *16*(1), 7–19. https://doi.org/10.1038/nrc.2015.5

Organization, G. R. (n.d.). What is the average glioblastoma survival rate? — Glioblastoma Research Organization. Retrieved from https://www.gbmresearch.org/blog/glioblastoma-survival-rate

Osawa, T., & Shibuya, M. (2013). Targeting cancer cells resistant to hypoxia and nutrient starvation to improve anti-angiogeneic therapy. *Cell Cycle*, *12*(16), 2519–2520. https://doi.org/10.4161/cc.25729

Osswald, M., Jung, E., Sahm, F., Solecki, G., Venkataramani, V., Blaes, J., . . . Winkler, F. (2015). Brain tumour cells interconnect to a functional and resistant network. *Nature*, *528*(7580), 93–98. https://doi.org/10.1038/nature16071

Park, J. H., & Lee, K. (2022). Current understanding of hypoxia in glioblastoma multiforme and its response to immunotherapy. *Cancers*, *14*(5), 1176. https://doi.org/10.3390/cancers14051176

Park, J., Kim, I., Han, S., Park, I., Kim, C., Bae, J., . . . Koh, G. Y. (2016). Normalization of tumor vessels by TIE2 activation and ANG2 inhibition enhances drug delivery and produces a favorable tumor microenvironment. *Cancer Cell*, *30*(6), 953–967. https://doi.org/10.1016/j.ccell.2016.10.018

Paul, S., & Lal, G. (2017). The molecular mechanism of natural killer cells function and its importance in cancer immunotherapy. *Frontiers in Immunology*, *8*. https://doi.org/10.3389/fimmu.2017.01124

Pearson, J. R., Cuzzubbo, S., McArthur, S., Durrant, L. G., Adhikaree, J., Tinsley, C. J., . . . McArdle, S. E. (2020). Immune escape in glioblastoma multiforme and the adaptation of immunotherapies for treatment. *Frontiers in Immunology*, *11*. https://doi.org/10.3389/fimmu.2020.582106

Razavi, S. M., Lee, K. E., Jin, B., Aujla, P. S., Gholamin, S., & Li, G. (2016). Immune evasion strategies of glioblastoma. *Frontiers in Surgery*, *3*. https://doi.org/10.3389/fsurg.2016.00011

Ross, S. H., & Cantrell, D. A. (2018). Signaling and function of interleukin-2 in T lymphocytes. *Annual Review of Immunology*, *36*(1), 411–433. https://doi.org/10.1146/annurev-immunol-042617-053352

Sabry, M., & Lowdell, M. W. (2017). NK cells and cancer. In *InTech eBooks*. https://doi.org/10.5772/intechopen.69658

Sameshima, T., Nabeshima, K., Toole, B. P., Yokogami, K., Okada, Y., Goya, T., . . . Wakisaka, S. (2000). Expression of emmprin (CD147), a cell surface inducer of matrix metalloproteinases, in normal human brain and gliomas. *International Journal of Cancer*, *88*(1), 21–27. https://doi.org/10.1002/1097-0215(20001001)88:1

Schulte, J., Aghi, M. K., & Taylor, J. (2021). Anti-angiogenic therapies in the management of glioblastoma. *Chinese Clinical Oncology*, *10*(4), 37. https://doi.org/10.21037/cco.2020.03.06

Sciumè, G., De Angelis, G., Benigni, G., Ponzetta, A., Morrone, S., Santoni, A., & Bernardini, G. (2011). CX3CR1 expression defines 2 KLRG1+ mouse NK-cell subsets with distinct functional properties and positioning in the bone marrow. *Blood*, *117*(17), 4467–4475. https://doi.org/10.1182/blood-2010-07-297101

Sejda, A., Grajkowska, W., Trubicka, J., Szutowicz, E., Wojdacz, T. K., Kloc, W., & Iżycka-Świeszewska, E. (2022). WHO CNS5 2021 classification of gliomas: a practical review and road signs for diagnosing pathologists and proper patho-clinical and neuro-oncological cooperation. *Folia Neuropathologica*, *60*(2), 137–152. https://doi.org/10.5114/fn.2022.118183

Shibuya, M. (2011). Vascular Endothelial Growth Factor (VEGF) and Its Receptor (VEGFR) Signaling in Angiogenesis: A Crucial Target for Anti- and Pro-Angiogenic Therapies. *Genes Cancer*, *2*(12), 1097–1105. https://doi.org/10.1177/1947601911423031

Shin, M. H., Kim, J., Lim, S. A., Kim, S., & Lee, K. M. (2020). NK Cell-Based immunotherapies in Cancer. *Immune Network*, *20*(2). https://doi.org/10.4110/in.2020.20.e14

Singh, N., Miner, A., Hennis, L., & Mittal, S. (2020). Mechanisms of temozolomide resistance in glioblastoma - a comprehensive review. *Cancer Drug Resistance*. https://doi.org/10.20517/cdr.2020.79

Sivori, S., Vacca, P., Del Zotto, G., Munari, E., Mingari, M. C., & Moretta, A. (2019). Human NK cells: surface receptors, inhibitory checkpoints, and translational applications. *Cellular & Molecular Immunology*, *16*(5), 430–441. https://doi.org/10.1038/s41423-019-0206-4

Slater, K., Bosch, R., Smith, K. F., Jahangir, C. A., García-Mulero, S., Rahman, A., . . . Kennedy, B. N. (2023). 1,4-dihydroxy quininib modulates the secretome of uveal melanoma tumour explants and a marker of oxidative phosphorylation in a metastatic xenograft model. *Frontiers in Medicine*, *9*. https://doi.org/10.3389/fmed.2022.1036322

Steven, A., & Seliger, B. (2016). Control of CREB expression in tumors: from molecular mechanisms and signal transduction pathways to therapeutic target. *Oncotarget*, *7*(23), 35454–35465. https://doi.org/10.18632/oncotarget.7721

Stillger, M. N., Chen, C., Lai, Z. W., Li, M., Schäfer, A., Pagenstecher, A., . . . Schilling, O. (2023). Changes in calpain-2 expression during glioblastoma progression predisposes tumor cells to temozolomide resistance by minimizing DNA damage and p53-

dependent apoptosis. *Cancer Cell International*, *23*(1). https://doi.org/10.1186/s12935-023-02889-8

Suck, G., Branch, D. R., Smyth, M. J., Miller, R. G., Vergidis, J., Fahim, S., & Keating, A. (2005). KHYG-1, a model for the study of enhanced natural killer cell cytotoxicity. *Experimental Hematology*, *33*(10), 1160–1171. https://doi.org/10.1016/j.exphem.2005.06.024

Temodar (temozolomide) dosing, indications, interactions, adverse effects, and more. (n.d.). Retrieved from https://reference.medscape.com/drug/temodar-temozolomide-342229

Thakkar, J. P., Dolecek, T. A., Horbinski, C., Ostrom, Q. T., Lightner, D., Barnholtz-Sloan, J. S., & Villanó, J. L. (2014). Epidemiologic and Molecular Prognostic Review of Glioblastoma. *Cancer Epidemiol Biomarkers Prev.*, *23*(10), 1985–1996. https://doi.org/10.1158/1055-9965.epi-14-0275

Tomar, M. S., Kumar, A., Srivastava, C., & Shrivastava, A. (2021). Elucidating the mechanisms of Temozolomide resistance in gliomas and the strategies to overcome the resistance. *Biochimica Et Biophysica Acta (BBA) - Reviews on Cancer*, *1876*(2), 188616. https://doi.org/10.1016/j.bbcan.2021.188616

Torsvik, A., Stieber, D., Enger, P. Ø., Golebiewska, A., Molven, A., Svendsen, A., . . . Bjerkvig, R. (2014). U-251 revisited: genetic drift and phenotypic consequences of long-term cultures of glioblastoma cells. *Cancer Medicine*, *3*(4), 812–824. https://doi.org/10.1002/cam4.219

Tran, T., Kim, Y., Duong, T., Thangaraj, J., Chu, T., Jung, S., . . . Jung, T. (2023). Natural killer cell therapy potentially enhances the antitumor effects of bevacizumab plus irinotecan in a glioblastoma mouse model. *Frontiers in Immunology*, *13*. https://doi.org/10.3389/fimmu.2022.1009484

Tsai, M. L., Chang, W., Chuang, C., Wu, K., Cheng, C., Sheu, C., . . . Hung, J. (2021). Cysteinyl leukotriene pathway and cancer. *International Journal of Molecular Sciences*, *23*(1), 120. https://doi.org/10.3390/ijms23010120

Visser, O., Ardanáz, E., Botta, L., Sant, M., Tavilla, A., Minicozzi, P., . . . Otter, R. (2015). Survival of adults with primary malignant brain tumours in Europe; Results of the EUROCARE-5 study. *European Journal of Cancer*, *51*(15), 2231–2241. https://doi.org/10.1016/j.ejca.2015.07.032

Vollmann-Zwerenz, A., Leidgens, V., Feliciello, G., Klein, C. A., & Hau, P. (2020). Tumor cell invasion in glioblastoma. *International Journal of Molecular Sciences*, *21*(6), 1932. https://doi.org/10.3390/ijms21061932

Wang, X., & Lin, Y. (2008). Tumor necrosis factor and cancer, buddies or foes? *Acta Pharmacologica Sinica*, *29*(11), 1275–1288. https://doi.org/10.1111/j.1745-7254.2008.00889.x

Wirsching, H., Galanis, E., & Weller, M. (2016). Glioblastoma. In *Glioblastoma* (pp. 381–397). https://doi.org/10.1016/b978-0-12-802997-8.00023-2

Wolfenson, H., Lavelin, I., & Geiger, B. (2013). Dynamic regulation of the structure and functions of integrin adhesions. *Developmental Cell*, *24*(5), 447–458. https://doi.org/10.1016/j.devcel.2013.02.012

Zhang, A. B., Mozaffari, K., Aguirre, B., Li, V. C., Kubba, R., Desai, N. C., . . . Wadehra, M. (2023). Exploring the past, present, and future of Anti-Angiogenic therapy in Glioblastoma. *Cancers*, *15*(3), 830. https://doi.org/10.3390/cancers15030830

Zhang, Z., Li, S., Zhang, B., Qiao, L., & Zhang, Y. (2020). T cell dysfunction and exhaustion in cancer. *Frontiers in Cell and Developmental Biology*, *8*. https://doi.org/10.3389/fcell.2020.00017